Fall 2019

Cyclophilin A Enhances HIV-1 Reverse Transcription in Human Microglial Cells

Zachary Michael Ingram
Missouri State University, Ingram13@live.missouristate.edu

CYCLOPHILIN A ENHANCES HIV-1 REVERSE TRANSCRIPTION IN HUMAN MICROGLIAL CELLS

A Master's Thesis

Presented to

The Graduate College of

Missouri State University

In Partial Fulfillment

Of the Requirements for the Degree

Master of Science, Cell and Molecular Biology

By

Zachary Michael Ingram

December 2019

CYCLOPHILIN A ENHANCES HIV-1 REVERSE TRANSCRIPTION IN HUMAN MICROGLIAL CELLS

Biomedical Sciences

Missouri State University, December 2019

Master of Science

Zachary Michael Ingram

ABSTRACT

Parenchymal microglia represent a susceptible cell type to HIV infection and contribute to HIV Associated Neurocognitive Disorders (HAND). Currently, HIV host-protein interactions in microglia are understudied, but relevant to the design of antiviral drugs. HIV replication events rely on host and viral proteins to evade an immune response while improve replication success. Post-fusion the HIV capsid is released into the cytoplasm and begins trafficking towards the nucleus. During transit viral RNA is transcribed to DNA through reverse transcription (RT). In addition, the HIV capsid that protects the reverse transcription complex disassembles in a step termed uncoating. Once the pre-integration complex reaches the nuclear envelope host-interactions facilitate nuclear import. In the cytoplasm the capsid acts as an interface for protein interactions including cyclophilin A (CypA). CypA is a cytoplasmic peptidyl prolyl isomerase that binds the CypA binding loop of CA. CypA has been known to enhance reverse transcription and nuclear import in a cell type dependent manner. Recent work in the CHME3 human microglial cell line indicates CypA enhances end point infectivity. Therefore, the goal of this study was to identify which replication events were altered by CypA. To characterize which replication event is altered reverse transcription, uncoating, and nuclear import were assessed. qPCR, cell based, and confocal microscopy experiments were employed to detect deficient replication in absence of CypA binding. Blocking CypA interaction with CsA treatment resulted in a significant decrease in the completion of reverse transcription. qPCR analysis indicated an effect on early RT products was not detectable until after 2 hours post-infection. Further, by quantifying 2-LTR circles as an indirect measurement of nuclear import loss of CypA binding led to a decrease in nuclear DNA. Preliminary results for uncoating suggest that CypA may not drastically alter uncoating kinetics, though replicate data is needed. Based on these findings we conclude that late reverse transcription is enhanced by CypA interaction. This work establishes a foundation for understanding how CypA influences HIV in microglia while contributing to the larger field studying HIV-CypA interactions.

KEYWORDS: HIV-1, reverse transcription, uncoating, nuclear import, cyclophilin a, microglia

CYCLOPHILIN A ENHANCES HIV-1 REVERSE TRANSCRIPTION IN HUMAN MICROGLIAL CELLS

By
Zachary Michael Ingram

A Master's Thesis
Submitted to the Graduate College
Of Missouri State University
In Partial Fulfillment of the Requirements
For the Degree of Master of Science, Cell and Molecular Biology

December 2019

Approved:

Amy E. Hulme, Ph.D., Thesis Committee Chair

Randi Ulbricht, Ph.D., Committee Member

Lyon Hough, Ph.D., Committee Member

Julie Masterson, Ph.D., Dean of the Graduate College

ACKNOWLEDGEMENTS

I would first like to thank Richard Martin for his encouragement during my application process to the Masters in Cell and Molecular Biology program. In addition, I would like to acknowledge RSTATS and Amber Yanez for her guidance on appropriate statistical testing. I would also like to thank Reece Stutzman and Caleb Likens for their assistance with the In Situ Uncoating Assay protocol troubleshooting. I am grateful for my thesis committee as completion of this project was not possible without their assistance. My committee members Dr. Hough and Dr. Ulbricht have been integral in advising and feedback as this project has progressed. Lastly, I would like to thank Dr. Hulme who under her support and guidance I have been able to grow as scientist.

TABLE OF CONTENTS

LIST OF TABLES

LIST OF FIGURES

INTRODUCTION

Overview

As treatment has improved HIV becomes a lifelong chronic disease resulting in growing populations of HIV positive individuals. With increasing lifespans, incidence rates of HIV-associated neurocognitive disorders (HAND) are on the rise. This spectrum of neurological disorders is attributed to the infection and prolonged activation of microglial cells throughout the central nervous system (1). While HIV research has been primarily focused on the susceptible T cell population in HIV infection, research into microglial cells is needed. During HIV replication, events prior to integration must be completed to establish infection. These early replication steps utilize both viral and host cellular machinery. Cyclophilin A (CypA), a cytoplasmic peptidyl prolyl isomerase, binds the CypA binding loop on the viral capsid and modulates infectivity in a cell type dependent manner (2, 3). CypA is responsible for isomerizing proline residues from *cis* to *trans* conformation in protein folding. How the binding of CypA and conformation of key proline residues impacts HIV replication is still unknown (4, 5). Despite decades of research a concise mechanism explaining the effect of CypA on HIV infection has not been established.

Microglia in HIV Associated Neurocognitive Disorders

A key component in maintaining homeostasis within the brain is the physical blood brain barrier (BBB). The BBB in a healthy individual prevents the passage of HIV into neural tissue. However, during HIV infection the BBB is compromised as perivascular macrophages (PVMs) are infected. PVMs are a resident brain macrophage that line the vasculature apart of the

basement membrane for the BBB. PVMs represent a susceptible cell type to HIV infection (6). Infection and ultimately disfunction of PVMs contributes to increased permeability of the BBB (7). Entry into the brain is primarily believed to occur through infection of monocytic cells that transport HIV past the BBB (8). Within the brain HIV infects astrocytes and parenchymal microglia cells. Infection of astrocytes does not produce replication competent virus, but the secretion of the viral Tat protein is neurotoxic (9). Maintenance of gap junctions is further compromised by the infection and dysregulation of astrocytes (10). The other primary cell type infected is parenchymal microglia. Unlike astrocytes, microglia can produce replication competent HIV and are relatively long-lived cells (11). Thus, it is believed that microglia act as the primary reservoir within the brain that maintain chronic HIV infection.

Within the brain parenchymal microglial cells assist in maintaining homeostasis. Microglial function is dependent on the gene expression state generally divided between ramified (resting) or activated phenotypes. Ramified microglia possess distinct processes stemming from the cell body allowing for environmental surveillance of activating signals. Activation of microglia results in a shift in morphology and gene expression profile. Once activated microglia appear ameboid and are capable of migration toward stimuli. Activated microglia carry out phagocytosis of pathogens and cellular debris. Clearance of cellular debris can promote apoptosis and is necessary for the maintenance of a healthy CNS. Additionally, the phagocytosis of pathogens is where similarities between macrophages are often drawn. The support that microglia provide extends past immune function as damaged neurons can undergo synaptic stripping mediated by microglia (12).

Chronic activation of microglial cells is implicated in a variety of neurodegenerative diseases and can result from the presence of pro-inflammatory stimuli. Established infection in

microglia contributes to the inappropriate activation as well as the proinflammatory viral protein, Tat. As HIV establishes a reservoir in the CNS cytotoxic effects from activated microglia drive neuronal damage. This CNS damage manifests in patients as a spectrum termed HIV-associated neurocognitive disorders (HAND) (13).

With the development of Highly Active Anti-Retroviral Therapies (HAART) a decrease in incidence rates of the most severe HAND classification, HIV-Associated Dementia (HAD), has been reported. However, Asymptomatic Neurocognitive Impairment (ANI) and Mild Neurocognitive Disorder (MND) are still a concern for the HIV positive population (1). Clinical research into HAND has progressed with the implementation of neuroimaging to track structural changes throughout the CNS (14). Understanding HAND at a clinical level is necessary but is additionally supplemented by molecular level research into HIV replication.

HIV infection within the CNS also establishes a viral reservoir which has proven to be a key determinant to developing a functional cure to HIV. The viral reservoir represents a subpopulation of infected cells not actively producing virions and thus escaping current methods for targeting infection. Viral reservoirs prevent the eradication of HIV as latently infected cells replenish viral loads upon later activation (15). In the interest of developing a cure all viral reservoirs must be eliminated. Primarily HIV research focuses on replication within T cell, dendritic, and macrophage cell lines while currently cellular and molecular research focused on microglia cells is lacking.

Overview of HIV Replication Events

Prior to entry of target cells, virions are enclosed within a lipid membrane with dispersed envelope proteins required in binding cell receptors. Binding of the viral gp160 envelope

complex, including gp41 and gp120, marks the beginning of the HIV replication cycle (Figure 1). HIV's tropism is restricted to CD4 positive receptor cells possessing either CCR5 or CXCR4 chemokine co- receptors. Binding is initiated through attachment of gp120 to a CD4 receptor and a chemokine co-receptor. Once attached, gp41 undergoes a conformational change and penetrates the host cell membrane before retracting. As gp41 retracts the viral membrane is pulled into proximity of the host cell membrane until direct contact initiates fusion of both viral and host membrane. Viral envelope proteins remain at the host membrane, while the capsid structure is released into the cytoplasm (16, 17).

Post-fusion a set of highly regulated, but poorly understood, events must occur prior to integration. The viral capsid begins trafficking along microtubules towards the nucleus (18). During transit viral ssRNA is transcribed by reverse transcriptase to dsDNA. Viral DNA associates with integrase and various accessory proteins to form the pre-integration complex (PIC). In addition, the intact capsid structure must undergo disassembly in a step called uncoating prior to nuclear import of the PIC. Once uncoated the PIC transverses the nuclear pore complex, an import mechanism which is required for lentivirus infection of nondividing cells. Integrase then facilitates integration of HIV dsDNA into the host genome establishing a provirus and permanent infection of the cell (Figure 2).

Once the provirus has been established replication events shift to the production of progeny virions or late replication steps. Late replication steps begin as long terminal repeats (LTR) marking the 5' and 3' ends of the integrated viral DNA recruit trans-acting elements for transcription of the viral genome (19). Viral mRNA is translated, and the viral proteins begin localizing near the host membrane in the assembly step. Immature virions then undergo budding with an envelope derived from the producer cell membrane. Free of the producer cell the viral

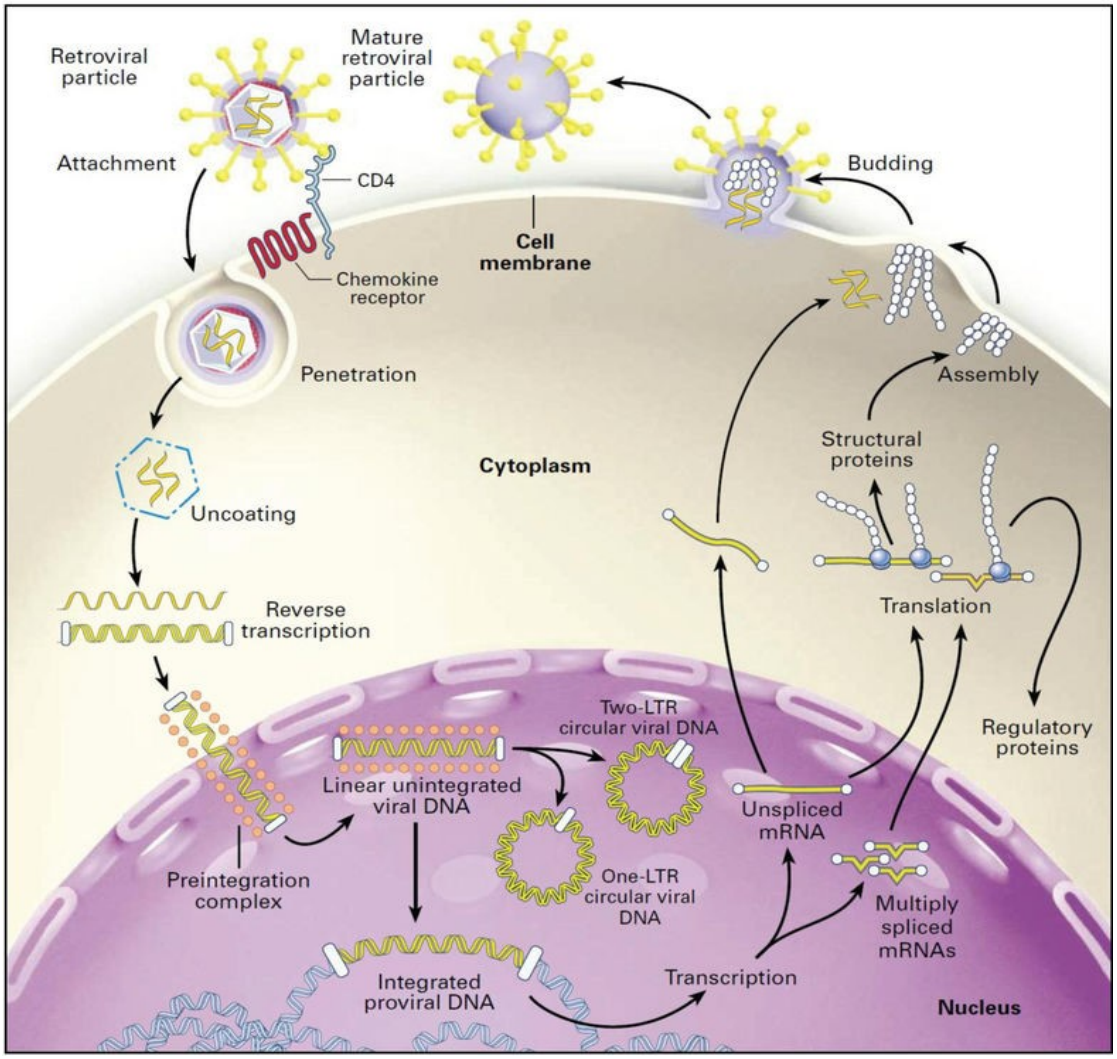

Figure 1. Schematic of the Complete HIV Replication Cycle. Early replication steps include attachment through integration. Following integration late replication steps facilitate production of progeny virions (20).

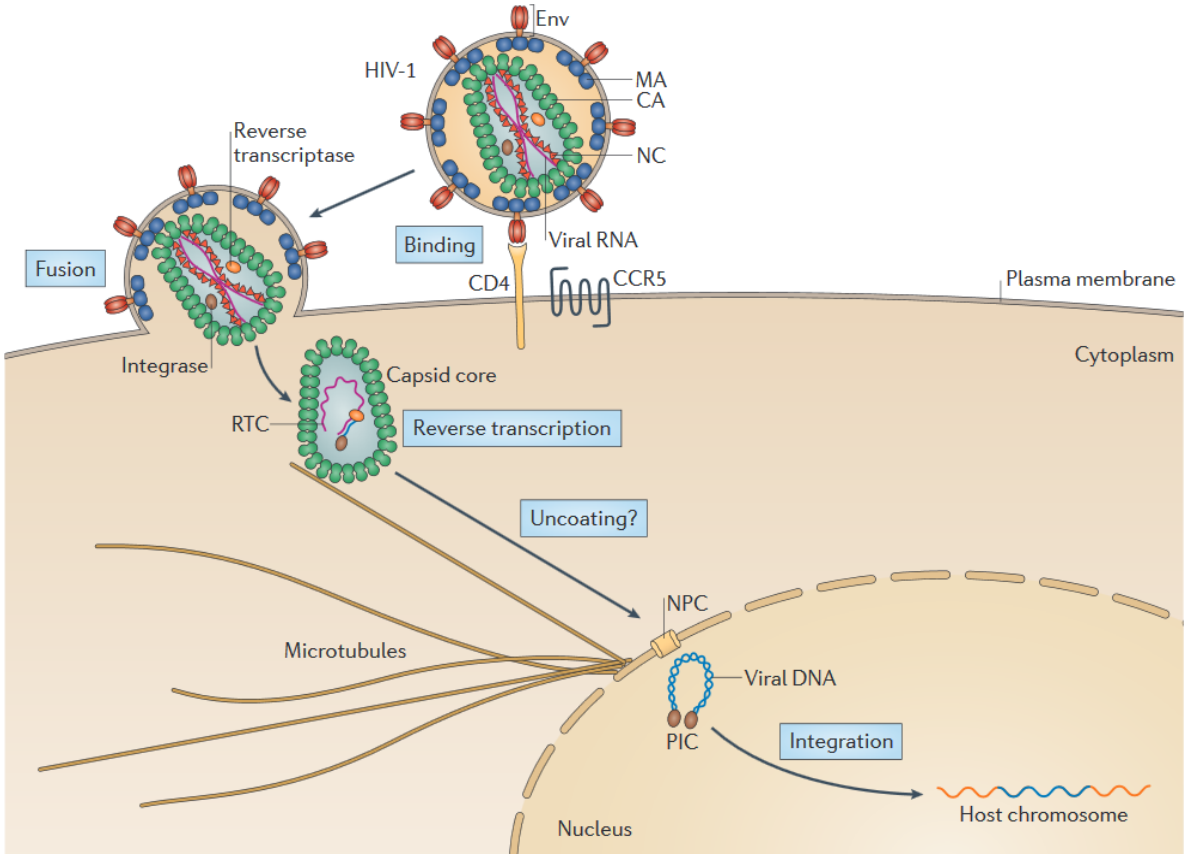

Figure 2. Overview of Early Replication Steps of HIV Infection. Viral gp120 binds the CD4 and chemokine co-receptor followed by gp41 initiated fusion. Viral capsid is released into the cytoplasm post fusion and traffics along microtubules towards the nucleus (21).

Gag polyprotein must then undergo cleavage mediated by HIV proteases initiating maturation. Uncleaved viral Gag consists of immature matrix, capsid (CA), nucleocapsid, and p6 proteins. Cleavage of Gag releases each protein and allows conformational change within the noninfectious virus particle. Assembly of the mature capsid structure and RNA enzyme complex represents the completion of maturation. The formation of mature viral particles marks the end of the HIV replication cycle with infectious virus particles now able to undergo binding (22, 23). The remainder of this literature review will focus on early replication events prior to integration specifically reverse transcription, uncoating, and nuclear import. Pre-integration steps are ideal targets for development of antiviral drugs as inhibition of these replication events prevents permanent infection of the cell. Additionally, cytoplasmic trafficking and nuclear import represent a timeframe in which interaction with host proteins is needed to complete replication steps.

Reverse Transcription

Reverse transcription begins with binding of reverse transcriptase to the ssRNA primer binding site (PBS) in the presence of host deoxynucleotide triphosphates (dNTPs) (Figure 3). Reverse transcription proceeds 5' to 3' until the 5' long terminal repeat region of the viral RNA is reached. As reverse transcriptase transcribes RNA to cDNA, a RNase H domain degrades the RNA part of the DNA: RNA structure. Reverse transcriptase then dissociates from the strand in a minus-strand strong stop step. This small ssDNA fragment represents early reverse transcription products and is able to bind to the 3' LTR region on the second viral RNA. Complementary base pairing of early RT products to the 5' LTR region completes the first strand transfer. Reverse

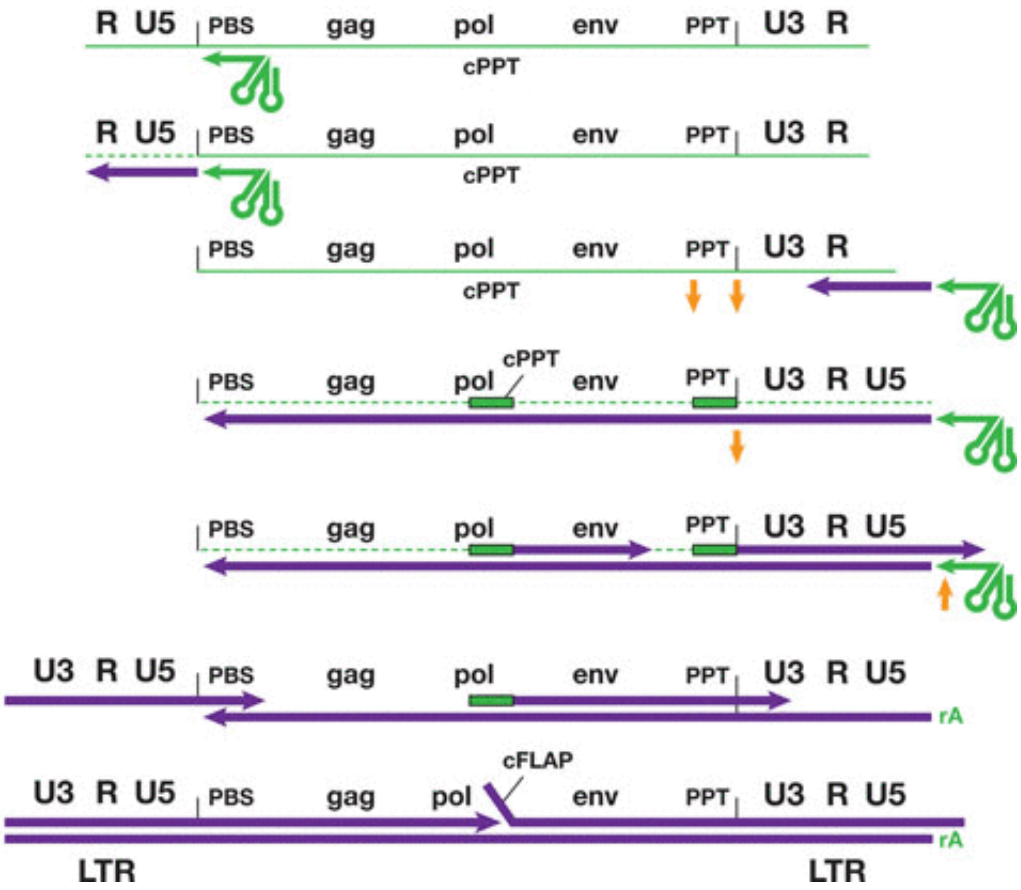

Figure 3. Stepwise Schematic of Reverse Transcription. Binding of reverse transcriptase at the primer binding site begins reverse transcription. During this process two distinct DNA products are detectable: early and late RT products. Early products represent the smaller DNA fragment after the minus-strand strong stop. Late RT products represent fully transcribed viral DNA (24).

transcriptase re-associates with the DNA: RNA structure and polymerizes along the RNA strand. RNase H activity degrades the majority of this second RNA excluding two purine rich regions (PPT). Upon completion of transcribing full-length cDNA reverse transcriptase binds the PPT and central PPT (cPPT) as a primer to continue transcription. Plus-strand strong stop occurs as the reverse transcription reaches the LTR region. The complementary PBS region facilitates the second strand transfer through transient base pairing allowing reverse transcriptase to complete synthesis of HIV dsDNA (25). Due to the two PPT regions multiple reverse transcriptase can transcribe simultaneously. As a result of the cPPT a DNA flap overhang is generated. The DNA flap has been linked to a role in nuclear import but is still not fully understood (26).

HIV Capsid and Uncoating

Upon completion of fusion, the viral capsid is released into the cytoplasm. The complete conical capsid consists of 1,000-1,500 CA monomers (21). CA monomers consist of two domains: a carboxyl-terminal domain (CTD) and amino-terminal domain (NTD). The NTD contains seven alpha helices, two beta hairpins, and a partially ordered loop region named the Cyclophilin A Binding loop. Secondary structures of the CTD include four α helices and a flexible linker bridging the NTD and CTD together (27, 28). Interfacing between adjacent CA monomers occurs at a major homology region (MHR) conserved across viruses. Mutations at key interface residues can prevent dimerization and formation of a mature capsid structure (28, 29). CA monomers interlink together form hexamers and pentamers. These hexamers and pentamer structures make up and maintain the unique cone shaped capsid (30) (Figure 4).

Within the capsid, the necessary components needed to establish infection are housed including the reverse transcription complex (RTC), integrase, and various accessory proteins.

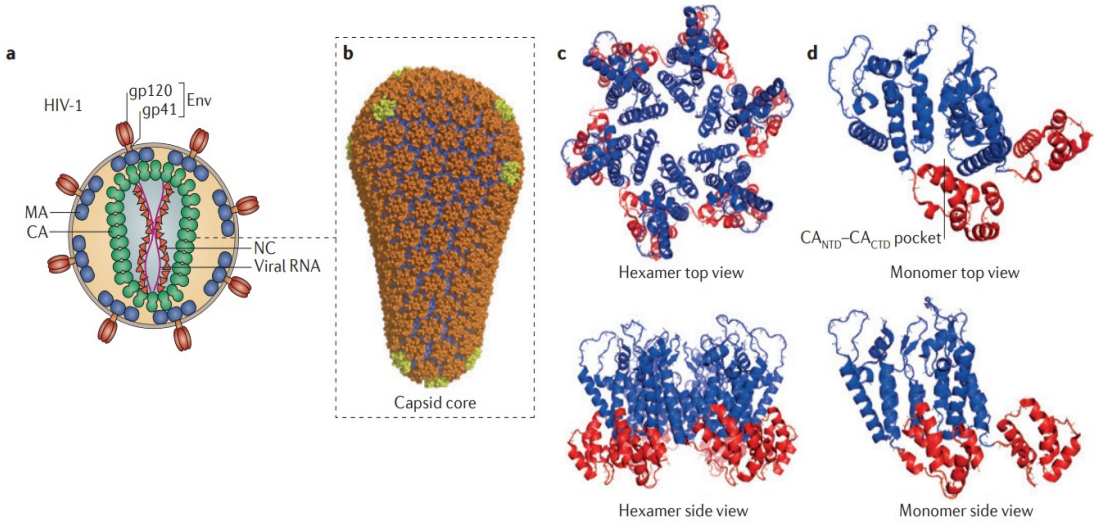

Figure 4. Mature Virion and Capsid Structure. A) Depiction of main proteins in mature unfused virions. B) Intact conical capsid structure consisting of CA protein forming hexamers (orange) and pentamers (yellow). C-D) Structural formation of CA formed hexamers (21).

Cytosolic sensors that would detect the internal components and raise an immune response are physically blocked by intact capsid. Contrary to this mandatory function, the capsid must also undergo a timely disassembly of the larger structure referred to as uncoating. Known hyperstable and unstable capsid mutants, with delayed or rapid uncoating kinetics, demonstrate suboptimal infectivity (31). Due to the opposing functions of the capsid, mutations to CA often result in decreases infectivity (32).

With the establishment of new methods for studying capsid increasing evidence suggests uncoating is not a single event. Rather, uncoating may be a multi-step process of structural loss. Initial capsid opening followed by a loss of the remaining lattice has been observed within two distinct assays. The capsid opening assay is carried out within a microfluidics device in which virus is adhered to a glass surface (33). Virus is produced with a GFP marker that becomes trapped within the capsid. The opening of the capsid corresponds to a loss in GFP signal compared to the initial level. Within this assay CypA-DsRed was introduced to bind CA monomers and indirectly label the capsid lattice. Interestingly, the loss of GFP often occurred before the loss of CypA-DsRed indicating biphasic uncoating was occurring. While the capsid opening assay is carried out within a microfluidics device an alternative assay has shown support for biphasic uncoating in cells.

Using fluorescent microscopy, the colocalization of CA stain and RNA staining is assessed. To carry out the RNA staining a 5-ethynul uridine (EU) stain is introduced which incorporates into viral RNA. A fluorescent dye is then ligated to the modified uridine allowing RNA labelling. Importantly, EU stain was only able to incorporate into viral RNA once the capsid has opened. By measuring colocalization of EU and CA staining over time two distinct uncoating events were observed (34).

The spatiotemporal aspects of uncoating are still not fully understood. Three main models of uncoating have been established to describe the coordinated events of uncoating (Figure 5) (21). Early attempts to define uncoating based the rapid disassembly model on the inability to isolate CA protein with the RTC (35, 36). Under this model the capsid disassembles shortly after fusion leaving the RTC free of CA monomers. Rapid disassembly represented the predominant model for uncoating for many years, but as methods for analyzing uncoating have improved evidence of intact capsids has contradicted this model. The unstable capsid mutant K203A has been shown to decreased infectivity in comparison to wild type capsid (32). The rapid loss of capsid subsequently effects downstream events leading to reduced nuclear import and integration (37).

Under the cytoplasmic uncoating model the capsid is maintained post-fusion and uncoating occurs during transit towards the nucleus. A combination of the In Situ Uncoating Assay and Cyclosporine (CsA) Washout Assay indicate that uncoating occurs in the cytoplasm. The In Situ Uncoating Assay utilizes GFP-Vpr labeled virus as well as immunostaining for CA protein. In this method, loss of p24 intensity co-localized at GFP puncta represents a visual measurement of uncoating that can be quantified across a time course (38, 39). Additionally, the CsA Washout Assay represents a high throughput method for measuring uncoating kinetics. The CsA washout assay relies on expression of the TRIM-Cyp fusion protein. TRIM-Cyp is thought to restrict uncoating similar to TRIM5α through formation of a net around the intact capsid lattice (40). TRIM-Cyp insensitivity occurs as intact capsid disassembles, though the amount of uncoated capsid needed for loss of TRIM-Cyp restriction is still not completely understood (39).Comparison of uncoating kinetics and reverse transcription kinetics have shown close association of events in favor of the cytoplasmic uncoating model. Under this model uncoating

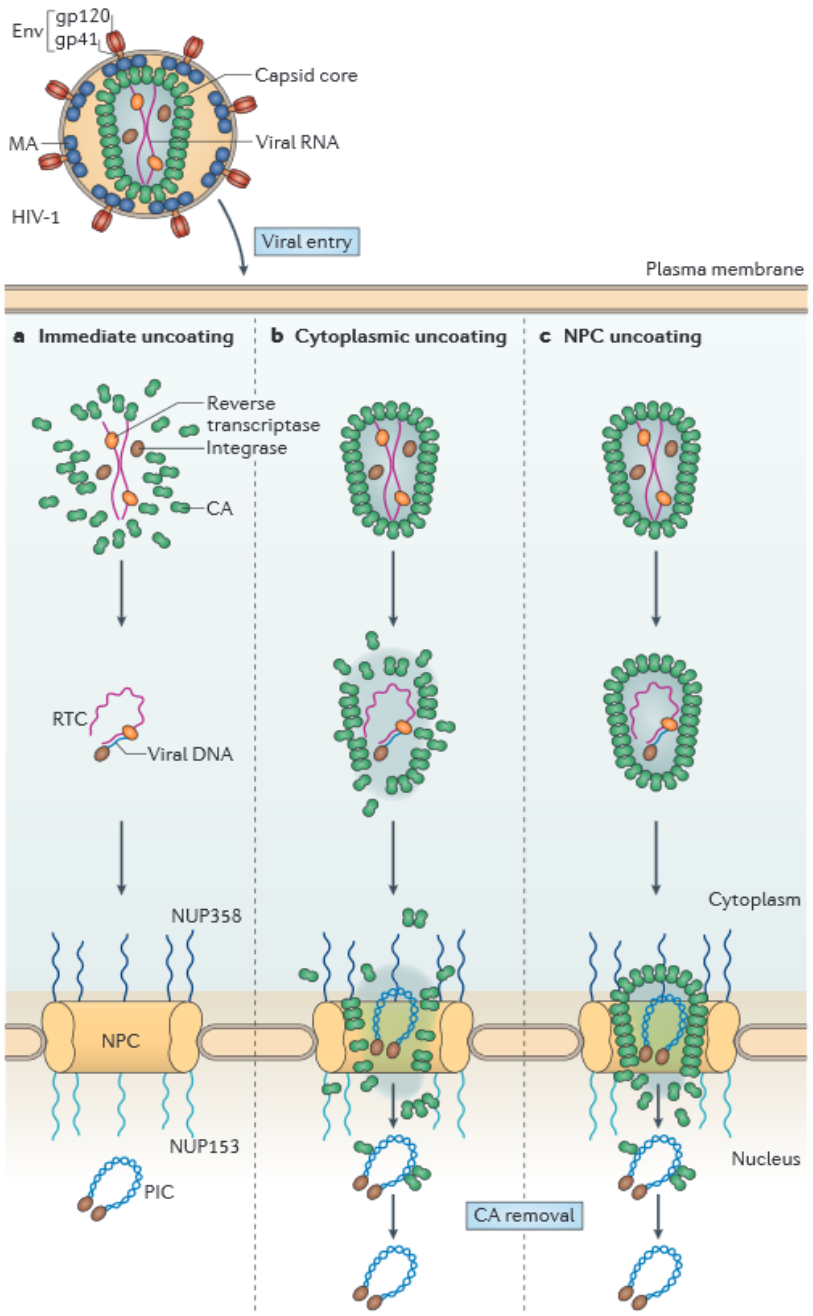

Figure 5. Models of Uncoating. A) Immediate uncoating is defined by rapid disassembly of the capsid structure post-fusion. The reverse transcription complex (RTC) traffics to the nucleus in absence of CA. B) Cytoplasmic uncoating occurs by intact capsid structure disassembling in route to the nucleus. Loss of capsid is necessary for nuclear import. C) Nuclear Pore Complex (NPC) uncoating capsid remains intact and is remodeled at NPCs to allow docking of the structure (21).

must occur prior to reaching nuclear pore complexes. Close association of microtubule stability and transport may play an additional role in regulating uncoating during cytoplasmic transit. Depolymerization of microtubules has been found to correlate with delays in uncoating kinetics. This mechanism is believed to be mapped to dynein and kinesin motors as specific targeting of either motor protein delays uncoating (41, 42).

The nuclear pore model of uncoating describes uncoating as occurring in association with the nuclear pore complexes (NPCs). This third model is described below with a general overview of nuclear import. The predominant models in the field are currently the cytoplasmic uncoating and NPC based models. While disagreement between the models exists, the possibility that partial capsid hexamers remain associated with the core following uncoating can accommodate both models.

Nuclear Import

To establish infection the pre-integration complex (PIC) consisting of integrase, viral dsDNA, and a myriad of accessory proteins must transit through nuclear pore complexes (NPC) into the nucleus. An exact model of nuclear import has yet to be defined as a variety of host proteins have been linked to this event. Deviation between cell lines further complicates the establishment of a clear mechanism of import. However, nucleophilic proteins that are a part of the PIC offer a starting point for understanding nuclear import. The ability to infect nondividing cells has been linked to an NLS apart of the viral integrase (IN). Loss of the identified motif inhibits nuclear accumulation of the PIC but is not tied to IN enzymatic function demonstrating the requirement of this motif for nuclear import (43). An additional component implicated in the import process is the DNA flap overhang generated during reverse transcription. This DNA flap

is a result of central initiation of reverse transcription at the central poly purine tract (cPPT). Mutations that remove this cPPT region result in strictly linear DNA accumulating near NPCs with faulty nuclear import (26).

Despite these necessary viral components for import a range of host proteins are also required to facilitate passage into the nucleus. Cleavage Polyadenylation Specificity Factor 6 (CPSF6), a cleavage factor for pre-mRNA processing, has been shown to interact directly with CA (44). Initial models of this interaction propose CPSF6 may assist in NPC translocation through binding CA associated with the nuclear basket (45). CPSF6-358, a truncated variant lacking the NLS, was found to accumulate in the cytoplasm and inhibit replication (44, 46). This mechanism has now been linked to nuclear import of CPSF6 dependent on the beta-karyopherin, TNPO3. Knockdown of TNPO3 has been shown to block infectivity, though this effect is now seen as indirect. Without TNPO3 CPSF6 accumulates in the cytoplasm. Binding of CPSF6 to the capsid lattice then prevents nuclear import. Restriction is abolished under TNPO3 KD when CPSF6 is expressed with an alternative NLS (46). Nuclear CPSF6 has more recently been shown to localize closely with Nup153 with both proteins capable of interacting with CA.

While PIC transit of NPCs has been viewed as separate from uncoating some speculate that uncoating of competent viral particles extends to interaction with NPCs. This model includes a docking event at NPCs (Figure 5) (47). Docking may require remodeling of capsid to meet the size requirements of NPC transport able to accommodate structure up to 39 nm (48). Intact capsid size at the smallest is 61-nm in width (47). Particle tracking of capsid associated RTCs were found to have increased residence time at the nuclear envelope (49). Capsid residence at NPCs suggests docking of capsids may occur, though size constraints are still not explained. Knockdown of Nup358, a cytoplasmic nucleoporin, abolishes both residence time and nuclear

import success (49, 50) . Further complicating the role of NUP358 in uncoating and import is the C-terminal cyclophilin homology domain capable of binding CA monomers (51, 52). Investigation of truncated variants of Nup358 lacking this homology domain show an independent role in HIV infection, but the possible interaction is still relevant (53). Additionally, Nup153, localized to the nuclear basket of NPCs, has been shown to be capable of CA binding further arguing that capsid interaction at NPCs is possible (54).

Interplay Between Early Replication Steps

Early models of HIV replication steps were predominantly represented as sequential unconnected events (Figure 2). As methods for studying each event have improved, viewing replication steps as individual events is no longer sufficient. Mounting evidence of interplay between uncoating, reverse transcription, and nuclear import has resulted in reevaluation of the HIV replication cycle. Early work based on the rapid disassembly model of uncoating defines disassembly as preceding initiation of reverse transcription. However, improved methods in studying uncoating support a direct correlation of reverse transcription kinetics and uncoating kinetics. Inhibition of reverse transcription by nevirapine, a non-nucleoside reverse transcriptase inhibitor, results in delayed uncoating kinetics demonstrating direct interplay (39). Further analysis of early reverse transcription has narrowed down the suspected uncoating initiator to the first strand transfer and elongation of cDNA (55). The role of reverse transcription in initiating disassembly of capsid highlights the cooperation of closely regulated events. Discovery of a novel CA pore structure in 2016 implicates intact capsid in benefitting reverse transcription (Figure 6). Successful reverse transcription of viral RNA to cDNA relies on availability to host deoxynucleotide triphosphates (dNTPs). Under the rapid disassembly uncoating model, reverse

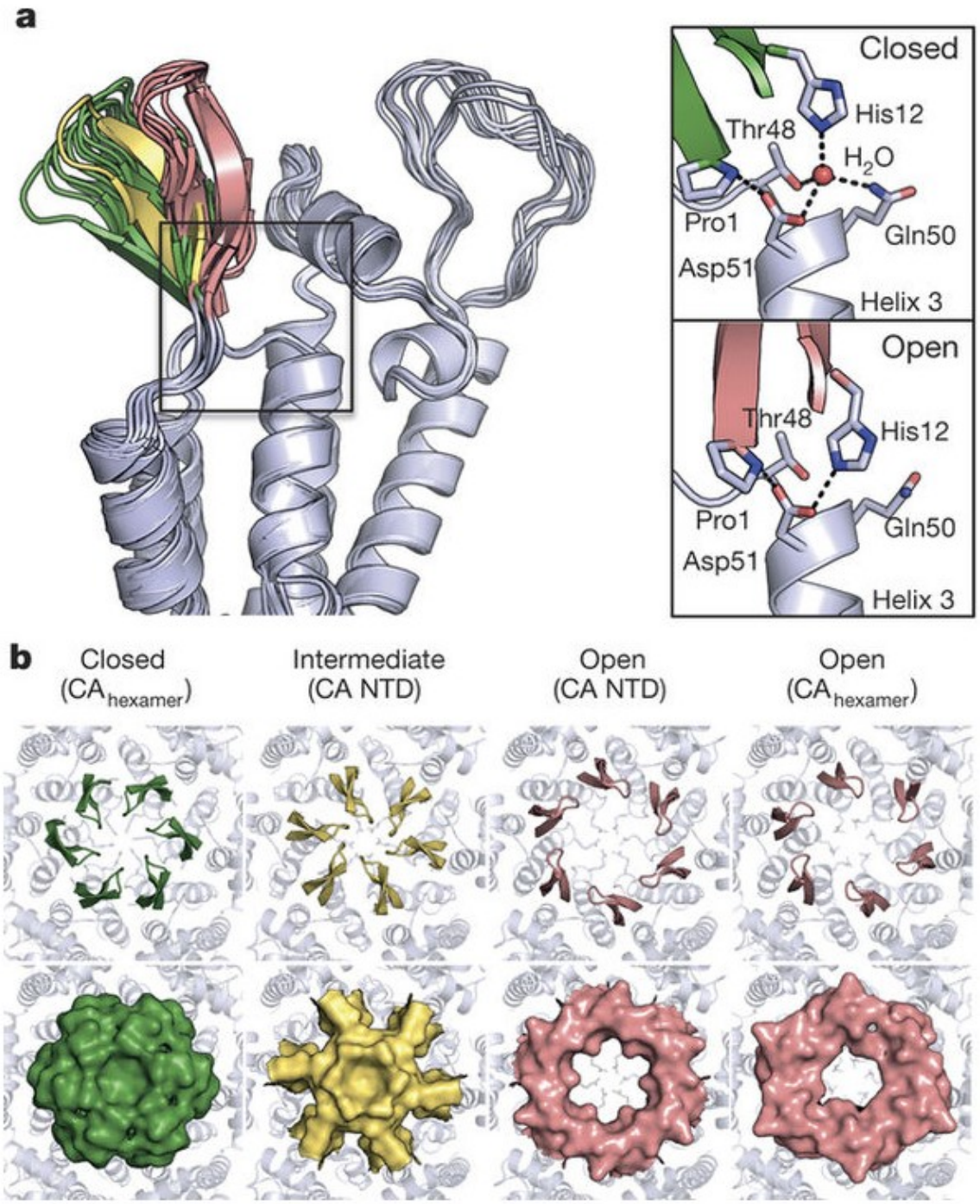

Figure 6. Modeling of H12 Hydrogen Bond Network Facilitating Capsid Pore Conformational Change. A) H12 apart of a β-hairpin structure facilitates a hydrogen bond network determining structural conformational. B) Modeling of the N-terminal domain pore in open, closed, and intermediate conformations (56).

transcriptase is free of a capsid structure allowing nucleotide incorporation. However, rapid uncoating kinetics are now known to correlate with decreased infectivity and are likely attributed to cytosolic sensor detection of viral nucleic acids in the cytoplasm (31). As the field moves further from the obsolete rapid disassembly model of uncoating dNTP incorporation must be explained in the presence of intact capsid. Functional analysis of histidine 12 (H12), present within a β-hairpin structure, revealed conformational changes resulting in a "molecular iris" dependent on the protonation state of the H12 imidazole side chain. H12 protonation has now been mapped to a novel pore structure on CA monomers. Histidine protonation results in an open pore conformation allowing size selective passage of dNTPs for reverse transcription. Size restraints of the pore structure prevent cytosolic sensor access to internal components, while allowing the recruitment of dNTPs. A positively charged internal ring of six arginine residues facilitates this process (56).

Hypothesized interactions of capsid structure at NPCs may tie uncoating and nuclear import together under the NPC docking model of uncoating. While NUP358 knockdown attenuates infectivity demonstrating necessity of this NPC; NUP358 knockdown in HeLa cells has been shown to alter integration sites. Specific capsid mutants G89V and P90A were shown to maintain infectivity in absence of NUP358 and integrate in areas of higher transcription density suggesting capsid structure may determine import and integration pathways. Alternatively, capsid mutant N74D and N75A were found to be less sensitive to NPC knockdown with an integration preference for lower transcription density areas (57). Altered integration sites and decreased infectivity are also observed with knockdown of the nuclear sided NUP153 (58).

Cyclophilin A in HIV-1 Replication

HIV encodes for 15 viral proteins responsible for maintaining structure, evading host defenses, and establishing infection. Due to this limited number of proteins to facilitate infection, viruses have coevolved alongside their host allowing for the use of host proteins to enhance replication. Therefore, interaction of HIV with host proteins represents an important area of study in understanding replication. One of the earliest host proteins identified to interact with HIV is the immunophilin cyclophilin A, an 18 kDa protein consisting of 165 amino acids found highly expressed and localized in the cytoplasm (59, 60) . Cyclophilin A (CypA) belongs to the immunophilin family of proteins consisting of cyclophilins, FK506 binding proteins, and parvulins. Immunophilins are characterized as peptidyl prolyl isomerases responsible for isomerizing proline residues between cis-trans conformations, as well as possessing a high affinity for specific immunosuppressive drugs. Cyclophilins are found highly conserved across mammals, bacteria, and plants with peptidyl prolyl isomerase activity (PPIase) activity and high binding affinity for cyclosporine A (CsA). Seven main cyclophilins are found in humans with varying localization to different organelles including the endoplasmic reticulum, mitochondria, nucleus, and the cytoplasm (59, 61, 62).

A hydrophobic binding pocket internalized within an eight-strand β barrel facilitates the CypA isomerase activity. Catalytic activity is primarily dependent upon nine residues making up the active site (60). The importance of PPIase activity encompasses protein folding as well as sustained complex formation in signaling pathways. Exposed proline residues apart of tertiary protein structure act as key substrates for CypA isomerization. In absence of PPIase activity isomerization of proline residues proceeds catalytically slow, highlighting the necessity of CypA. In this regard CypA acts as a protein chaperone facilitating isomerization from the unstable cis

confirmation to the relatively stable trans isomer (5). Binding of target proline substrates can also result in sustained complex formation beyond transient interaction for signal transduction. Early work in the 1990s studying CypA and HIV led to identification of CypA packaging into budding immature virions during assembly (63, 64) . CypA incorporation is dependent on proline rich regions of uncleaved HIV gag polyprotein P222. Simian Immunodefiency Virus (SIV) is a lentivirus closely related to HIV that is unable to incorporate CypA. However, upon generating chimeric SIV with proline rich Gag from HIV CypA become packaged into new virions (63). Much of the early work studying CypA in HIV infection has been centered on the incorporation from producer cells and was viewed as necessary for successful infection. However, contradictory data published in 2004 has compromised this model of CypA function in infection (65). Relevance of CypA in HIV infection has shifted within the field from incorporation during assembly to CypA interaction with the capsid prior to uncoating.

Intact capsid cores post-fusion have been known to interact with CypA since 1996, though the importance of CypA binding in infection is still not completely understood (Figure 7) (3). HIV-1 CA monomers contain a flexible proline loop termed the Cyclophilin A Binding Loop (66). This flexible CypA binding structure is centered on six main residues: H87, A88, G89, P90, I91, and A92. Mutation of CypA binding loop residues drastically reduces CypA association or fully abolishes binding (3). Additionally, distal residues away from the loop have been shown to alter CypA impact on infection (67). Within the CypA binding loop the P90 residue acts as the CypA substrate while G89 maintains loop flexibility (66). P90 residues in trans conformation, as opposed to cis, are predominantly found in the presence of CypA validating predicted peptidyl prolyl isomerase activity (4). Capsid mutants G89A and P90A establish the importance of the G89 and P90 residues as these mutants are unable to bind CypA.

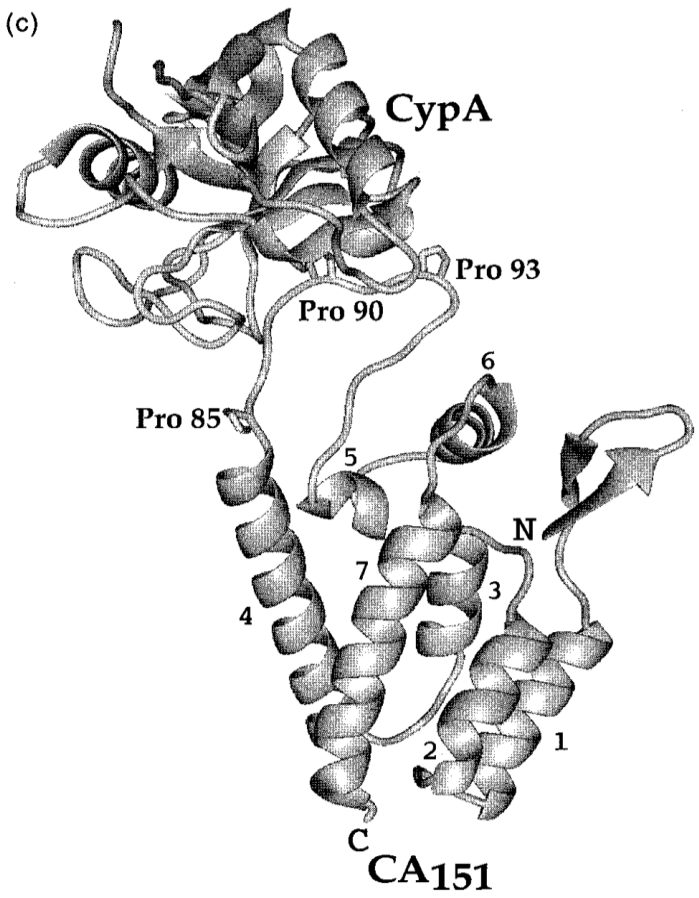

Figure 7. Cyclophilin A Binds P90 within the Cyclophilin A Binding Loop. HAGPIA residues apart of the partially ordered loop of CA monomers acts as the key substrate for cyclophilin A binding (68).

Though structurally similar, lentiviruses HIV-2 and SIV lack the required residues needed to naturally bind CypA. Early work in confirming the CypA binding loop function led to the generation of chimeric SIV capsid, which can bind CypA indicating functional conservation of this structural region (66).

Cyclosporine A (CsA) binds with high affinity directly within a hydrophobic binding pockets characteristic of cyclophilins. CsA-cyclophilin complex formation is thermodynamically favorable resulting in competitive binding of CypA. Presence of CsA results in saturation of unbound CypA as well as disruption of current CypA binding interactions. As a result of the high affinity CsA treatment is used a tool to pharmacological disrupt CypA binding. Complexing with CsA facilitates an immunosuppressive role of CypA through direct inhibition of Calcineurin. Calcineurin, a calmodulin and calcium dependent serine-threonine phosphatase, is required for removal of target phosphate groups on nuclear factor of activated T cells (NFAT). CsA-CypA inhibits the NFAT signaling pathway through complexing with calcineurin blocking the catalytic subunit and ultimately preventing T cell activation (69, 70). The binding pocket on CypA and the catalytic activity are closely associated as mutations to CypA that drastically reduce CsA affinity alter PPIase function to a similar degree (71, 72). This high binding affinity of CsA to CypA is often used when studying CypA as treatment of cells with CsA containing media allows for saturation of CypA as well as disruption of any CypA in complex with other proteins.

Generalizing the importance of this association of CypA-CA has been difficult as the CypA role in infectivity varies between cell lines, obscuring the establishment of a clear mechanism. CypA-CA interaction in infection of CD4+ T cells, macrophages, and dendritic cells has been demonstrated in enhancing infection. Disruption of the CypA interaction through knockdown or CsA treatment lowers HIV-1 infectivity in these cell lines (2, 73). Infection of

HeLa cells contrasts with primary monocyte derived macrophages and T cell lines as infection is independent of CypA (57, 73). Identification of a mechanism of CypA modulated infectivity must account for specific altered replication events. Extensive work has been focused on the significance of CypA during early replication steps due to the CypA and capsid interaction. The early replication steps of interest include reverse transcription, uncoating, and nuclear import as these steps align with CypA interaction. Research characterizing CypA modulation of infectivity has shown a correlation of CypA with the completion of reverse transcription across a wide range of cell lines. Primarily, the absence of CypA binding through CsA interference correlates to a decrease in late reverse transcription products (73). How the CypA-CA interaction relates to reverse transcription is still unclear.

Cofactor interaction with capsid also raises questions as to the stabilization effects contributing to altered uncoating kinetics. CypA activity is known to isomerize G89-P90, but the implications of this structural modification, if any, is still not known (4). Cryo-electron microscopy data has identified CypA may bridge adjacent CA monomers through a noncanonical binding site. Structural simulations indicate this novel secondary binding site comparatively has reduced binding interaction, though may facilitate capsid stabilization through increased binding avidity (74). However, functional analysis of the proposed secondary binding site was unable to show alterations in binding affinity. The contradictory finding has raised concerns that the novel binding site was misidentified (75). Regardless, the loss of CypA binding has been shown to correlate with faster cytoplasmic uncoating and reduced CA upon reaching the NPC (49). Alterations to uncoating kinetics may suggest CypA influences uncoating kinetics. As the development of cell-based assays for studying uncoating kinetics improve this potential effect of CypA in stabilization will likely see more focus.

Transport of the PIC across the nuclear envelope has been predominantly mapped to Nup358 (RanBp2), a large nucleoporin. Nup358 consists of four Ran-binding domains, an alpha helical region, eight zinc finger regions, a SUMO E3 domain, and a cyclophilin homology domain at the C-terminus (51). Nup358's cyclophilin homology domain has been demonstrated to bind capsid while possessing comparatively weak PPIase activity to CypA. Protein homology of the Nup358 Cyp homology domain to CypA structurally can bind the CypA binding loop. In contrast to CypA however, Nup358 modelled steric clashes demonstrate Nup358 is unable to bind CsA due to a recessed hydrophobic binding pocket making it insensitive to CsA treatment (52). Knockdown of Nup358 results in decreased infectivity without altering late reverse transcription products. Nuclear import regarding Nup358 is further complicated by infection with the P90A capsid mutants that maintains infectivity in Nup358's absence. A similar phenotype is observed in wild type virus upon CsA treatment suggesting CypA binding may play a role in nuclear import pathways. Alteration of nuclear import without CypA binding in HeLa cells extends further to integration targeting in areas of higher transcription activity (57).

Post-fusion HIV must undergo transit towards the nucleus, reverse transcribe RNA to DNA, uncoat the capsid structure, and passage through nuclear pore complexes. The capsid structure represents a key point of contact for HIV to utilize host proteins to modulate infectivity. These host-protein interactions as a result can potentially alter the rate of reverse transcription, kinetics of capsid uncoating, and nuclear import success. Despite decades of research into the CypA-CA interaction, a clear mechanism has not been established for infectivity modulation. As HIV research shifts focus to host protein interactions, the mechanism of CypA enhancement on infectivity represents a major area of study. Research into host factor interactions during early replication events provide insight into potential targets for drug development. As models of early

replication favor an interdependent explanation of reverse transcription, uncoating, and nuclear import CypA mediated enhancement of infectivity may also span multiple steps.

Cyclophilin A in HIV-1 Infectivity in the CHME3 Cell Line

Cyclophilin A has been previously been shown to enhance HIV replication in a cell type dependent manner (73). The variable nature of CypA in HIV replication is commonly observed as having an enhancing effect on early replication or no observable change. While T cell and macrophage-based cell lines have seen extensive investigation of this host-factor interaction the role of CypA in microglial cell infection has not been established. To determine if CypA alters HIV infectivity in microglial cells the CHME3 human microglial cell line was used to carry out a CsA Addition Assay. Cyclosporin A (CsA) is an immunosuppressive drug that binds the hydrophobic pocket on CypA required to bind HIV CA (3, 69). The addition of CsA containing media across a time course allows for controlled disruption of CypA binding. Endpoint infectivity can then be quantified using the GFP reporter gene which is a part of the HIV GFP genome. Successful integration of the viral genome leads to expression of GFP allowing a direct correlation between GFP and success of early replication steps. Any effect of CypA interaction on infection is then represented by differences in percent GFP positive cells relative to the vehicle ethanol control. Synchronized infection was carried out with addition of either CsA or ethanol containing media at 0, 0.25, 0.50, 0.75, 1, 2, 3, 4, and 5 hours post-infection. Percent GFP positive cells quantified by flow cytometry indicated a decrease in infectivity when CsA was included at early time points (Figure 8). The observed decrease in infectivity implicates CypA in enhancing reverse transcription, uncoating, or nuclear import during the first 5 hours of infection. Due to the cytoplasmic localization of CypA it is unlikely that HIV-1 binding, fusion,

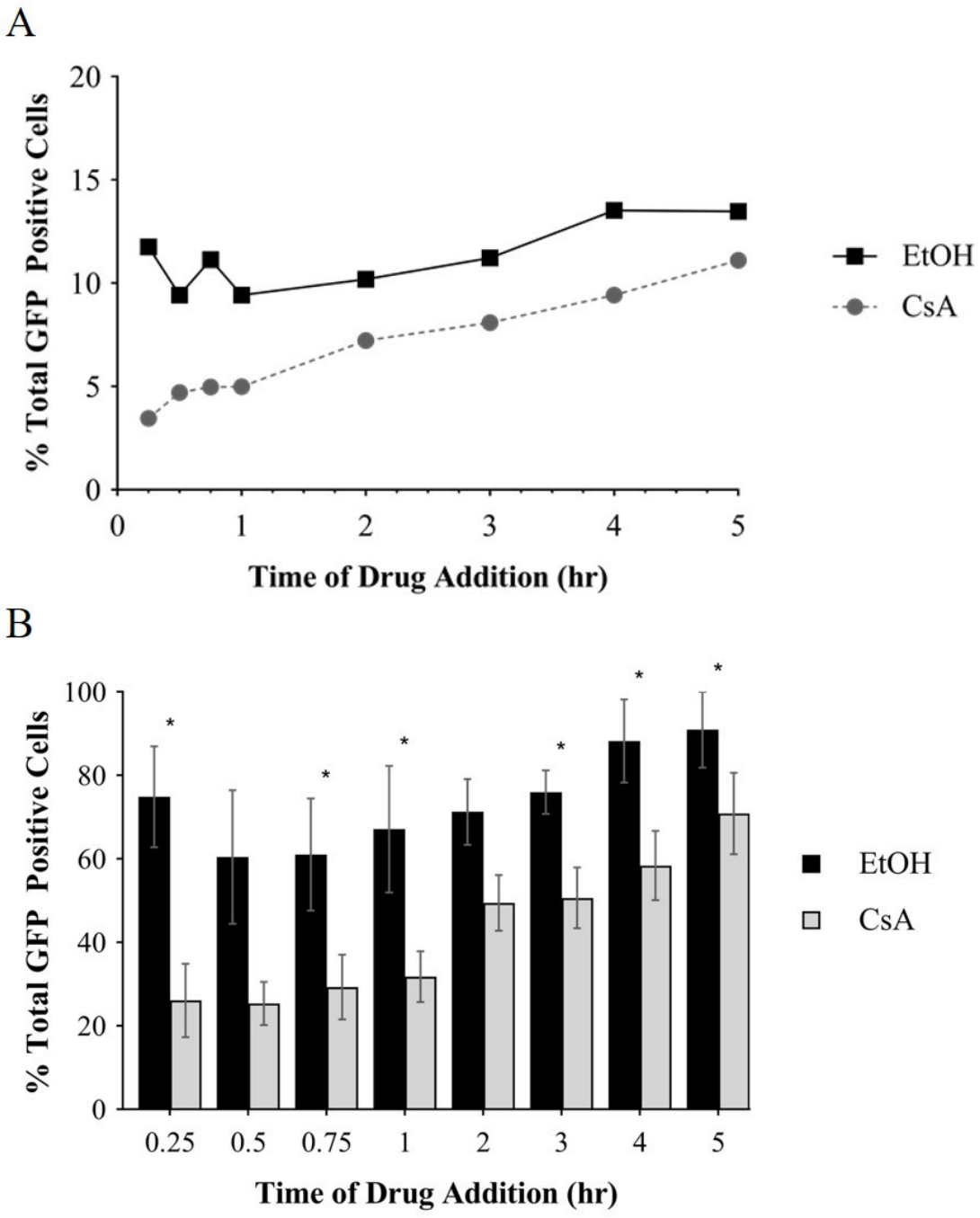

Figure 8. CsA Addition Assay in CHME3 Cells. Infection of CHME3 cells was carried out in triplicate with addition of CsA or ethanol containing media at each timepoint. A) A representative run of an individual CsA addition experiment without normalizing to a constant infection condition. B) Results of the CsA Addition Assay normalized to a constant infection condition. Data from three independent experiments were averaged and used to calculate percentage of GFP and SEM. Statistical significance was determined by a Student's T-Test. *, $P < 0.05$. Error bars represent ±SEM

and integration are altered.

Hypothesis and Aims

Initial work in the CHME3 cell line indicates that CypA enhancement of HIV-1 infectivity occurs at time points associated with early replication steps (Figure 8). CypA is unable to interact with the capsid pre-fusion and direct effects post-nuclear import are unlikely due to cytoplasmic localization of CypA. Relevant replication steps then include reverse transcription, uncoating, and nuclear import. Due to the overlapping nature of the early events, multiple steps may encompass CypA mediated enhancement.

While some data show the effects of CypA correlate with a decrease of RT products it is currently thought that reverse transcription proceeds mainly by viral machinery (73). The lack of CypA interaction with the RTC may suggest an indirect effect stemming from altered uncoating kinetics. At the onset of this research it was hypothesized that uncoating would directly be impacted by CypA binding and not RT due to literature indicating a potential stabilizing role (33, 75). It was also anticipated that nuclear import would see a decline without CypA binding as loss of binding alters import pathways (57). However, any effect on nuclear import may also represent a downstream effect due to changes to reverse transcription and uncoating. Therefore, to address each replication event corresponding experiments were carried out. The effect of CypA on reverse transcription and nuclear import were characterized through qPCR analysis. To assess any alterations in uncoating caused by CypA the In Situ Uncoating Assay was utilized to track relative CA signal over time.

MATERIALS AND METHODS

Cell Lines and Pharmaceuticals

Institutional Review Board approval was not required for the use of human cell lines in this research. The CHME3 microglial cell line was provided by the Naghavi lab at Northwestern University (76). CHME3 cells were cultured in 100 x 20 mm Falcon culture dishes (Corning) with 1X DMEM (Corning), 1X Penicillin Streptomycin L-Glutamine (Corning), 10% FBS, and 0.91 mM Sodium Pyruvate (Corning™). The 293T HEK cell line was received from Northwestern University from the Hope Lab. 293T HEK cells were cultured in 1X DMEM with 100 U/ml penicillin, 100 U/ml streptomycin, and 292 μg/ml L-glutamine (PSG). Both cell lines were maintained at 37°C with 5% CO2. All human cell lines were handled within a laminar flow hood and split once 80% confluence was reached.

CHME3 cells were split by washing cells with 1X PBS. Cells were placed in the incubator with 3 ml of trypsin for several minutes to detach cells. Addition of 7 ml of CHME3 media to the plate inactivated trypsin activity. Gentle washing of the plate ensured cell detachment before transferring cell solution to a new plate. 293T HEK cells were split by aspirating media and adding 1 ml of trypsin. Following a trypsin wash the plate was aspirated and placed at 37°C for 2-3 minutes. Once cells were visibly detached 10 ml of media was added to inactivate the trypsin and resuspend the cells. 1 ml of detached 293T cells were transferred into 10 ml of media and stored at 37°C.

Cyclosporine A (CsA) was made up in ethanol with a working concentration of 2.5 μM and stored at -20°C. Nevirapine (NVP) was prepared in DMSO with a final concentration of 5 μM and stored at -20°C. Polybrene solution was used at a final concentration of 10 μg/mL at

kept at -20°C. Polyethyleneimine (PEI) was stored in aliquots in ddH_2O at 4°C and used at 1 mg/mL. DEAE Dextran was prepared in water, stored at 4°C, and used at 10 µg/mL.

Virus Production

To safely utilize HIV for research purposes within a BSL2 facility single round replication incompetent virus was produced and used throughout all experiments. An HIV-GFP reporter virus with a frame shift mutation to the envelope gene prevents further replication of the virus. To allow for a single use virus envelope protein the vesicular stomatitis virus glycoprotein (VSV-G) is included as a second plasmid during transfection and harvesting of HIV. Vesicular stomatitis virus glycoprotein (VSV-G) pseudotyped HIV-GFP reporter virus was produced through transfection of 293T HEK cells at 80-90% confluence with polyethylenimine (PEI). 6 µg of HIV-GFP and 4 µg of Cytomegalovirus VSV-G plasmid were aliquoted into a transfection mix with 40 µL of PEI and 1 ml 1X DMEM. The solution was incubated at room temperature for 15 minutes before adding dropwise directly onto the tissue culture plate. Plates were incubated at 37°C for 24 hours before replacing the transfection media with the standard 293T media. Further incubation was carried out for 16-18 hours prior to harvesting virus. Culture media was transferred into a 20 mL Luer-Lok Tip syringe (BD) with a 0.45 µm syringe filter (Millex-HV). Filtered solution containing virus was aliquoted into cryovials and stored at -80°C.

Viral Titration

Viral titers were carried out in 293T HEK cells by plating out cells at 10,000 cells/well onto a 96 well plate. On the day of infection media was replaced with polybrene containing media. Virus was added and serial diluted for: 1:2, 1:4, 1:8, 1:16, 1:32, 1:64, 1:128, and 1:256

viral dilutions. A previously assayed stock of virus was used as a positive control. Negative control included a minimum of three wells with only polybrene containing media. Plates were centrifuged at 1,200 x g at 16°C using a ThermoFisher Scientific Sorvall Legend X1R centrifuge for 1 hour with media replacement post-spinoculation and incubated overnight. 24 hours post-infection media was changed. Cells were fixed 48 hours post-infection with trypsin and 2% paraformaldehyde in PBS. Fixed plates stored at 4°C until analysis of %GFP positive cells by flow cytometry.

Flow Cytometry

Percentage of GFP positive cells were quantified using a BD Accuri C6 Flow Cytometer and BD CSampler™ Software. Analysis of resuspended cell samples were run on the fast fluidics setting with run limits of 10,000 events or 80 µL. FSC-H threshold was set to 100,000. Cell background was removed by setting the GFP gate minimum to the non-infected cell background average. Flow cytometry data was analyzed in Microsoft Excel.

Plasmid Purification

Transformation of HB101 *Escherichia coli.* *E.coli* cryopreserved at -80°C in glycerol were slowly thawed on ice. *E.coli* was aliquoted at 66 µL into individual test tubes. Cultures to be transformed with the 2-LTR plasmid received 0.07 ug of plasmid DNA. *E.coli* to be transformed with the Hu β-Actin plasmid received 244 µg of DNA. Following a 10-minute incubation on ice following plasmid addition the test tubes were heat shocked by placing the tubes in a 42°C water bath for 50 seconds. The bacteria were placed back on ice for 2 minutes. Cultures received 1 mL of LB before being allowed to recover post-heat shock by incubating for

60 minutes at 37°C with shaking (220 rpm). 100 µL of the cultures were plated onto Ampicillin agar plates and incubated at 37°C overnight. Individual colonies were selected from the transformed *E. coli* and added to a LB culture containing Ampicillin (1 mg/mL) and incubated overnight at 37°C with shaking.

Qiagen plasmid MaxiPrep. Transformed bacterial cultures were grown in 100 µg/µL Ampicillin LB overnight at 37°C and 220 RPM. Cultures were used following the Qiagen Plasmid MaxiPrep protocol to extract plasmid DNA.

Confirmation of 2-LTR and human β-Actin plasmids. Plasmid extract were quantified using a ThermoScientific nanophotometer with acceptable A260/A280 ranges of 1.8 to 2.0. Agarose gel electrophoresis was carried out on a 1% agarose gel including ethidium bromide with a 1 kilobase NEB quick-load purple DNA ladder. 2 µL of each plasmid was added to a loading mix of 20 µL including 1X loading dye. Samples were loaded onto the gel and run at 120V for 45 minutes with 1X TAE running buffer. DNA samples were imaged with UV and product size was determined using the DNA ladder to confirm 2-LTR and Hu β-Actin Plasmids.

Cyclosporine A (CsA) Addition Assay

The CsA Addition Assay was utilized to determine what possible effect CypA may have on HIV-1 infection of the CHME3 microglial cell line. Cells were plated out at 6,000 cells/well in triplicate on 96-well plates. On the following day after plating cells were infected with HIV-GFP in 10 µg/mL polybrene and spinoculated at 1,200 x g, 16^{o}C for 1 hour. Addition of warm replacement media-initiated fusion of the virus and beginning the time course. At 0, 0.25, 0.5, 0.75, 1, 2, 3, 4, and 5 hours post-infection media was aspirated and replaced with CsA or EtOH containing media. 24 hours post-infection media was replaced with new drug containing media.

Infection was allowed for 48 hours before harvesting all wells at 48 hours post-infection with trypsin and 2% Paraformaldehyde in PBS. Harvested cells were stored in parafilm wrapped 96-well plates at 4°C until % GFP positive cells were quantified through Flow Cytometry. A student T-test was carried out in Microsoft Excel between CsA and ethanol treatment at each timepoint. Statistical significance was determined based on a P value below 0.05.

Nevirapine (NVP) Addition Assay

CHME3 cells were plated out at 6,000 cells/well in a 96-well plate with 100 uL per well in triplicate. Following an overnight incubation at 37°, the cells were infected with HIV-GFP in either CsA or EtOH containing media with 10 ug/mL polybrene. The plate was spinoculated for 1 hour at 1,200 x g, 16^{o}C to synchronize infection. After removal from the centrifuge the wells were aspirated and received 100 ul of warm replacement media containing either CsA or ethanol. Addition of the replacement media initiated the time course for 0, 1, 2, 3, 4, 6, and 8-hour conditions. Control conditions included virus in constant NVP and virus with no drug addition. At the respective time point for each set of wells media was replaced with NVP containing media while maintaining the corresponding drug. The plate was left to incubate overnight at 37^{o}C before replacing the media 24 hours post-infection. 48 hours post-infection the cells were harvested by washing in trypsin and fixing with 2% paraformaldehyde in PBS. The plate was sealed with Parafilm and stored overnight at 4^{o}C. Flow cytometry was used to quantify % GFP positive cells. A student T-test was carried out in Microsoft Excel between CsA and ethanol conditions for each timepoint. Statistical significance was determined based on a P value below 0.05.

Quantitative Polymerase Chain Reaction (qPCR)

qPCR primer efficiency and optimization. To determine primer efficiency a serial dilution of β-actin, HIV-GFP, and 2-LTR plasmids were carried out. Plasmids were prepared into five standards each with the highest concentration at 2.5 ng/µL. Samples were loaded in triplicate onto PCR tube strips (Bio-Rad) at 5 ul so that all reactions did not exceed 12.5 ng of plasmid DNA per reaction. Primers were included at 5 µM in 10 µl of SsoFast EvaGreen supermix (Bio-Rad). Ambion Nuclease-Free Water (ThermoFischer Scientific) was added to bring the total reaction volume to 20 µl. PCR tubes were sealed with the corresponding Optical Strips (Bio-Rad) and briefly centrifuged down prior to being placed into the thermocycler. qPCR was carried out using CFX Connect Thermal Cycler 96FX2 (Bio-Rad 1855201) with the Bio-Rad CFX Manager 3.1 software. The primer efficiency program was carried out with an initial denaturation at 95°C for 30 seconds followed by a 5 second 95°C step before annealing for 5 seconds at 60°C. SYBR fluorescence levels were assessed following the annealing step before repeating this cycle 44 times. Once 44 cycles had been completed a melt curve analysis was carried out with a 65°C step for 5 seconds and a 95°C denaturation step for 50 seconds with continuous quantification of SYBR fluorescence. Primer efficiency was calculated by plotting Cycle quantification (Cq) values from the 5-point standard. The slope for each primer set was then used to calculate primer efficiency (Figure 9).

Optimal annealing temperatures were assessed for Early RT and 2-LTR primers by carrying out an annealing gradient at 57.7°C, 60.6°C, 63.0°C, 64.3°C, and 65.0°C for 5 seconds. All other steps of the program are as previously described. DNA products were then run on a 1% agarose gel for electrophoresis. Imaging of DNA products by UV was carried out to confirm expected DNA products without contaminants.

Infection of cells and sample preparation for qPCR analysis. CHME3 Cells were plated out at 100,000 cells/well in 24-well plates. Following overnight incubation at 37°C cells were infected with HIV-GFP with 10 ug/mL polybrene in either CsA or ethanol containing media by spinoculation for 1 hour at 1,200 x g, 16°C to allow binding of HIV, but prevent fusion. Post-spinoculation the media was aspirated and replaced with warm CsA or ethanol containing media to initiate synchronized fusion. The time course is started with plates kept at 37°C. Time points for assessing early RT products included 0, 1, 2, 4, and 12 hours post-infection. Quantification of 2-LTR circles was carried out with conditions for 0, 6, 12, and 24 hours post-infection. At each time point respective wells were harvested with trypsin by washing the well plates before adding equal amounts of media and transferring to Eppendorf tubes. Control conditions included uninfected cells and infected cells under constant NVP treatment. Control conditions were harvested at 24 hours post-infection. Harvested samples were centrifuged to produce a cell pellet at 300 x g. Remaining solution was carefully aspirated off while not disturbing the cell pellet. Isolated cell pellets were then stored overnight at –20 °C. Genomic DNA extraction of CHME3 cell pellets were carried out using Qiagen DNeasy Blood & Tissue Kits with DNeasy Mini Spin Column Kit. Standard protocol followed throughout DNA extraction except for a 100 µL elution step. DNA samples quantified with Thermo Scientific NanoDrop™ 2000 Spectrophotometers (ND-2000) and the associated software with an acceptable purity range of 1.7-2.0 for the A260/A280 ratio.

A DpnI restriction enzyme (NEB) digest was carried out to remove any carry over HIV-GFP plasmid that may have been contaminating the sample. Digest of extracted genomic DNA were carried out in 100 uL reactions using 78 uL of DNA with 2 uL DpnI (400 U/mL) in 1X

CutSmart® Buffer (NEB) and Nuclease-Free Water (Ambion) for 4 hours in a water bath at 37°C. Samples were stored at 4 °C overnight prior to use for qPCR.

qPCR analysis. β-Actin, Early RT, and 2-LTR primer sets were prepared for a final concentration of 5 µM for 20 µl PCR reactions (Table 1). 2X SsoFast EvaGreen supermix was included with Nuclease-Free Water constituting the remaining volume up to a volume of 15 µl per reaction. 15 µl of the qPCR mastermix was loaded into each PCR tube. Digested genomic samples were then added at 5 µl and not exceeding 50 ng of DNA per reaction bringing the final volume to 20 µl. Each sample was loaded in triplicate as technical replicates. Samples were heated initially for 30 seconds at 95.0 °C. Denaturation was carried out for 5 seconds at 95.0 °C followed by a 5 second at 60.0 °C. SYBR signal from each reaction was quantified following the last step of the cycle. The program proceeded through 44 cycles before completion. Reactions ended with a melt curve analysis through 5 seconds at 65.0°C and 95.0 °C. Data analysis was carried out using the Pfaffl method to determine relative fold change between CsA and ethanol treated conditions. Previously determined primer efficiencies were used during fold change calculations. Statistical significance was determined by a student T-test between CsA and ethanol for each timepoint. Additionally, fold change relative to the 0-hour post-infection in CsA or ethanol was quantified to calculate increase in DNA products over the time course as an additional amplification check. Statistical significance was calculated using a Mixed ANOVA followed by a post-hoc t-test with Bonferroni correction. Following qPCR DNA samples were stored at -20°C for long term storage.

qPCR troubleshooting assay. CHME3 cells were plated out onto 24-well plates following the previously described qPCR protocol with the inclusion of duplicate wells for each condition. One well per reaction followed the qPCR 2-LTR protocol while the duplicate received

A. $\text{Primer Efficiency (E)} = 10^{(-1/\text{Slope})} - 1$

B. $$\text{Relative Expression Ratio} = \frac{(E_{\text{Target}})^{\Delta Cq(\text{control-experimental})}}{(E_{\text{Housekeeping}})^{\Delta Cq(\text{control-experimental})}}$$

Figure 9. Primer Efficiency and Relative Fold Change Equation. A) Primer efficiency equation using the slope of the primer standard curve. B) Relative fold change equation using primer efficiencies and Cq values.

Table 1. qPCR Primer Sequences

Primer Target	Primer Sequence (5' to 3')
β-Actin	Forward: TCACCCACACTGTGCCCATCTATG
	Reverse: CAGCGGAACCGCTCGTTGCCAATGG
Early RT	Forward: GCTAACTAGGGAACCCACTGCTT
	Reverse: ACAACAGACGGGCACACACTAC
2-LTR	Forward: AACTAGGGAACCCACTGCTTAAG
Circles	Reverse: TCCACAGATCAAGGATATCTTGTC

NVP containing media at the respective time point and was not harvested. At 24 hours post-infection media was changed. At 48 hours post-infection wells that received NVP containing media were harvested via trypsin and 2% paraformaldehyde in PBS. Samples transferred to Eppendorf tubes and stored at 4°C before analysis via flow cytometry to determine % GFP positive cells. Comparison of analyzed qPCR data and flow cytometry data was carried out to determine if infection was successful.

Agarose gel electrophoresis. Agarose gel electrophoresis was carried out with a 1% gel containing ethidium bromide. 15 ul of PCR samples were loaded into each well. Current was passed through the rig at 120 V for 45-60 minutes before UV imaging with a Kodak Gel Logic 200 Imaging System with the Kodak Molecular Imaging Software.

In Situ Uncoating Assay

In situ uncoating assay protocol. Glass coverslips stored in 70% ethanol were transferred to individual wells on a 24-well plate and treated for 15 minutes with 500 ul of EmbryoMax 0.1% Gelatin in ultrapure water for cell adherence. CHME3 cells were plated onto glass coverslips in 24 well plates at 120,000 cells per well and incubated overnight. Dual-labelled virus with HIV-GFP and S15-mTomato were used to infect the plated cells at a 1/10 dilution with 1X DEAE Dextran. Cells were spinoculated for 1 hour at 1,200 x g, 16°C. Post-spinoculation all wells were aspirated to remove unbound virus. The time course was begun with warm replacement media for time points at 0, 1, 2, and 4 hours. At the respective time points coverslips were fixed with 4% paraformaldehyde in PBS for 15 minutes before washing with 1X PBS. Plates were stored overnight in 1X PBS at 4°C. Coverslips were then permeabilized with 0.05% Triton X in PBS for 15 minutes followed by a 40-minute block period with 10% FBS in

1X PBS. Primary staining was carried out overnight with anti-p24 mAb 241-D (NIH AIDS Research and Reference Reagent Program) in antibody solution (10% FBS in 1X PBS). Coverslips were washed with 1X PBS and stained with anti-human α-647 Cy5 secondary antibody for 1 hour in antibody solution. Coverslips were then mounted onto glass slides using Fluoro-gel with Tris Buffer. Slides dried at room temperature for 2-3 hours before storage at 4^{o}C. Slides were imaged within 1 week of coverslip mounting via confocal microscopy. Confocal microscopy was carried out with a Leica DMi8 inverted microscope using Lecia LAS X software for GFP, dTomato, and Cy5 punctate.

Optimization of staining and virus verification. Modifications of the staining protocol or testing of dual-labelled virus stocks were carried out as described for the In Situ Uncoating Assay. However, coverslips were fixed immediately following infection at 0 hpi.

Fixing and imaging virus on glass. Glass coverslips stored in ethanol were transferred onto 24-well plates followed by several 1X PBS washes. Coverslips were treated with 0.01% Poly-L-Lysine solution for 15 minutes followed by three 1X PBS washes. Virus solutions were prepared at 1/10 dilution in CHME3 media before adding 400 ul per well. Plates were spinoculted for one hour at 16°C and 1,200 x g in a centrifuge. Post-spinoculation procedures and staining were carried out as described.

Semi-automated virus counting. Counting and assessment of fluorophore signal was carried out in FIJI. Each condition analyzed within this assay utilized a minimum of 10 images per slide to ensure a sufficient sample size near or above 1,000 GFP particles. Background for each channel was manually removed in the Lecia LASX software by determining the base background in the mock and secondary only conditions. Once adjusted max projected images were imported to ImageJ. Imported images were split into green, red, and blue channels. Green

channels underwent automated thresholding with the IsoData algorithm settings. Regions of interest (ROI) were manually drawn to include areas that encompass visible cell morphology and avoid inclusion of particles adhered to glass. Particle analysis was then carried out with size parameters set to 0.7 um to 2.0 um. The size range was selected based on past literature for particle reference size and with inclusion of smaller particles that contained multiple fluorophores (77). ROIs created from the particle analysis were then overlaid onto the red and blue Channels. ROIs were analyzed for maximum pixel value for each channel. Data was exported into Microsoft Excel for data analysis. Within Excel dTomato values were sorted into S15 negative particles with zero-pixel values and S15 positive for non-zero-pixel values. Capsid positive particles were sorted based on values above 0 for max pixel intensity. Mean max intensity was calculated for each condition and plotted in Prism as a column scatter plot.

RESULTS

Characterizing the Role of Cyclophilin A in Reverse Transcription

Virus titration. Flow cytometry-based experiments that use HIV-GFP are not sensitive enough to detect multiply infected cells. By maintaining infectivity below 50% the probability that cells will be infected by multiple virus is reduced. To determine the amount of virus needed to achieve <50% GFP positive cells 7/26/18 virus stocks underwent viral titration. Serial dilution was carried out alongside a stock of virus that had previously been confirmed as infectious. Adjustments for cell background fluorescence were carried out using mock infected cells. Based on this virus titration a 1/10 dilution was chosen for future experiments (Figure 10).

qPCR primer efficiency. To investigate if CypA enhances infectivity of microglial through promoting reverse transcription, early and late RT products were quantified by qPCR. Primers targeting the R-U5 region for early RT products were selected from previous literature (78). Detection of late RT products was carried out with U5-Gag targeting primers (79). Primers for Human β-Actin were used to normalize the data to a housekeeping gene for fold change calculations. Primer amplification efficiencies were first calculated to ensure accurate quantification of relative fold changes (Table 1). Primers with 100% amplification efficiency result in doubling of the template DNA at each cycle during qPCR. However, 100% amplification is unlikely as the inclusion of PCR inhibitors and primer secondary structure can lower efficiency. A 5-point dilution standard was created for both human β-Actin and HIV-GFP plasmids to assess the amplification efficiencies. Each standard dilution of plasmid underwent a 1/10 serial dilutions from a known starting concentration. Primers for each target were then used to amplify the known standards. Cq values were deemed acceptable based on linear R^2 value

above 0.97 for each 5-point standard (Figure 11). Primer efficiencies were calculated by using the determined slope for each primer set. Primers with 100% amplification are represented by an equation slope of –3.3.

β-Actin amplified with 77% efficiency and a slope of –4.01 (Figure 11A, Table 2).The early RT primers were found to have a slope of –4.33 corresponding to 70% efficiency (Figure 11B, Table 2). Out of initial concerns of a primer efficiency difference greater than 5% the Pffafl method was selected to calculate relative fold change in future experiments. Use of the Pfaffl method, rather than the ΔΔCt method, improves reproducibility by accounting for variability between primers (80).

The role of cyclophilin A in early reverse transcription. With primer efficiencies calculated, relative quantification of early RT products can be carried out. Plated CHME3 cells were infected with HIV-GFP in constant CsA or ethanol containing media. At 0, 1, 2, 4, and 12 hours post-infection individual wells were harvested. As a negative control mock infected cells underwent CsA or ethanol treatment. In addition, a set of wells received the reverse transcription inhibitor, Nevirapine (NVP), blocking reverse transcription. Cell pellets for each time point then underwent genomic DNA extraction. As a precautionary step all samples were digested for 4 hours with DPN1. DPN1 targets a methylated sequence found on genomic DNA. HIV-GFP plasmid used during virus production is susceptible to digest allowing any contaminating plasmid to be removed. Once samples were digested respective primers were used to quantify targets by qPCR. Relative fold change of early RT products was calculated for 0, 1, 2, 4, and 12 hours post-infection to compare relative differences between CsA and ethanol conditions. To determine fold change Cq value for CsA treatment is subtracted from the corresponding ethanol Cq reaction for each primer set. The resulting ΔCq value is then used as the exponent over the

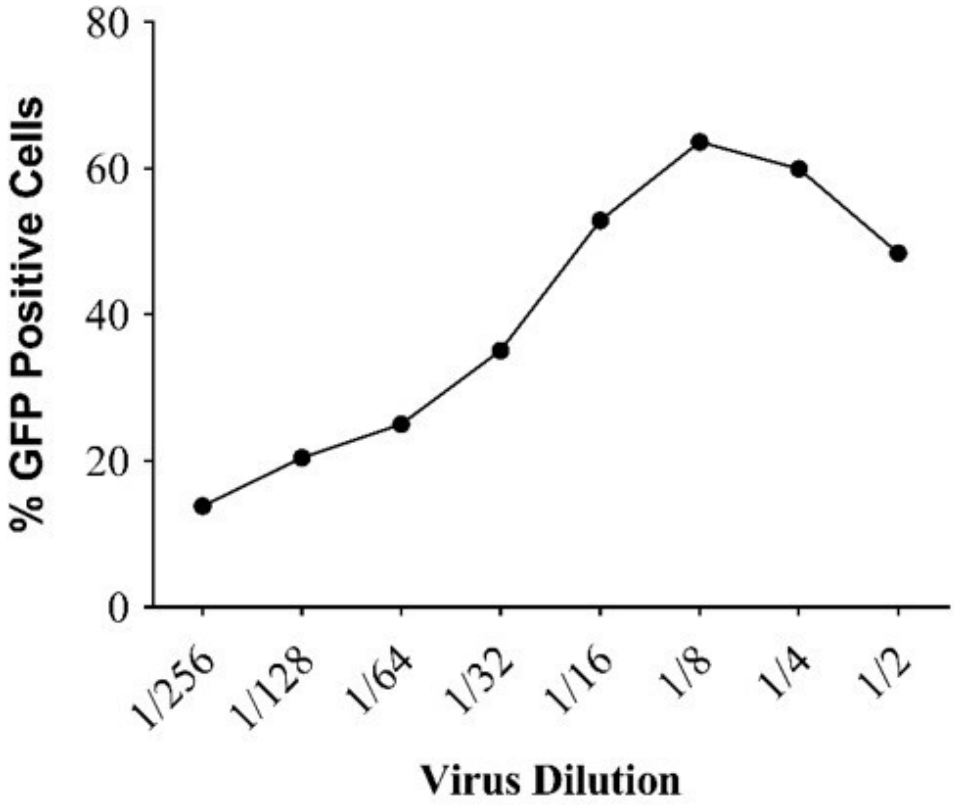

Figure 10. Titration of VSV-G HIV-GFP virus. The 7/26/18 stock of HIV-GFP virus underwent a serial dilution for titration in the 293T HEK cell line. Infectivity was quantified by percentage of GFP positive cells by flow cytometry. Titration data used to select the appropriate dilution of virus for future experiments.

Table 2. Calculated Primer Efficiencies

Primer Target	Efficiency	Pfaffl Efficiency
Early RT	0.70	1.70
β-Actin	0.77	1.77
2-LTR	0.80	1.80

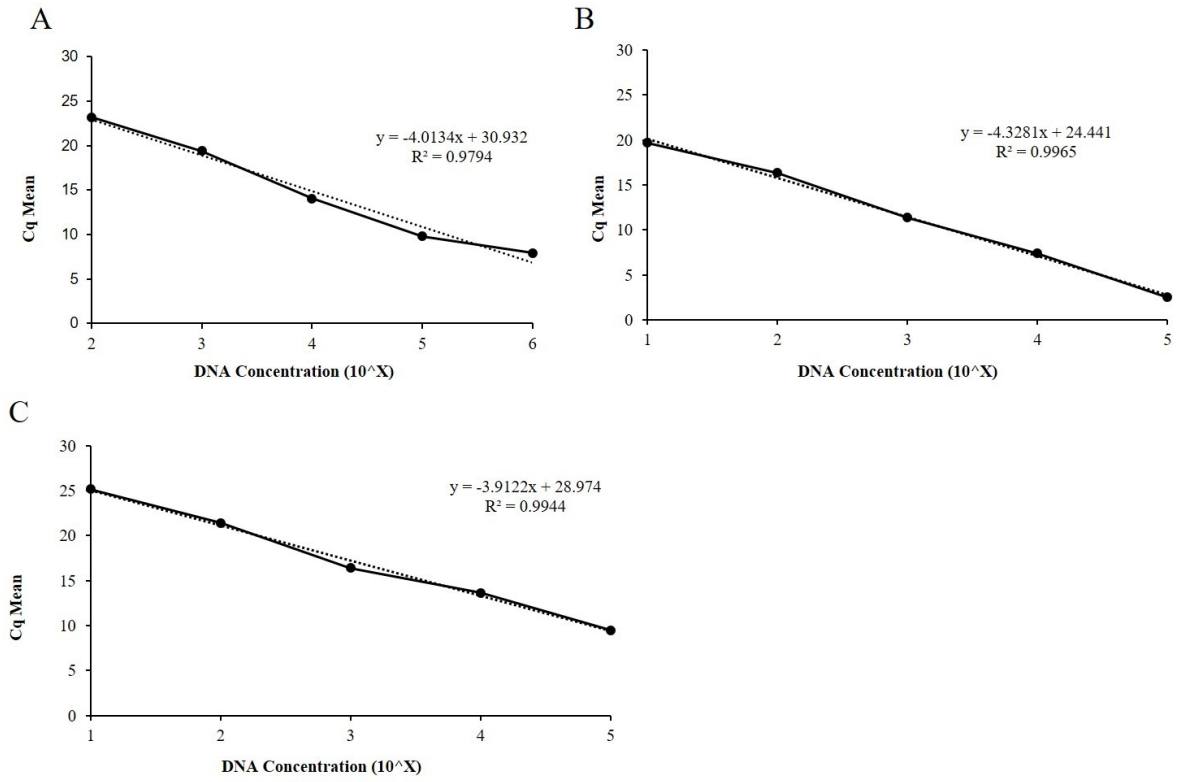

Figure 11. Primer Efficiency of β-Actin, Early RT, and 2-LTR Primers for qPCR. Plasmids underwent serial dilution to generate a 5-point standard curve. Amplification was assessed for each primer set and plotted as a Cq mean. Slopes of each plot equation were then used to calculate primer efficiency. A) β-Actin primer efficiency plot generated using a plasmid containing β-Actin sequences. B) Early RT primer efficiency plot from amplification of an HIV-GFP plasmid. C) 2-LTR circle primer efficiency plot following amplification of a plasmid containing the U5-U3 2-LTR region.

primer efficiency to calculate a non-normalized fold change. Fold change is normalized for any differences in DNA concentration by taking the target fold change divided by the housekeeping target fold change (Figure 9).

Reverse transcription products are expected to increase over time signifying the progression of infection. To assess the accumulation of RT products fold change was calculated relative to the 0-hour time point. Fold change was determined by treating control treatment as the 0-hour Cq value (Figure 9). The 0-hour time point should represent no RT products therefore fold change is expected to increase over time. Increasing amounts of early RT products were initially detected. However, the no template control (NTC) amplified with a Cq value within 5 cycles of the experimental reactions signifying contamination (Figure 12A). Melt curve analysis was carried out to ensure an individual product was amplified within NTC and experimental reactions. Single melt peaks were identified within each condition suggesting an individual amplicon. Comparing melt temperature between the 12-hour post infection reaction and NTC revealed only a 1.5^{o}C difference suggesting similar product size (Figure 12B). To address the possibility of primer dimers the 12-hour ethanol samples were run on a 1% agarose gel alongside the NTC products. Imaging of the gel revealed identical product size between the experimental and NTC sample near the expected 77 base pair size for the early RT products (Figure 13).

Initially, qPCR reactions were prepared in a primary laboratory space where HIV-GFP plasmid had previously been extracted. To remove any risk of environmental contamination qPCR reactions were set up in a separate lab space with dedicated PCR micropipettes. Subsequent qPCR runs indicated inconsistent contamination of the NTC samples (data not shown). To further remove sources of contamination qPCR samples were prepared in a ventilated cell culture hood. All materials excluding primers, master mix, and DNA samples

were exposed to UV for 15 minutes prior to setting up reactions. Following these alterations, a consistent reduction in NTC Cq values was observed. All qPCR was prepared following these precautions in later experiments with no observed contamination (Figure 12C-12D).

With the NTC reactions no longer indicating contamination early RT samples were prepared and quantified for relative fold change. Despite increasing RT products observed in initial experiments later experiments failed to show accumulating products (data not shown). Infectivity of HIV-GFP in CHME3 cells, off-target effects of ethanol, plasmid contamination, and low DNA template number were next investigated to identify the cause in failure to accumulate early RT products.

Viral titration in CHME3 cells. The virus titration of the 7/26/18 HIV-GFP stock had previously been carried out in the 293T HEK cell line, but not the CHME3 cell line. To ensure that failed infection was not the cause of low RT products infectivity in CHME3 cells was assessed. Infection was carried out through serial dilution as previously described. A confirmed infectious virus stock was included for positive control (data not shown). Triplicate wells underwent mock treatment to adjust cell background fluorescence. Infectivity of CHME3 cells was comparable to past viral titers in the 293T HEK cells across all serial dilutions (Figure 14A, Figure 10).

Off-target effect of ethanol. During the experiment CsA and ethanol containing media is used to disrupt CypA binding or act as a vehicle control. The inclusion of any drug may have off target effects within cells that could alter replication events. Within failed experiments CsA and ethanol treated cells did not demonstrate an increasing trend in early RT products. To ensure that the presence of ethanol was not disrupting replication a viral titration was carried out in CHME3 cells with ethanol containing media at a $1/2000^{th}$ dilution. As a positive control for

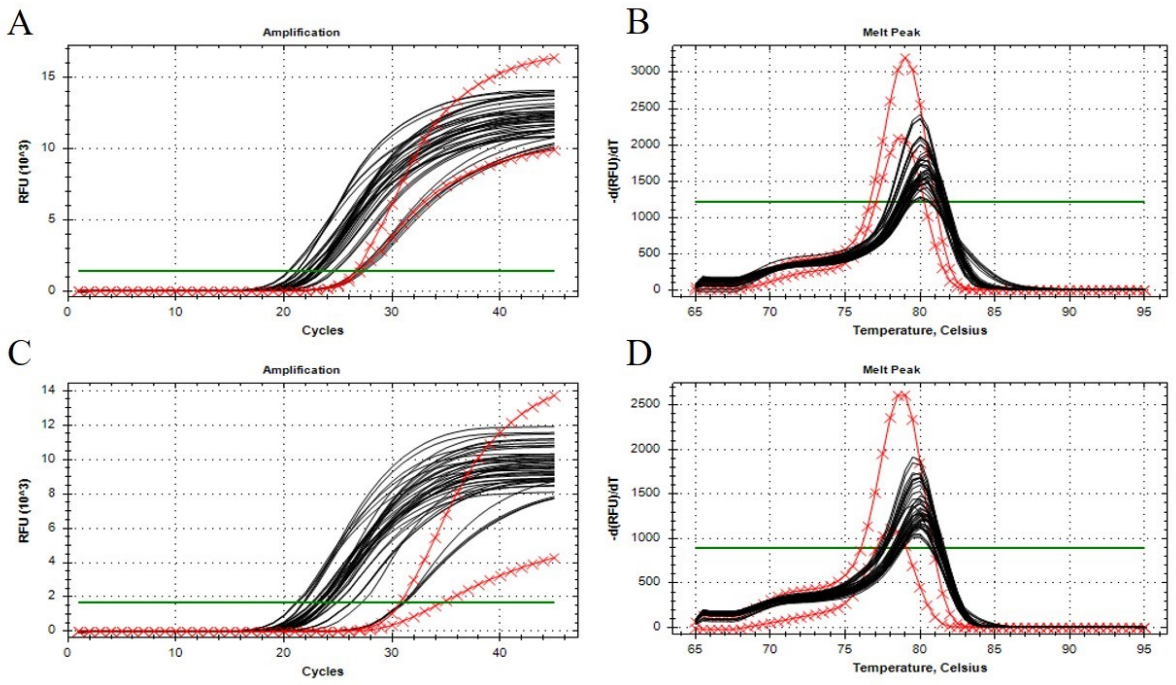

Figure 12. Early Amplification of NTC Control Reactions. Amplification and melt curve plots for qPCR of early RT products. Black lines represent experimental samples. Red lines with X marks indicate the no template control (NTC). A) Amplification plot demonstrating contaminated NTC based on early amplification relative to experimental reactions B) Melt curve analysis of contaminated NTC imposed over experimental reactions C) Amplification plot of reactions prepared in cell culture hood with acceptable NTC amplification. D) Melt curve analysis of reactions set up in cell culture hood.

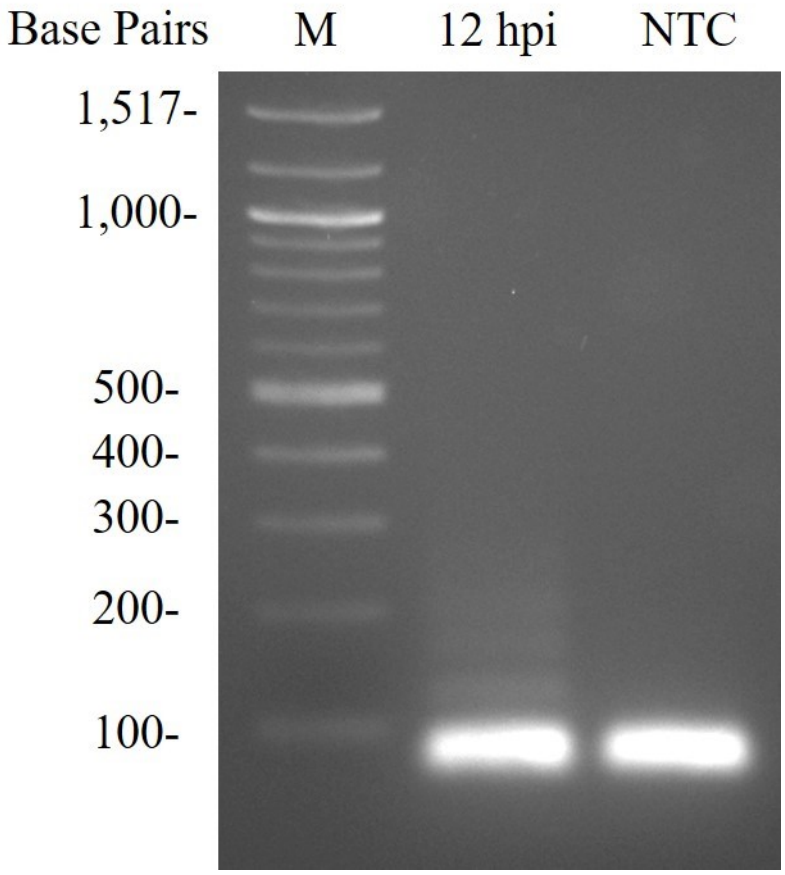

Figure 13. Agarose Gel Electrophoresis of NTC and 12 Hour Post-Infection Products. qPCR products were run on a 1% agarose gel for 1 hour at 120V. Expected early RT product size is 77 base pairs.

infectivity a set of wells were infected without addition of any drug. In the presence of ethanol infectivity was comparable in CHME3 cells relative to the control indicating that the inclusion of ethanol was not inhibiting early replication steps (Figure 14B). Over the 1/20 to 1/4 dilution range a decrease in infectivity without ethanol treatment was identified. Despite the decrease, higher and lower concentrations of virus were similar in infectivity. The observed decrease in infectivity may be due to confounding variables such as exposing microglial cells to < 37°C during initial infection of the plated cells.

Extended DPN1 digest. Prior to qPCR all DNA extracts undergo a 4-hour DPN1 digest that targets a methylated sequence found on genomic and plasmid DNA. Failure to remove contaminating plasmid would reduce accuracy in measuring early RT products. In addition, presence of plasmid DNA within the 0-hour samples may shift the baseline Cq. Out of concern that contaminating plasmid was not being completely digested a set of extracted samples underwent two 4-hour digests followed by qPCR. Cq values were compared within the same sample after the first and second digest period. Extended digest resulted in later Cq values suggesting some contaminating amplicons were removed (Table 3). A shift in +0.95 cycles in the mock treated samples suggests a near 50% reduction in template DNA. Experimental samples for 0, 4, and 12 hours post-infection indicated later cycle numbers at +0.37, +0.65, and +0.96, respectively. Despite the shift in Cq, plotting the relative fold change to the 0-hour failed to demonstrate a gradual increase in products (Figure 15). At the 12-hour post-infection time point products indicated an increase in early RT products, but 4 hours post-infection failed to show increased products. Therefore, the lack of increasing products prior to 12 hours post-infection was not due to contaminating plasmid altering the calculated fold change.

Low DNA template number. It is expected that detectable amounts of early RT

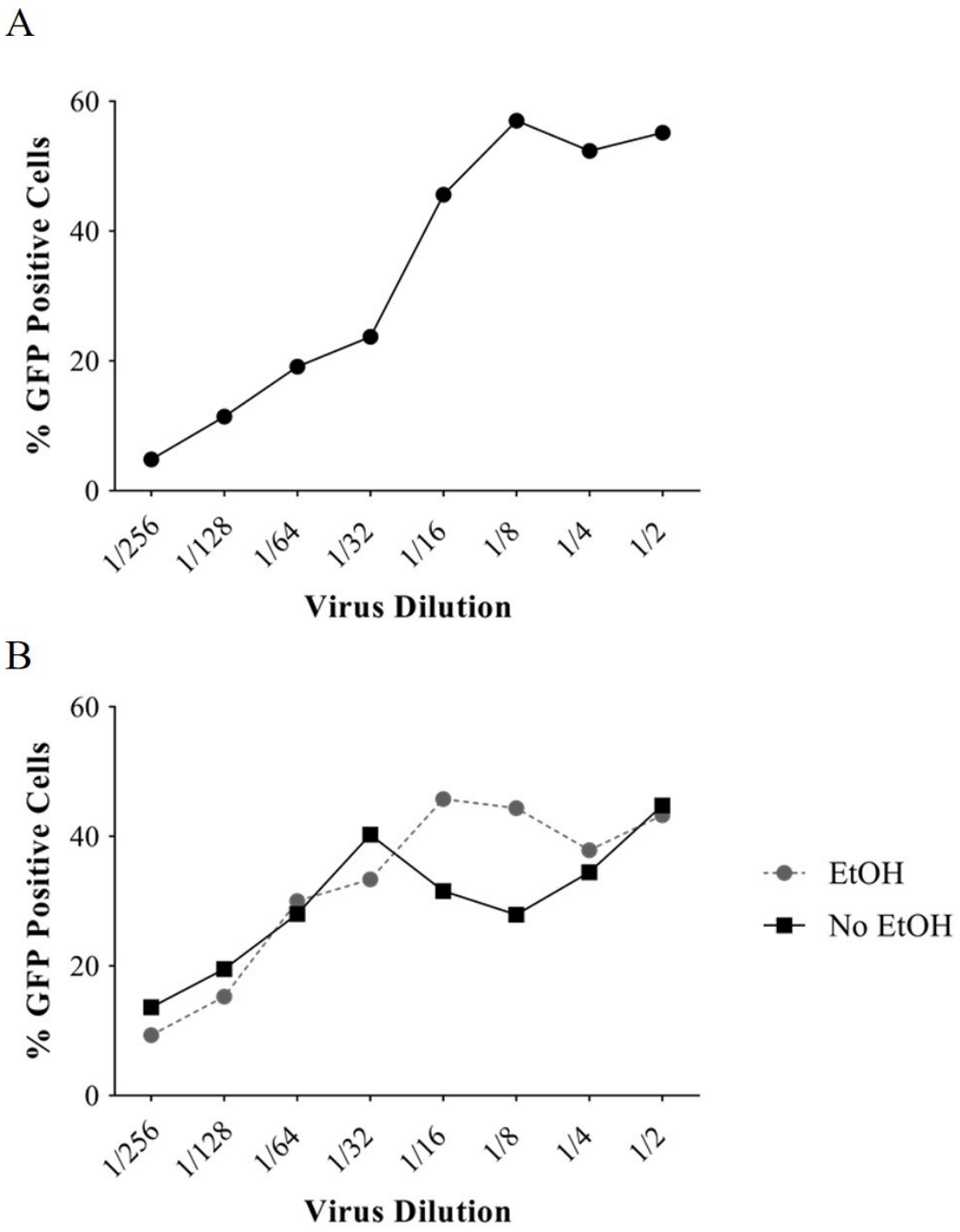

Figure 14. Confirmation of CHME3 Infectivity by Viral Titration. Viral titration of the 7/26/18 HIV-GFP stock was carried out in CHME3 cells to confirm infectivity. A) Infectivity of HIV-GFP in the CHME3 cell line over a serial dilution. B) Comparison of HIV-GFP infectivity in ethanol treated and no treatment CHME3 cells.

Table 3. Cq Values for Single and Extended Digests

Time of Harvest (hr)	Intial Digest Cq	Extended Digest Cq	Cq Difference
Mock	23.46	24.41	+ 0.95
0	23.16	23.53	+ 0.37
4	22.47	23.12	+ 0.65
12	23.16	24.12	+ 0.96

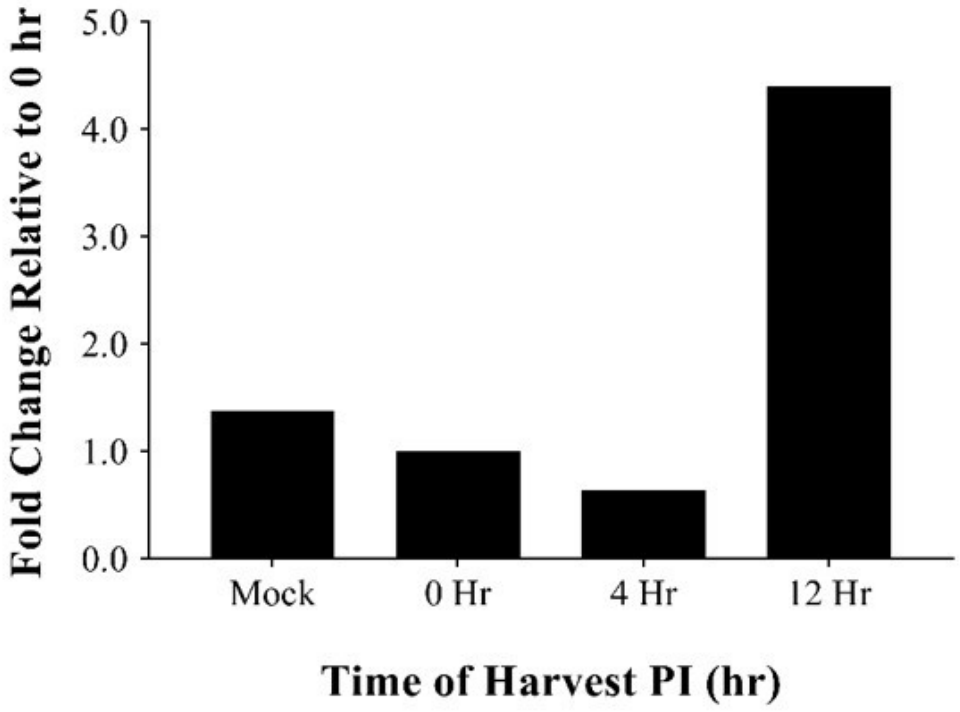

Figure 15. Accumulation of Early RT Products After a DPN1 Digest. Cells treated with ethanol underwent DNA extraction followed by two 4-hour DPN1 digests. Digested samples then underwent qPCR for early RT products. Fold change relative to the baseline 0-hour was plotted to track increasing products over time.

products should be present by 1-hour post-infection, however, qPCR for early RT products often did not detect increased fold change until 12-hours post infection (Figure 15). Therefore, a lack of detection of increasing products at early timepoints may indicate low template DNA number per reaction. To confirm CHME3 cells were being infected a troubleshooting assay was designed to confirm end point infection under the same conditions that RT products were being prepared. VSV-G HIV-GFP includes a GFP reporter gene that allows for detection of infected cells by flow cytometry. Therefore, endpoint infectivity can be compared to increasing RT products within the same experiment. Duplicate conditions were infected across a time course in ethanol containing media. At 0, 2, 4, and 12 hours post-infection one set of wells were harvested and prepared for qPCR as previously described. At these same time points, a duplicate well received ethanol containing media with NVP to prevent reverse transcription at the time of addition. Infection of these cells was carried out to 48 hours post-infection before harvesting all wells for flow cytometry. A mock treated well was included as a negative control for background. Percent GFP was then quantified as an indirect measure of infectivity and compared to the relative fold change of early RT products.

Quantification of the qPCR samples for early RT did not demonstrated an increasing trend in products in line with previous experiments. Additionally, early RT products peaked at 2 hours post-infection at 2.33-fold change and decrease at 4- and 12-hours post-infection. The comparative flow cytometry data indicates an increasing completion of integration from 2 to 12 hours post-infection as expected for infection. With the NVP addition at 12 hours post-infection infectivity reached a maximum of 30 percent GFP positive cells (Figure 16A-B). The increasing percentage of GFP positive cells over time in the flow data, but a lack of increase in qPCR products suggests low levels of amplicons are not properly amplified. While the trend in peak

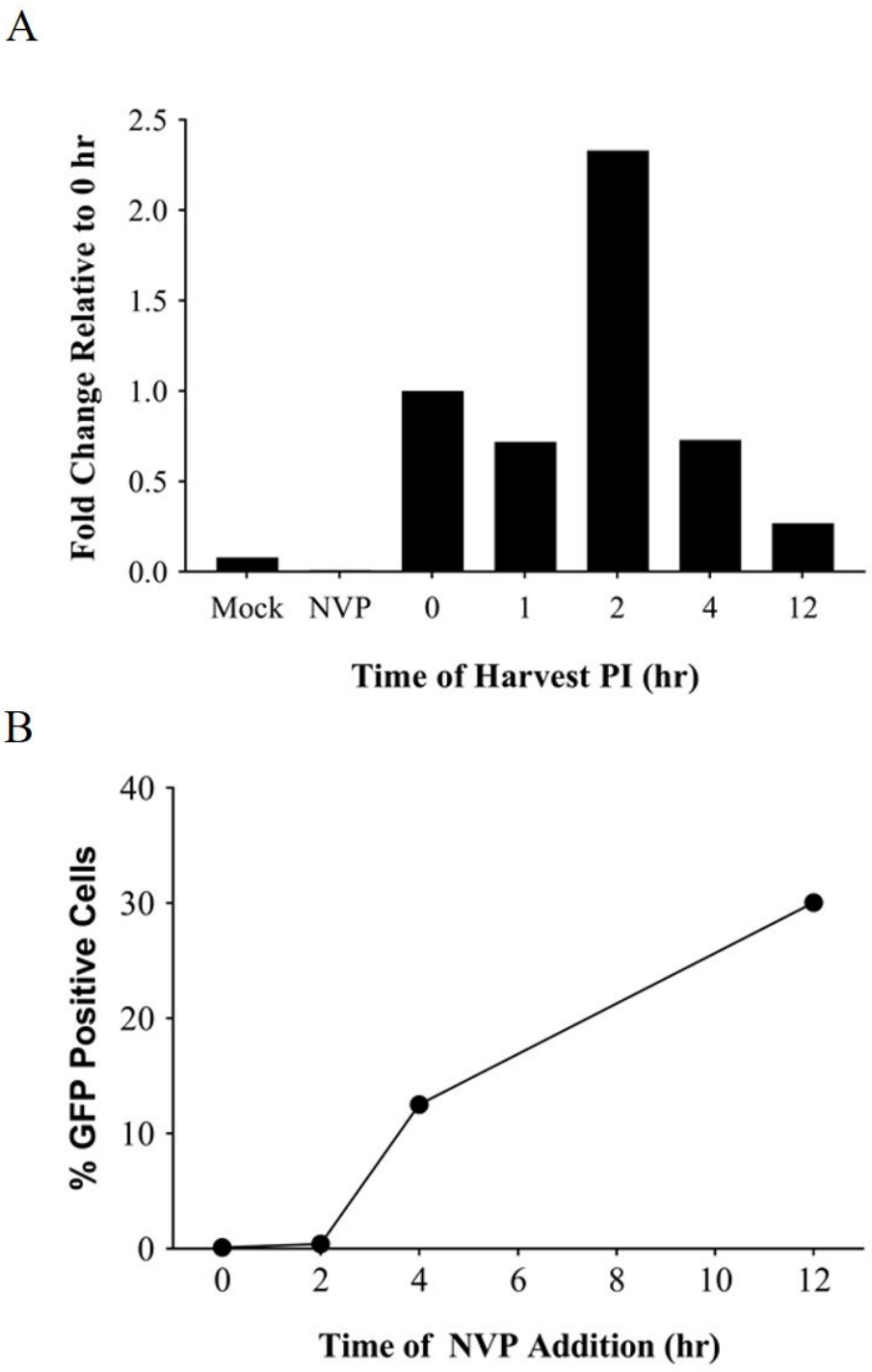

Figure 16. Early Reverse Transcription Troubleshooting Assay. Side-by-side qPCR and flow cytometry assays to track infection over a time course under ethanol treatment. A) qPCR of early RT products relative to the 0-hour time point. Plot represents the relative product level over time. B) Flow cytometry of cell samples treated with NVP containing media at each time point. Percentage GFP positive cells indirectly represents end point infectivity.

products differed from previous failed runs the lack of product at later time points suggests a failure to detect accumulating products.

Completion of early RT product qPCR. Continued troubleshooting and subsequent runs for early RT qPCR eventually yielded three successful experiments. The fold change ratio between CsA and ethanol treated cells was found to be near 1.0 for the first 2 hours of infection. However, at the 4- and 12-hour time points CsA treated conditions indicate decreases in fold change of 0.70 and 0.51, respectively (Figure 17A, Table 4). A fold change of 1.0 indicates that relative amounts of early RT products are identical between CsA and ethanol. Therefore, the near 1.0-fold change at 0, 1, and 2-hours post-infection suggests that CsA treatment does not affect the amount of early RT products. However, the decrease in fold change at 4- and 12-hours post infection indicates a reduction in early RT products when cells are treated with CsA.

To track the increase of CsA and ethanol individually the fold change for each time point was compared to the 0-hour post-infection condition. Plotting these data in this way revealed an increasing amount of early RT product under ethanol treatment. Surprisingly, CsA treated cells indicated a peak in products at 2 hours post-infection with no apparent increase past this time point (Figure 17B). Carrying out a mixed ANOVA on these data revealed a statistically significant difference between treatment groups and timepoints. Data was then split on treatment to assess changes between time. A post hoc dependent t test was then carried out with a Bonferroni correction (Table 5-6). Statistical significance was only detected between the CsA hour 1 to 2 and CsA hour 4 to 12. While all other comparisons were statistically insignificant a large effect size was detected through calculating Cohen's d suggesting time has an impact on the accumulation of RT products (Table 5-6).

Quantification of late RT. Due to difficulty in quantifying RT products by qPCR the

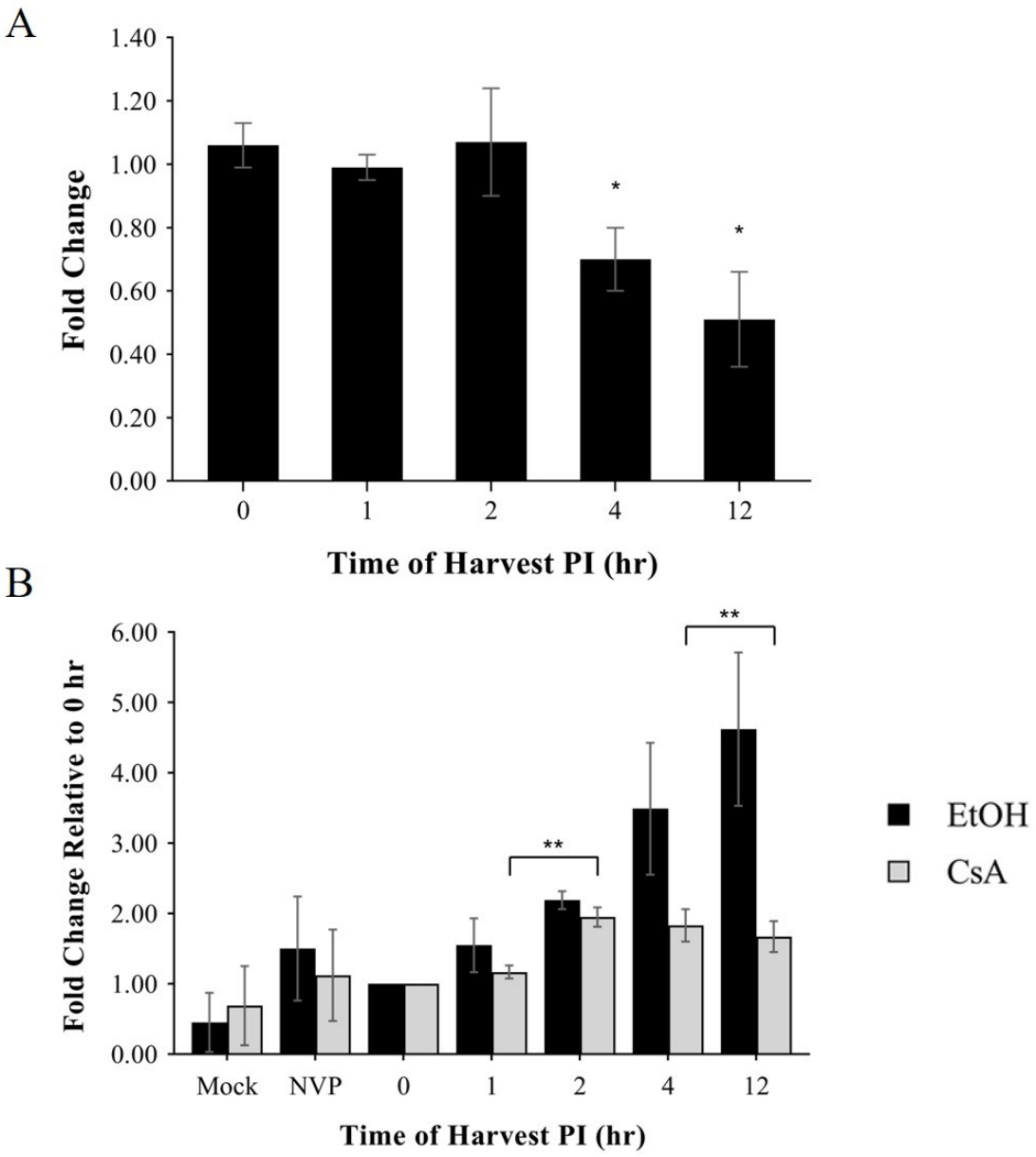

Figure 17. qPCR of Early RT Products Under CsA or Ethanol Treatment. CHME3 cells were infected with CsA or ethanol containing media to assess if CypA binding altered early reverse transcription. Fold change calculated from the average of three independent experiments. Error bars represent ±SEM. A) CsA fold change was set relative to the ethanol control. By comparing decreases in fold change ratio, the effect of CypA on products can be determined. Statistical significance was determined by a Student's T-Test between CsA and ethanol at each time point. *, $P < 0.05$. B) Relative accumulation of early RT products relative to the 0-hour timepoint. Fold change was calculated from identical Cq data used in 9A. A mixed ANOVA was carried out before splitting factors on treatment followed by a post-hoc Student T-Test with Bonferroni correction. **, $P < 0.01$

Table 4. Early RT qPCR Fold Change Ratio CsA/EtOH.

Time of Harvest (hr)	Fold Change
0	1.06
1	0.99
2	1.07
4	0.70
12	0.51

Table 5. Post Hoc Analysis of CsA Early RT Accumulation

Variables		p-value	Cohen's d
Mock	NVP	0.745	-0.22
Mock	Hour 1	0.424	-0.58
Mock	Hour 2	0.095	-1.74
Mock	Hour 4	0.201	-1.09
Mock	Hour 12	0.248	-0.93
NVP	Hour 1	0.953	-0.04
NVP	Hour 2	0.391	-0.63
NVP	Hour 4	0.452	-0.54
NVP	Hour 12	0.544	-0.42
Hour 1	Hour 2	0.007	-6.76
Hour 1	Hour 4	0.155	-1.29
Hour 1	Hour 12	0.224	-1.00
Hour 2	Hour 4	0.745	0.22
Hour 2	Hour 12	0.449	0.54
Hour 4	Hour 12	0.005	7.85

Table 6. Post Hoc Analysis of Ethanol Early RT Accumulation

Variables		p-value	Cohen's d
Mock	NVP	0.463	-0.52
Mock	Hour 1	0.200	-1.09
Mock	Hour 2	0.084	-1.83
Mock	Hour 4	0.127	-1.46
Mock	Hour 12	0.051	-2.45
NVP	Hour 1	0.951	-0.04
NVP	Hour 2	0.379	-0.65
NVP	Hour 4	0.123	-1.49
NVP	Hour 12	0.172	-1.21
Hour 1	Hour 2	0.239	-0.96
Hour 1	Hour 4	0.089	-1.80
Hour 1	Hour 12	0.058	-2.29
Hour 2	Hour 4	0.274	-0.86
Hour 2	Hour 12	0.166	-1.24
Hour 4	Hour 12	0.351	-0.70

NVP addition assay was used to assess late RT. This time of addition assay utilizes NVP containing media at specified time points to inhibit further reverse transcription. If the virus has completed reverse transcription, later replication steps are not blocked and can be quantified by percent GFP positive cells. Virus that has not completed reverse transcription at the time of NVP addition are inhibited and cannot integrate. By infecting triplicate reactions in constant CsA or ethanol containing media reverse transcription completion was assessed for 0, 1, 2, 3, 4, 6, and 8 hours post-infection. A mock infected condition as the negative control allowed for background fluorescence to be adjusted. In addition, all time points were normalized to a 48-hour constant infection condition as a positive control. Infection of microglial cells in CsA or ethanol containing media with addition of NVP demonstrated a reproducible increase in percent GFP positive cells after 2 hours post-infection (Figure 18A). Ethanol treated cells were found to have a statistically significant increase of infectivity and completion of reverse transcription compared to CsA treated cells at all-time points beyond 2 hours post-infection (Figure 18B, Table 7).

Determination if CypA Binding Alters Uncoating Kinetics

Cyclophilin A binds to capsid monomers at the CypA binding loop and may alter stability and uncoating kinetics. To identify if CypA binding alters uncoating kinetics the In Situ Uncoating Assay was utilized. The In Situ Uncoating Assay is a confocal microscopy based experiment relying on the use of dual-labelled HIV. In addition to the VSV-G and HIV-GFP plasmids used during transfection GFP-Vpr and S15-dTomato plasmids are included. Viral protein R (Vpr) is an accessory protein that associates with the Reverse Transcription Complex (RTC) (35). The GFP tagged Vpr therefore allows for tracking of RTCs within cells. As HIV virions bud from the producer cell the viral membrane is established from the producer cell

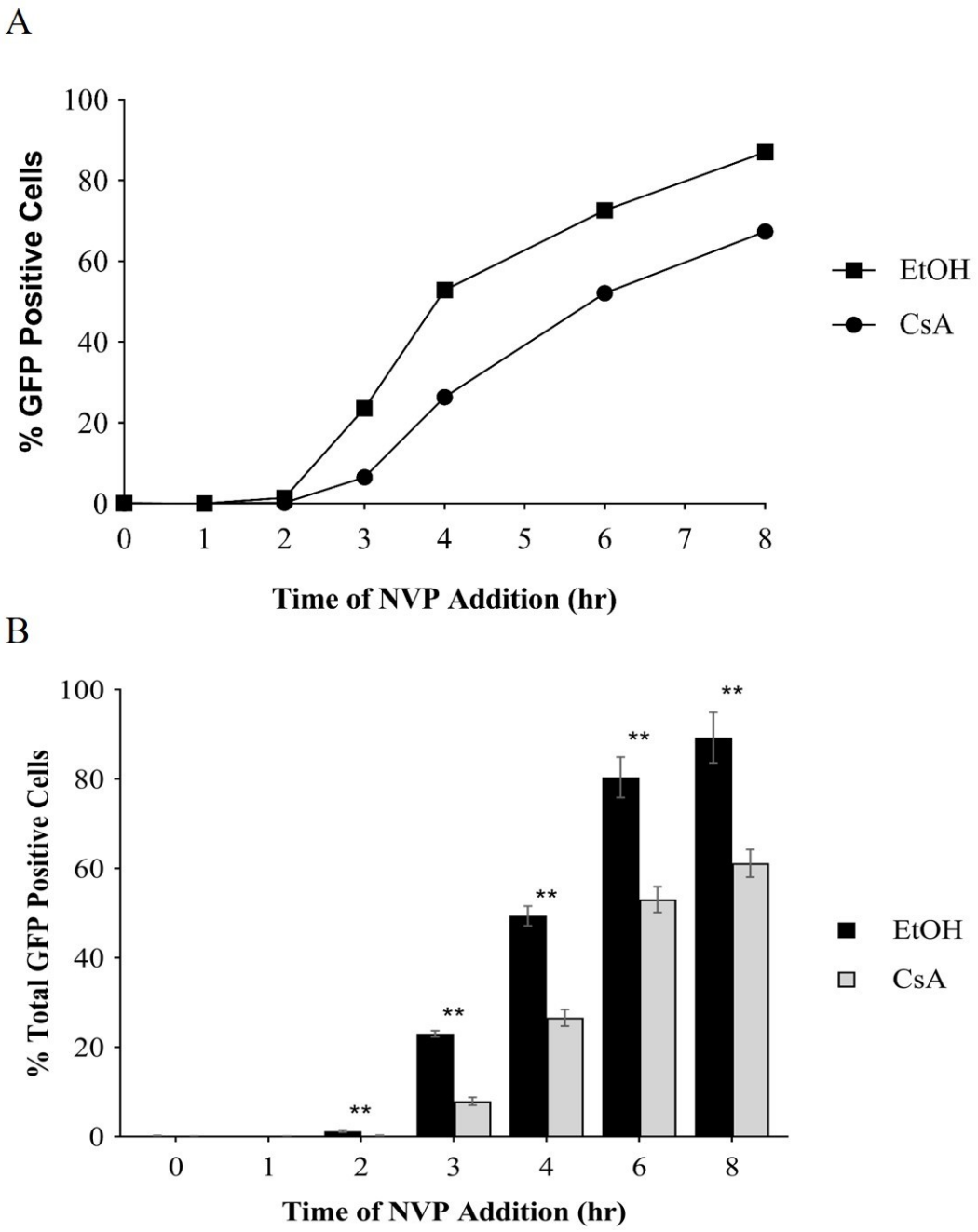

Figure 18. NVP Addition Assay with CsA or Ethanol Treatment. CHME3 cells were infected under constant CsA or Ethanol treatment. NVP containing media was added to block further reverse transcription at each time point while maintain CsA or ethanol treatment. Percentage of GFP positive cells normalized to a constant infection. A) Representative run of the NVP Addition Assay from a single experiment. B) Results of the NVP Addition Assay in CHME3 cells. Data averaged from three individual experiments. Error bars denote ±SEM. Statistical significance was determined by carrying out a Student's T-test between treatments for each time point. **, $P < 0.01$

Table 7. NVP Addition Assay Normalized Percentage of GFP Positive Cells

Time of Addition (hr)	% GFP Positive Cells (CsA)	% GFP Positive Cells (EtOH)
0	0.07	0.15
1	0.07	0.08
2	0.25	1.22
3	7.94	23.00
4	26.62	49.39
6	53.07	80.39
8	61.16	89.27

membrane. To account for any unfused virus the viral membrane is labelled with S15-dTomato. S15-dTomato consists of the N-terminal segment of c-Src conjugated to a dTomato fluorophore. The 15 amino acid sequence of c-Src contains a glycine residue that following myristoylation anchors into the cell membrane (38, 81). The S15 tagging of cell membranes extends to the viral envelope allowing fusion to be tracked based on the presence of signal (38). As fusion occurs, the dTomato signal is lost allowing unfused virus (dTomato+ virions) to be excluded from analysis (Figure 19).

The experiment begins by first adhering cells onto gelatin subbed coverslips. Cells are then infected with dual-labelled virus across a time course with paraformaldehyde fixation at each time point. Coverslips undergo immunohistochemistry for CA with a Cy5 conjugated secondary antibody. Once stained coverslips are mounted and imaged with a confocal microscope. GFP signal within cells are used to locate virus. The overlap of dTomato and Cy5 signal or lack thereof is then used to determine if a virus has fused or uncoated. Virus indicating GFP positive and dTomato negative is sorted as fused virus. Virus is further organized into coated or uncoated categories based on the Cy5 signal presence. Within the Cy5 positive count the max intensity is measured for each virus counted. The average was then calculated from all max values for each timepoint representing the mean max intensity. Differences in intensity between conditions can then be used to identify general trends in uncoating (Figure 20).

Establishment of a semi-automated virus counting protocol in FIJI. Following the completion of imaging slides for virus verification or the In Situ Uncoating assay data analysis was carried out. This analysis involves categorizing GFP tagged virus as positive or negative for capsid and membrane markers. At the onset of this work the protocol relied on manual counting through a counter deciding the category for each virus. By analyzing these data manually bias is

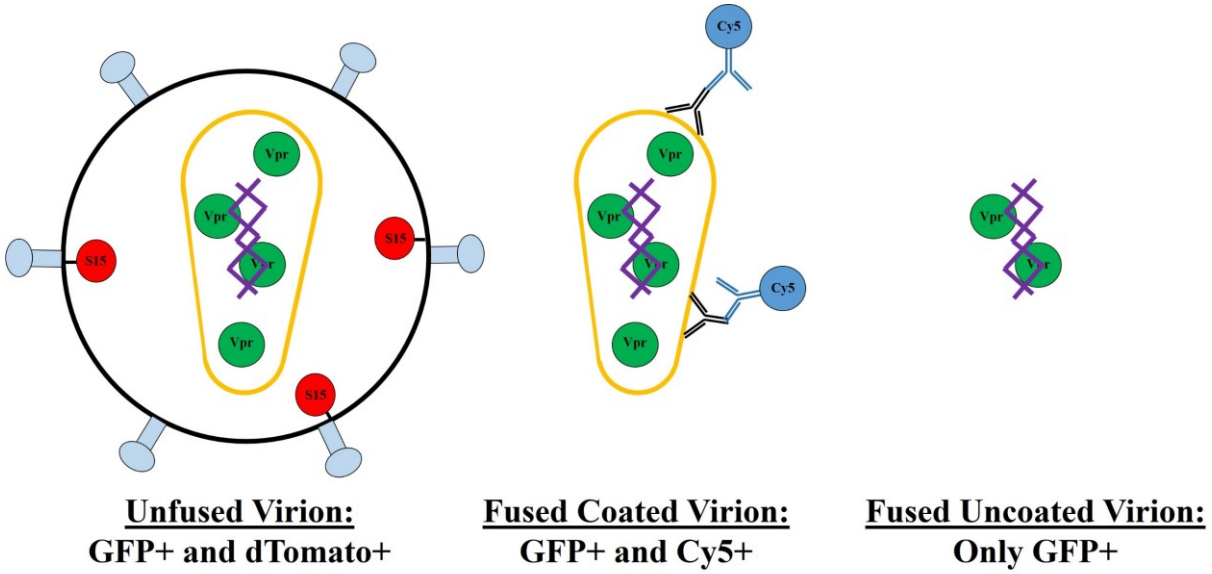

Figure 19. Schematic for Dual Virus Labelling. Dual-labelled virus is produced with GFP-Vpr and S15-dTomato. GFP-Vpr marks the viral core during infection. S15-dTomato associates with the viral membrane allowing fusion to be assessed. Antibody staining using a Cy5 conjugated secondary antibody allows CA to be visualized. Structure and molecule sizes are not representative of actual sizes.

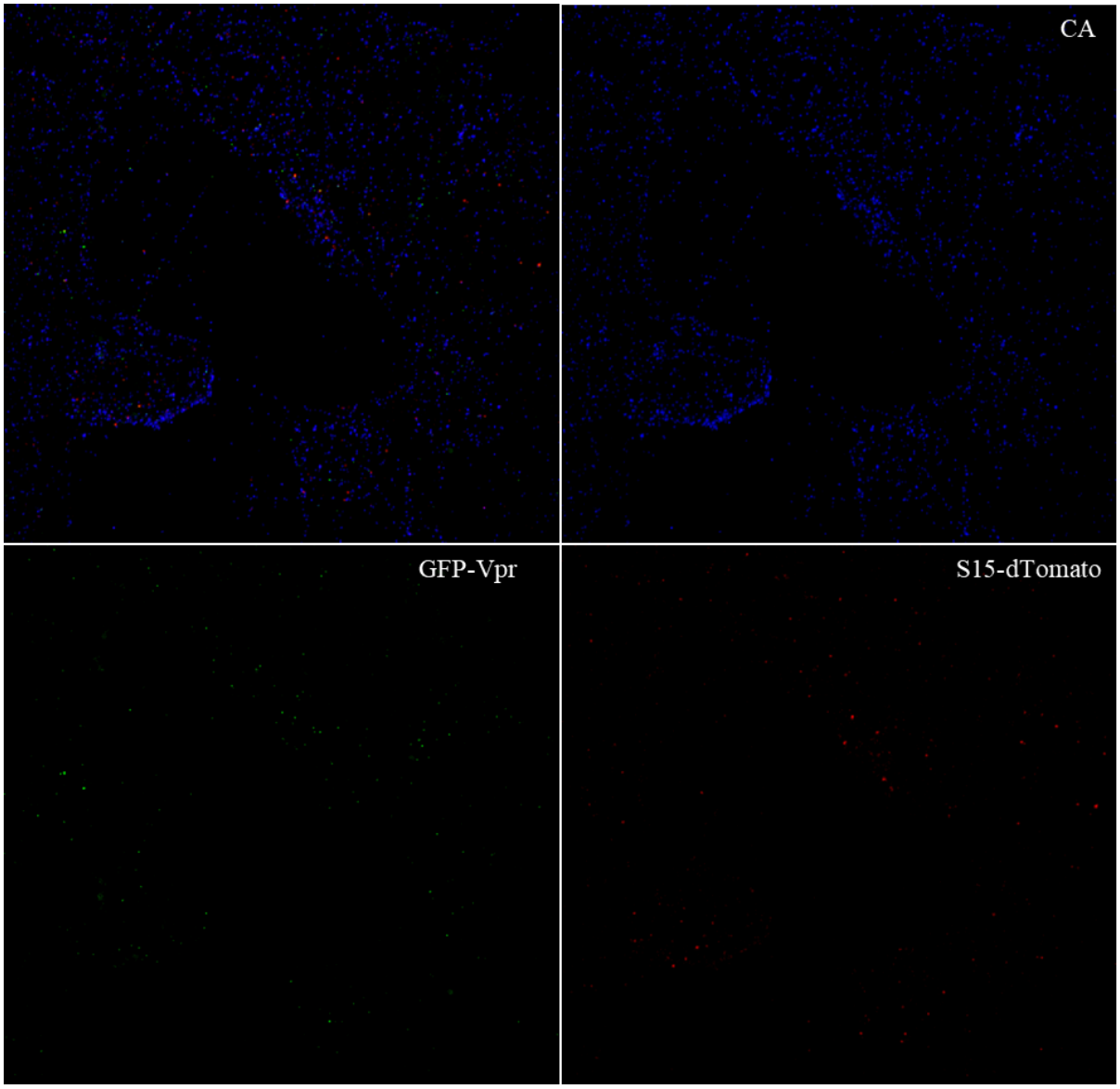

Figure 20: Representative Image from the In Situ Uncoating Assay. Dual-labelled virus was used to infect CHME3 followed by staining for CA. All panels were psuedocolored blue, green, and red for CA, GFP-Vpr, and S15-dTomato, respectively. Top left panel indicates the merged channels for detecting virus.

introduced through subjective sorting that can vary from individual to individual. Further, manual image analysis is time consuming for the number of images processed per experiment.

To streamline the procedure for data analysis a semi-automated method was designed. The benefit in establishing a semi-automated protocol includes shortening time of analysis, increasing precision of virus detection, gating virus size, and creating uniform standards across multiple users. Currently no freely available software exists solely for the purpose of the In Situ Uncoating assay. Additionally, available cell counting plugins are not well suited for quantification of near pixel size objects such as virus. FIJI was selected as the image processing software for analysis due to the open source nature of the program. FIJI is an enhanced version of the freely distributed ImageJ software developed by the National Institutes of Health (NIH). The software is commonly updated with scripting capabilities suited to the creation of macros and plugins. Thus, the flexibility of the software in customizing data analysis is well suited for semi-automated virus counting.

Before exporting images into FIJI, background intensity was manually removed in Leica Application Suite X (LAS X). LAS X is a proprietary software used with Leica microscopes for imaging and processing. Mock infected cells that underwent the staining procedure were included to gauge background fluorescence in each channel. Imaging was carried out by capturing individual focal planes of the cell generating a Z-stack of different Z-slices. The image then underwent max projection in which the Z-stacks were combined to create a 2D image representing 3D data. Background was removed by adjusting the baseline signal intensity for each channel based on the cell only condition. The appropriate intensity range was then set on all images before exporting a max projected snapshot as a Tif file. Once images were adjusted for background and exported imaged files were opened into FIJI. The initial max projected image

consists of a merge of GFP, dTomato, and Cy5 channels. In this format particle analysis cannot be carried out. The initial image is then split into green, red, and blue channels to represent each fluorophore. Of the three fluorophore labels GFP-Vpr represents the viral complex within the cell and therefore was chosen as the primary marker for particle analysis.

With GFP representing viral complexes the green channel then underwent thresholding. Thresholding allows for pixels within an image to be sorted into separate categories-based on signal intensity. For the purpose of this method, background and GFP signal are sorted appropriately prior to particle analysis. While manual thresholding does exist within the program setting a threshold value for background and objects is subjective. To avoid any variability between images the auto-threshold option was therefore utilized. Auto-thresholding is a plugin included within FIJI with various methods for global thresholding. Images initially underwent the “Try all” method for auto-thresholding. By choosing the "Try all” option all available thresholding methods are run and presented in unison. This allowed for each algorithm to be compared for how well objects were segmented without including background. IsoData method was then selected for auto-thresholding based on the algorithms ability to separate background from virus without introducing artifacts (Figure 21). Iterative Self-Organizing Data Analysis Technique (IsoData) thresholding method groups pixels into categories based on intensity. Average pixel values are then compared to an initial threshold. Pixels are then regrouped over several iterations until the change in grouping number falls below a determined threshold (83, 84).

Once a thresholding method was selected particle counting parameters were then established (Figure 22). FIJI’s particle analysis tool allows for circularity and size ranges to be set prior to quantification. Circularity restrictions allow for particles that appear too oblong to be

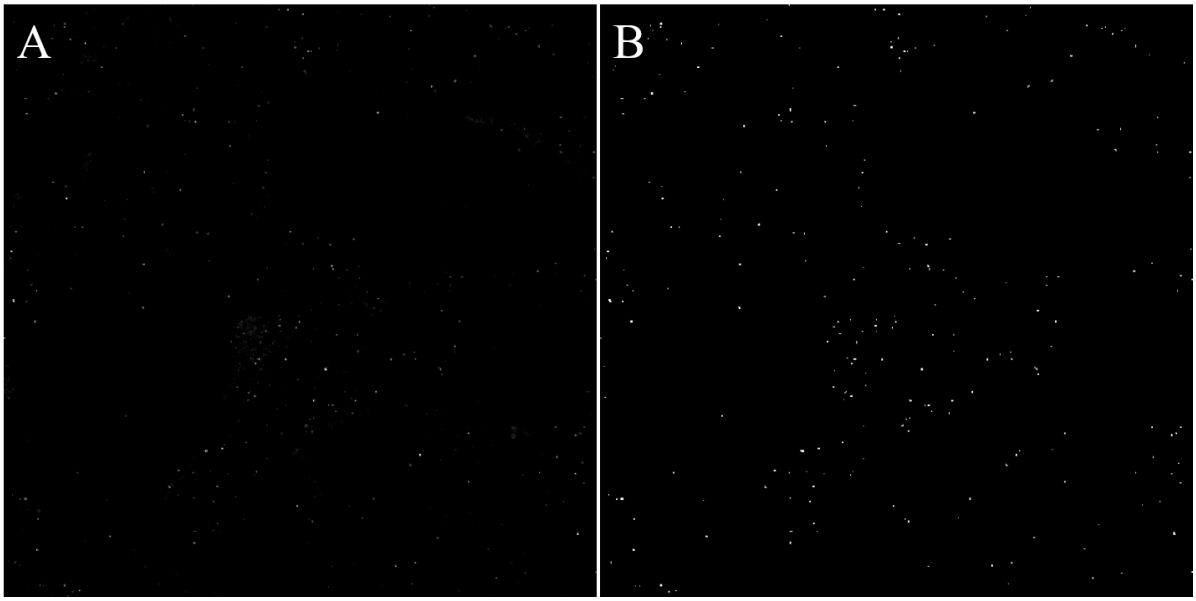

Figure 21: Automated IsoData Thresholding of GFP Signal. Merged images were split into separate channels with the green channel undergoing auto-thresholding in FIJI. A) Representative image of a pre-thresholding green channel representing GFP-Vpr. B) Representation of the same image following IsoData auto-thresholding.

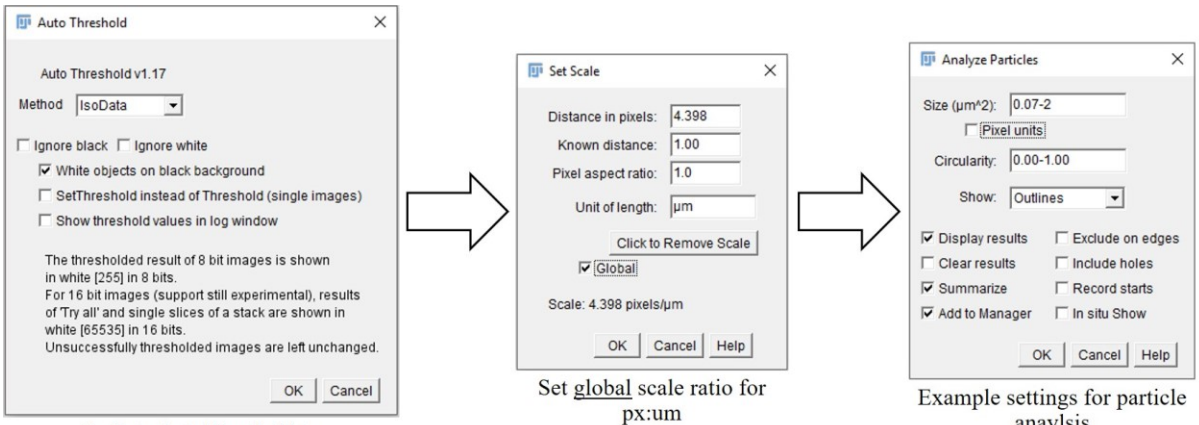

Figure 22. Schematic of Thresholding and Particle Analysis Protocol in FIJI. The auto thresholding tool is found under Image > Adjust > Auto Threshold. Algorithm method can then be selected from the drop-down menu. Global scale settings can be set under the Analyze > Set Scale menu. Pixel-to-distance ratio can then be altered and set to globally include all images opened. The particle analysis tool is opened through Analyze > Analyze Particles. Prior to analysis images must be processed through thresholding.

excluded from counting. Adjacent virus that cannot be resolved as two objects would then be ignored based on circularity. However, due to the near pixel size of GFP-Vpr all virus was categorized as perfectly circular (data not shown). Therefore, the circularity parameter could not be used to exclude overlapping virions with abnormal shape. Restriction of particles too large to count as single virions were then gated based on area (um^2). Gating for size requires the adjustment of the global scale setting within FIJI prior to analysis. Based on indicated pixel and um size of each image the global pixel ratio was set to 4.398 pixels (px):1 um. Referencing previous use of the In Situ Uncoating Assay a range of 0.07-2 um was selected (77). Using these values as a starting point a size restriction of 0-2 um was initially used to verify signal overlap of dual-labelled viral stocks. The stricter range of 0.07-2 um was found to exclude particles with dTomato and CA positive signal but selects for a virus within the distribution while excluding sizes at the small and large extremes. By choosing the range of 0.07-2 um background signal below 0.07 um is excluded with larger objects beyond 2 um removed from analysis (data not shown).

With size parameters established images were analyzed for virus count and signal intensity. Following particle analysis, each GFP particle is stored in the Region of Interest (ROI) manager (Figure 23). ROIs record the coordinates, size, and shape of each particle on an image needed in analysis. The total count of GFP particles is then saved to a Microsoft Excel sheet. With the total count saved the red and blue channels can then be measured. Selecting either red or blue channels all ROIs can be overlapped onto the image. Choosing the ‘Measure’ option in the ROI manager records each spot for maximum intensity. Pixel values are then exported into Excel to match the corresponding particle counted. Once all data per image has been moved into Excel the percentage of GFP spots that are CA or S15 positive can be determined from the total

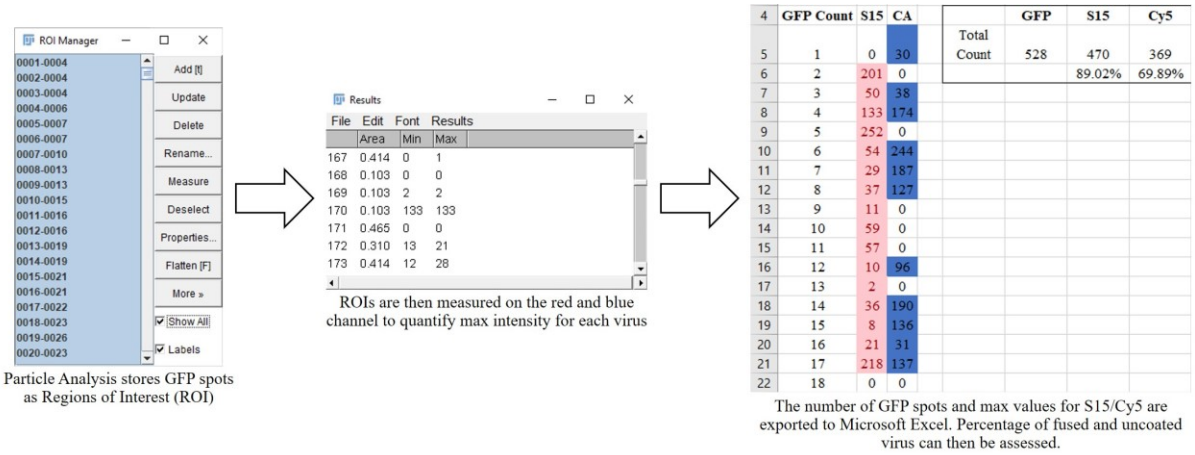

Figure 23. Schematic of In Situ Uncoating Assay Data Analysis. Regions of interest (ROIs) are saved to the ROI manager following particle analysis. Each GFP particle can then be measured for maximum intensity on the red and blue channels. Exporting values into Microsoft Excel allows for categorizing virus for each image. Percentage of overlap can also be determined with this initial analysis.

population. Using the Filter tool in Excel unfused is then hidden allowing Cy5 mean max fluorescence to be calculated.

TRITC and dTomato laser settings. The established protocol for imaging dual-labelled virus separates each fluorophore into a respective channel. Imaging for each fluorophore under previous use of the protocol utilized excitation and emission wavelengths for TRITC to detect the dTomato labels. General excitation and emission maximums for TRITC correspond to 555 nm and 580 nm, respectively. dTomato fluorophores have a maximum excitation at 554 nm and emission at 581 nm. While maximum excitation and emission are nearly identical for TRITC and dTomato excitation and emission spectrums differ. dTomato spectrums encompass a similar range of wavelength with increased intensity in contrast to TRITC (Figure 24). Functionally, this leads to higher fluorescence emission at longer wavelengths. In previous works the use of TRITC laser settings was considered appropriate for dTomato labels.

To further optimize the In Situ Uncoating Assay protocol the use of dTomato laser settings was investigated. dTomato spectra data was first imported into the LAS X software to create a user defined setting. A prepared slide with dual-labeled virus on CHME3 cells was then imaged sequentially by TRITC and dTomato laser settings. Comparatively, using the dTomato settings resulted in visibly brighter emission using the same slide (Figure 25). Using the semi-automated counting protocol particle counts were compared for each image. Size restriction for counting was set to 0.07-2 um revealing a TRITC particle count of 339. In contrast, dTomato settings drastically increased particle count to 2,203 particles (Table 8). Under the dTomato settings sensitivity was improved for particle analysis relative to TRITC spectra. Thus, the working protocol was altered to further optimize membrane label detection.

71-31 and 241-D primary antibody. During initial runs of the staining protocol the

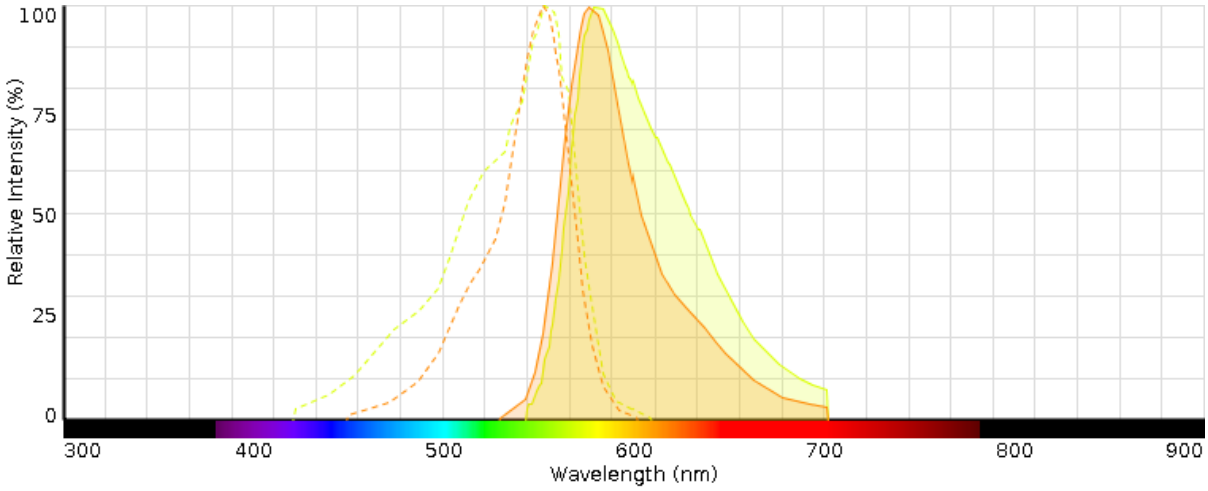

Figure 24. TRITC and dTomato Spectra Overlap. TRITC and dTomato excitation and emission histograms plotted by wavelength and intensity. TRITC spectra is represented in orange with dTomato in yellow. Excitation wavelengths are indicated as dashed lines regions. Emission wavelengths are shown with solid boundaries (86).

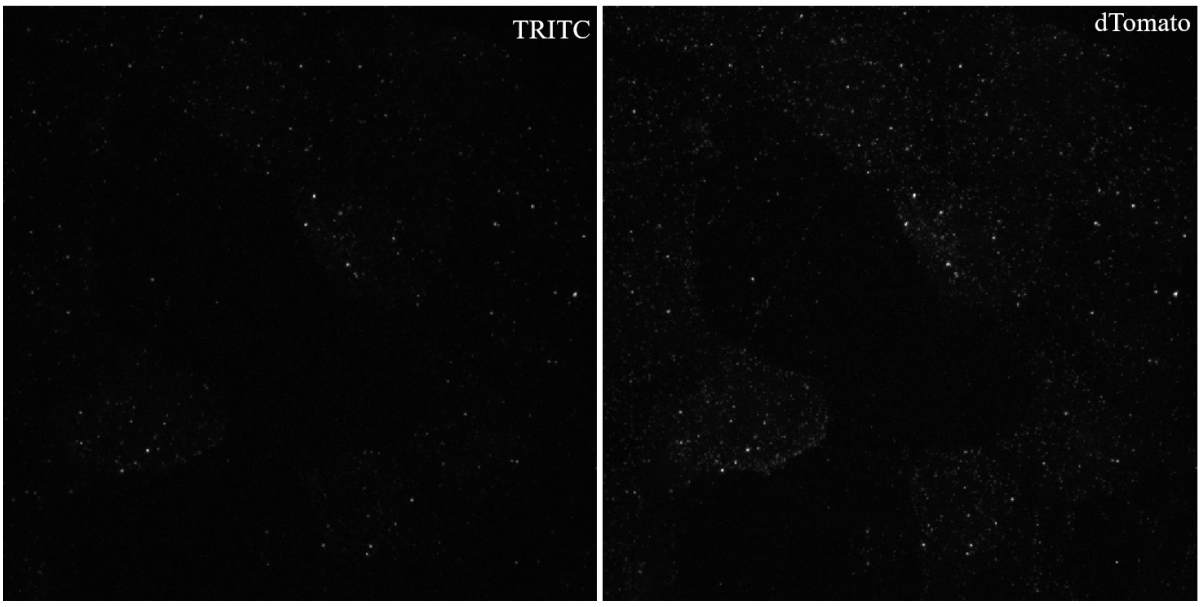

Figure 25. Virus imaged with TRITC compared to dTomato Laser Settings. Representative images of dual-labelled virus infecting CHME3 cells. TRITC and dTomato imaging was carried sequentially over an identical region of cells.

Table 8. TRITC and dTomato Particle Count Comparison

Laser Setting	Total Particle Count
TRITC	339
dTomato	2,203

primary and secondary antibodies were assessed for appropriate staining. In some instances, staining with the 71-31 CA primary antibody resulted in high levels of staining (data not shown). Within the In Situ Uncoating Assay CA signal intensity is the primary measurement in analysis. Excessive staining then increases the risk that adjacent virus CA signal may overlap. If virus lacks CA but appears CA positive there is no way to differentiate the false positive virus. Out of concern of over staining the 241-D anti-CA primary antibody was compared against the 71-31 antibody. A GFP-Vpr only stock of virus was used to compare general levels of staining. Following imaging, the 71-31 antibody appeared to show an overall higher amount of stain around GFP punctate foci. 241-D staining was dispersed around the GFP punctate with less staining of areas lacking GFP foci (Figure 26). These data may indicate that 241-D within this protocol has reduced staining of CA. However, upon particle analysis for GFP count the 71-31 antibody images were found to have a higher number of GFP foci relative to 241-D. Across three images for the 71-31 antibody 7,657 GFP particles were counted. In contrast, 241-D staining only had 2,305 GFP particles across three images (Table 9). While both conditions were prepared identically it appears there is a difference in the number of virus per image. It cannot be ruled out that the high area of staining in 71-31 was a result of more virus and therefore more capsid than the 241-D images. Regardless, based on the decrease in CA staining observed the 241-D primary antibody was used in later experiments.

Single labelled virus with S15-dTomato or GFP-Vpr. Initial attempts at producing dual-labelled virus resulted in poor overlap with dim dTomato signal (data not shown). During the production of virus 293T HEK cells are transfected with four plasmids. If transfection efficiency for GFP-Vpr or S15-dTomato is sub-optimal overlap and signal intensity may be lost. Additionally, if either fluorophore containing plasmid has low purity or quality transfection

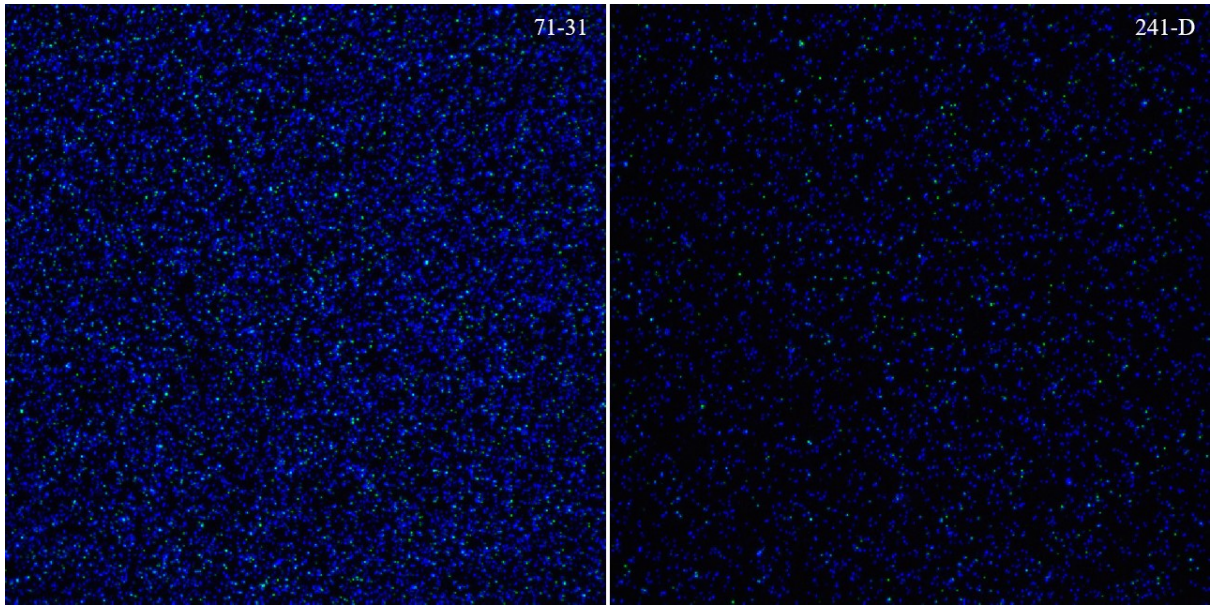

Figure 26. Comparison of Staining with 71-31 and 241-D Primary Antibodies. Staining was carried out either a 71-31 or a 241-D primary antibody. Shown are representative max projected images of virus on glass.

Table 9. GFP Count across Three Images for 71-31 and 241-D Primary Antibodies

Primary Antibody	Total GFP Count
71-31	7,657
241-D	2,305

efficiency may be further compromised. To assess the quality of the fluorophore from each plasmid single labelled virus was created with either S15-dTomato or GFP-Vpr. Virus stocks were then used to infect CHME3 cells and imaged allowing the intensity and quantity of labelling to be observed. GFP-Vpr only virus underwent particle analysis with a total of 3,293 particles across two images. In contrast, S15-dTomato labelling appeared scarcer in cells with reduced intensity above background at 440 particles (Figure 27, Table 10). While a difference in particle count was observed both fluorophores were detectable indicating the GFP-Vpr and S15-dTomato can properly label virus.

Virus verification. A core requirement of the In Situ Uncoating Assay is virus with a high percentage of labelling and staining. Virus lacking GFP-Vpr is not detected during particle analysis making the presence of GFP a requirement. Further, >80% labelling of detectable S15-dTomato is required for a virus prep before it can be used in the In Situ Uncoating Assay. Low dTomato incorporation can result in unfused virus being included during analysis. By counting unfused virus intensity of CA signal can be skewed as GFP and CA are in proximity within the viral envelope. Production of dual-labelled virus with high S15 overlap becomes further complicated as the staining procedure introduces Triton-X to permeabilize membranes. The permeabilization step is required to allow antibodies into fixed cells during staining. However, the viral membrane is derived from producer cell membranes and is also permeabilized leading to a loss in the initial S15 label. Thus, the >80% dTomato requirement extends to virus that has undergone the full staining procedure. Along with S15, dual-labelled virus requires a >50% staining overlap with GFP. Balancing membrane labeling and staining highlights the need for virus verification.

To carry out the In Situ Uncoating Assay a virus stock must first be prepared and

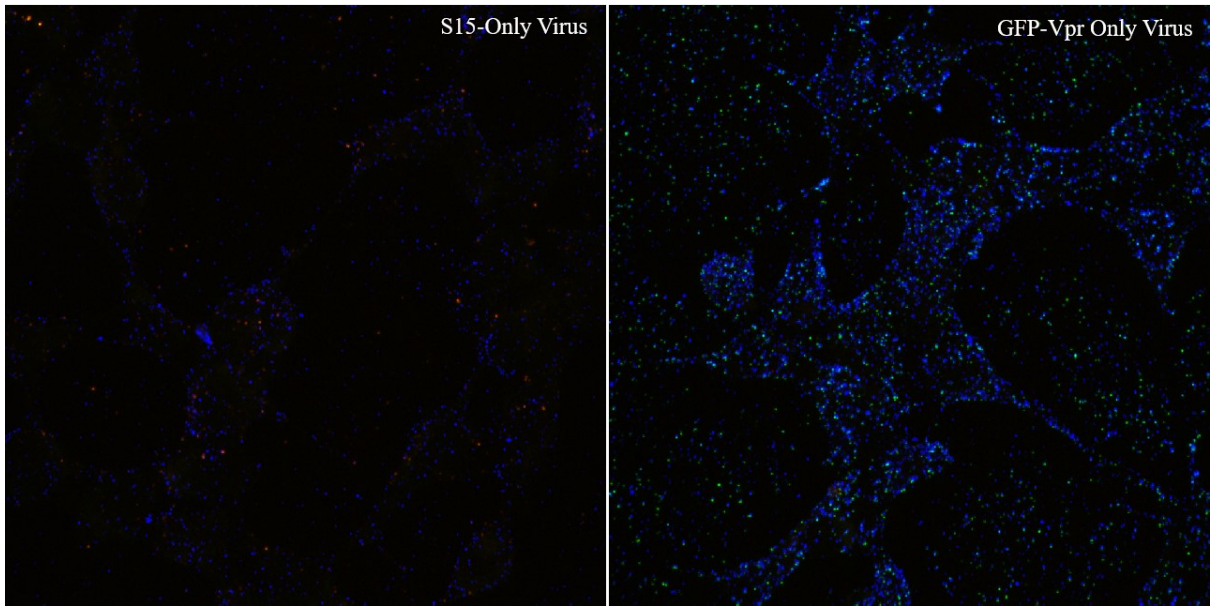

Figure 27. Assessment of Individual S15-dTomato and GFP-Vpr Labelling. Single labeled virus was generated with inclusion of the S15-dTomato or GFP-Vpr plasmid at the time of transfection. CHME3 cells were infected with single labeled virus, stained for CA, and imaged for GFP, dTomato, and Cy5 signals. Shown are max projected images, adjusted to remove background.

Table 10. Particle Analysis of Dual-Labelled HIV for GFP-Vpr or S15-dTomato

Virus	Particle Count
GFP-Vpr Only	3,293
S15-dTomato Only	440

confirmed for high signal overlap. Production of dual-labelled virus with virus verification was first carried out. The full In Situ Uncoating Assay is carried out in cells but requires time for proper cell confluence. Poor cell adherence to glass can also occur leading to failed experiments and loss of virus stocks. To reduce the time to verification of viral stocks virus was plated directly onto glass rather than cells, stained, and imaged. This process follows the previous protocol while foregoing the use of cells removing time for confluence. Glass coverslips were first treated with Poly-L-Lysine as an adherent to create a positively charged surface. Virus was then introduced to the coverslips allowing adherence and immediately centrifuged at 1,200 x g, 16°C for 1 hour. Virus was immediately fixed, and staining was then carried out allowing capsid overlap to be imaged. Once slides were imaged the semi-automated counting protocol was utilized for labelling analysis.

Over the course of the verification process numerous virus stocks were prepared and harvested using variable amounts of viral plasmids. By imaging each prep of virus, the appropriate amount of S15 to GFP-Vpr was assessed based on appropriate signal co-localization (Figure 28). Virus stock from 10-27-18 were initially chosen for virus verification using the semi-automated method. Using the semi-automated method, the 10-27-18 stock was found to have a S15 labelling of 79.87% following staining. CA staining was considered low, but acceptable at 59.84% (Figure 28, Table 11). While near the required labelling threshold the 10-27-18 stock was depleted over the course of optimizing the experiment. Later experiments were carried out using the 9-23-19 A stock of dual labelled virus (Table 11).

In situ uncoating assay. After extensive optimization of the In Situ Uncoating Assay protocol the experiment was carried out once. Cells plated on glass coverslips received either CsA or ethanol containing media with the addition of dual fluorophore-labelled HIV. Infection

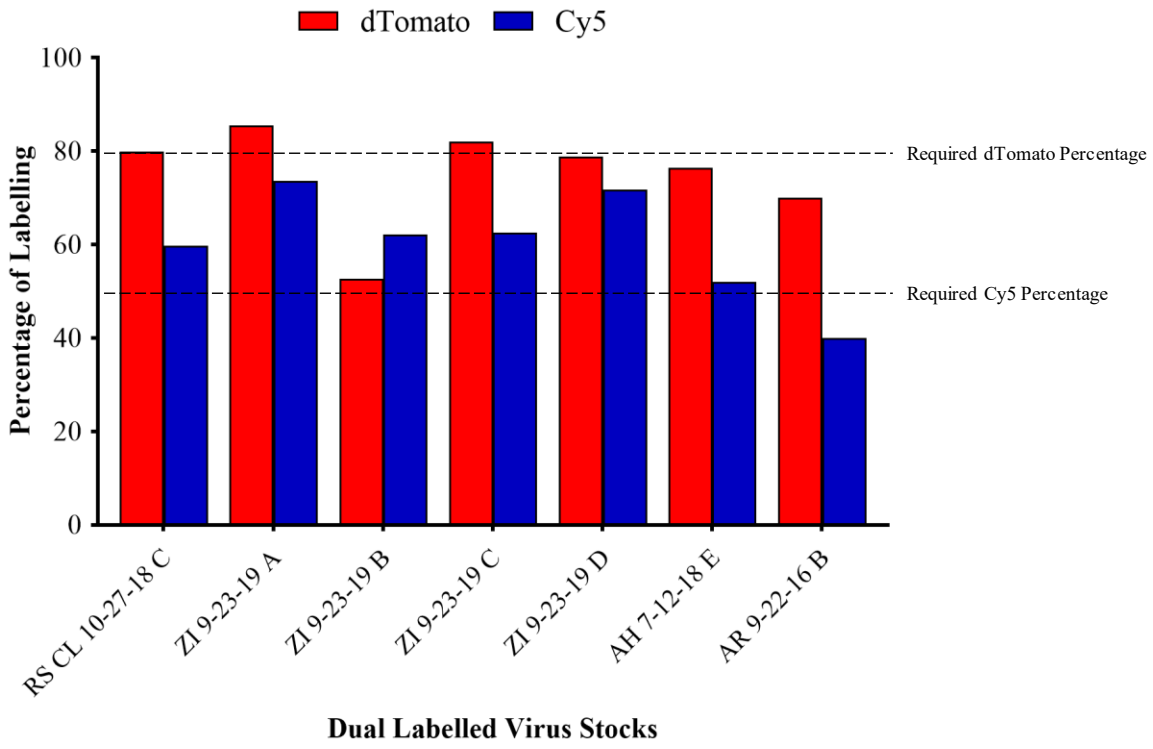

Figure 28. Percentage of Label Overlap for Dual-Labelled HIV-GFP. Dual-labeled virus stocks were imaged on glass. GFP particle count was carried out in FIJI following the semi-automated counting protocol. Total percentage of dTomato and Cy5 positive virus was calculated for each viral prep.

Table 11. Labelling Percentage of Dual-Labelled HIV-GFP Stocks

Viral Stock	Total GFP Count	Percentage of dTomato Labelling	Percentage of Cy5 Labelling
RSCL 10-27-18C	889	79.87	59.84
ZI 9-23-19 A	2,067	85.53	73.68
ZI 9-23-19 B	1,616	52.78	62.25
ZI 9-23-19 C	1,509	82.11	62.62
ZI 9-23-19 D	1,480	78.85	71.82
AH 2018 E	750	76.53	52.00
AR 2016 B	1,016	70.00	40.00

was synchronized by spinoculation before beginning the uncoating time course. At 0, 1, 2, and 4 hours post-infection cells were fixed with paraformaldehyde. Coverslips then underwent overnight primary antibody staining for CA. Secondary antibody staining was carried out with a Cy5 conjugated antibody for CA detection. As a control, mock-infected cells underwent staining or no staining to measure cell background. To ensure that secondary staining was specific for the 241-D primary antibody a 0-hour post-infected condition was used that only received the secondary antibody. Lastly, to validate the S15-dTomato labelling and Cy5 CA staining a coverslip underwent 4 hours of infection with constant baflomycin A. Baflomycin A is a V-ATPase inhibitor that blocks endosomal fusion of the VSV glycoprotein and therefore blocks VSV-G HIV fusion (85). Following staining and mounting of the coverslips onto glass slides cells were imaged for GFP, dTomato, and Cy5 signal. Up to ten images were taken at each timepoint to acquire >100 fused virions. In all conditions the number of fused virions exceeded 100 with the exception of the ethanol treated 4-hour time point. Only 71 fused virions were detected after imaging the ethanol 4-hour coverslip (Figure 29A). Utilizing the newly established semi-automatic counting protocol fused virions were analyzed for Cy5 signal to measure relative CA.

The BafA control allows for a maximum CA intensity to be set as it is expected that few virions will have fused or uncoated. Surprisingly, the total population of BafA treated virus included 1,951 virions with 63% lacking any detectable CA signal resulting in a mean max CA signal of 38.17 (Figure 29A). Out of concern that poorly stained virions were skewing the average signal BafA virions were reanalyzed with only virions with CA signal above 0. Removing uncoated virions resulted in a population of 1,155 and an average signal of 60.73. An additional control for maximum signal overlap is the 0-hour post-infection conditions, which

should indicate relatively high CA signal. In contrast to the BafA control, staining of the 0-hour virions was relatively high at 85 percent CA positive under CsA and ethanol treatment. CA signal at 0 hours post-infection were 52.66 under CsA treatment and 41.99 with ethanol treatment.

Beyond the 0-hour timepoint average signal intensity was assessed for CsA and ethanol conditions (Figure 29A). A decrease in signal as infection progresses is expected as capsids uncoat. When CypA binding was blocked with CsA the signal intensity was recorded as 40.02 at 1-hour post-infection. At 2- and 4-hours post-infection with CsA the CA signal decreased to 36.52 and 23.73, respectively. In contrast, at 1-hour post-infection with ethanol the CA signal was 29.79 and increased over time with 38.16 at 2-hours post-infection and 77.20 at 4-hours post-infection. Surprisingly, maximum CA intensity was reached at 4 hours post-infection under ethanol treatment.

Next, CA signal average between groups were compared to determine if CypA alters uncoating timing (Figure 29A). The initial hypothesis was that CypA binding may stabilize the capsid leading to higher CA signal under ethanol treatment. At 0, 1, and 2 hours post-infection CA signals were similar when CsA or ethanol was present. CA signal at 4 hours post-infection did reveal a difference between treatments with CsA CA signal decreasing and ethanol treatment increasing. Across all conditions the widest range in intensities was at 4 hours post-infection from 23.73 in CsA to 77.20 in ethanol. Scatter plot representation of virions between groups remained comparable except for the 4-hour ethanol timepoint, which lacks a larger population of near 0 CA virions.

An alternative way to represent uncoating in the In Situ Uncoating Assay is to categorize fused virions into uncoated or coated virions based on the absence or presence of any CA signal

(82). By sorting virions into uncoated based on 0 CA signal values the progression of uncoating was tracked. Plotting these data in this way it would be expected that the percentage of uncoating would increase with time. Under CsA treatment the fused virion population indicates an increasing trend in uncoating up to 4 hours post-infection (Figure 29B). In contrast, ethanol treatment uncoating followed a more erratic trend that peaked at 2 hours post-infection decreasing to 3 percent uncoating at 4 hours post-infection.

To verify that CsA treatment had no effect on fusion the percent of fused and unfused virions was calculated. Over the time course fusion was expected to increase under CsA and ethanol treatment. Total number of S15-dTomato positive virions relative to the total virion count was used to assess fusion (Figure 30). The BafA fusion control included only 8 percent fused virions at 4 hours post-infection from a total of 1,951 virions. In contrast, the 0-hour CsA and ethanol time points demonstrated the maximum percentages of fused virions at 45 and 33 percent, respectively. At 1-hour post-infection fusion decreased to 11 percent with CsA and 14 percent with ethanol. A general increase in fusion was observed for each treatment from the 1 hour to the 4-hour time points with fusion reaching 31 percent. No drastic differences between treatments were identified within this single experiment.

Characterizing the Role of Cyclophilin A in Nuclear Import

Optimizing infection for qPCR of 2-LTR products. To characterize if CypA influences nuclear import 2-LTR circles were quantified by qPCR. 2-LTR circles are formed following nuclear import as non-homologous end joining (NHEJ) pathways recognize and ligate together the 5’ and 3’ long terminal repeat (LTR) regions (86, 87). The specific localization of 2- LTR circles allow for an indirect quantification of nuclear import by qPCR (Figure 1). Primers

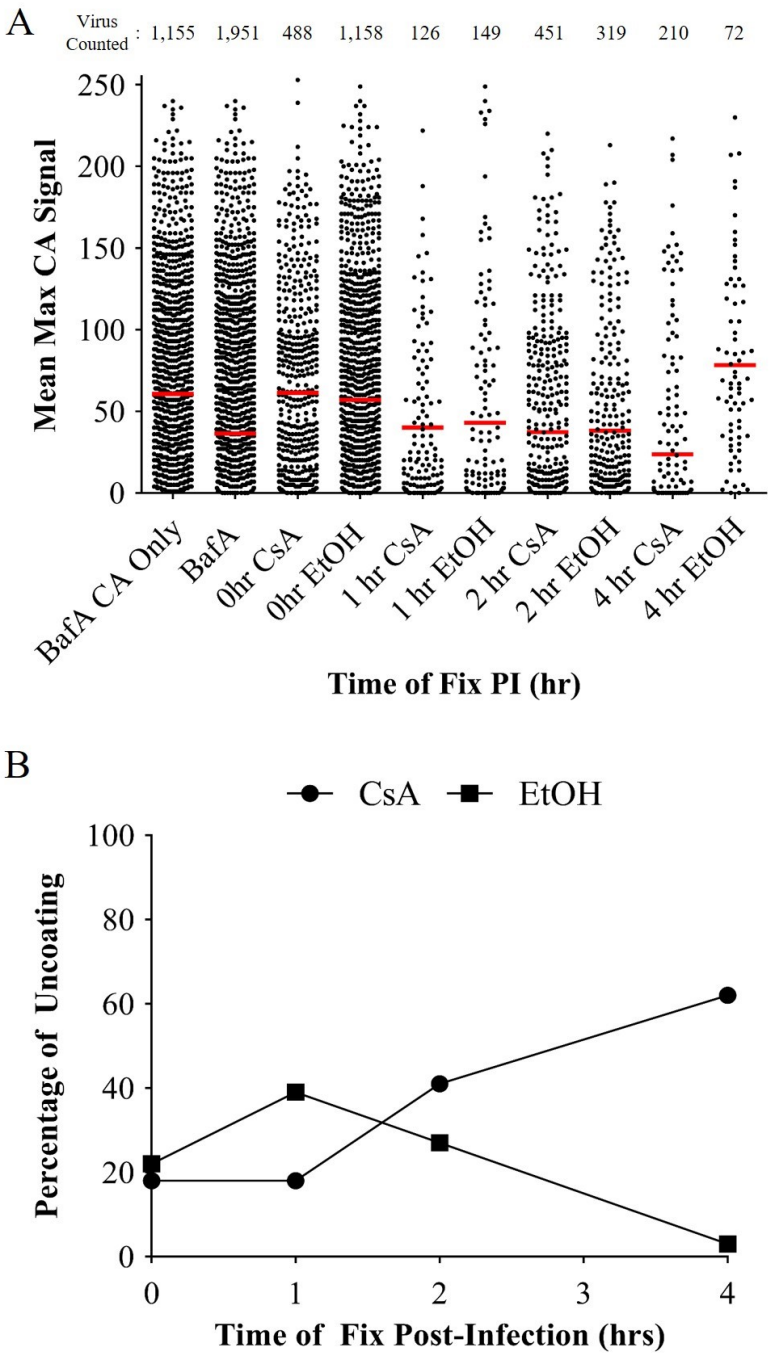

Figure 29. In Situ Uncoating Assay Results. Data shown is representative of an individual experiment. A) Cy5 signal intensity is represented as a scatter plot to assess uncoating. CA signal average is shown by the horizontal red bar. Value above each column indicates the total number of fused virions included for analysis. Pixel intensity for CA ranges from 0-255. B) Fused virions were sorted into coated or uncoated groups based on any Cy5 signal above 0 or virions with a signal of 0. Percentage of uncoating was calculated based on total fused virion counts for each image set.

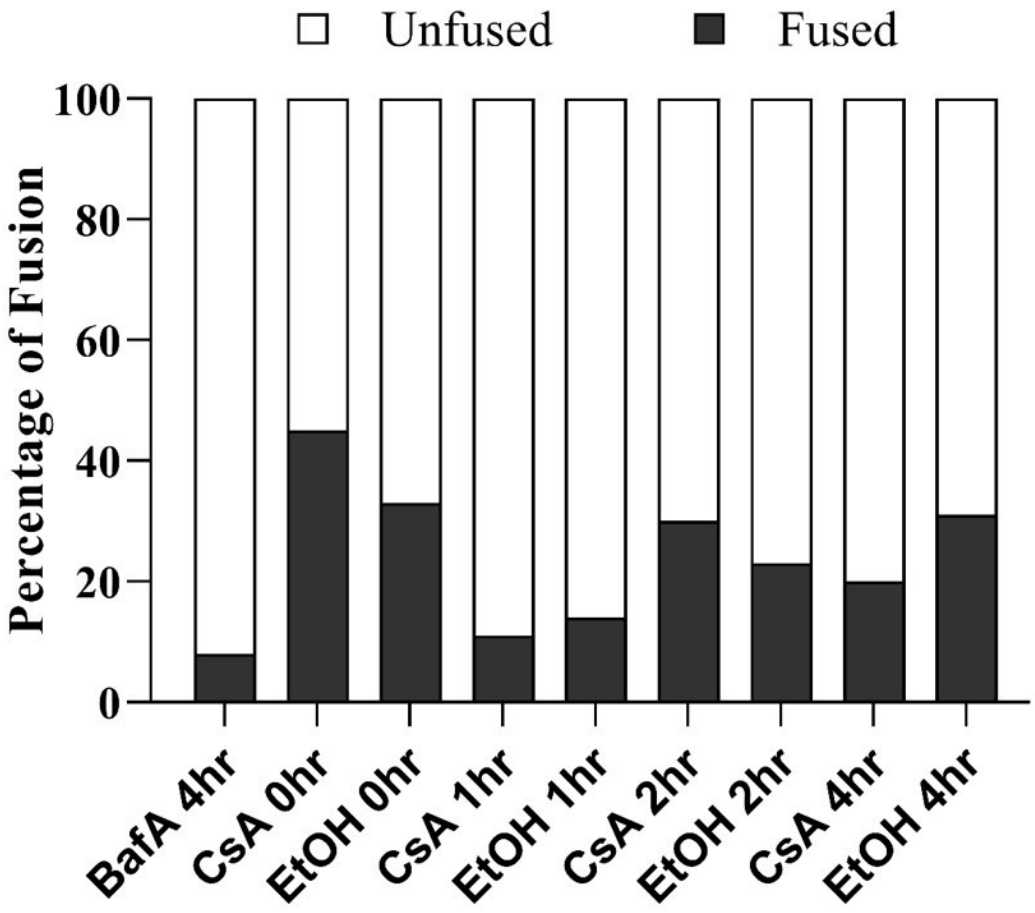

Figure 30. Representation of Fusion from the In Situ Uncoating Assay. As an additional verification of the In Situ Uncoating Assay data was analyzed for percentage of fused virions. Fused virions were then further sorted into coated or uncoated groups. Data shown represents one independent experiment. Percent of fusion at each time point is represented from the total number of particles analyzed. Data shown is representative of an individual experiment.

designed to amplify the unique U5-U3 junction apart of 2-LTR circles allow qPCR detection. In line with the early RT qPCR analysis using the Pfafll method, the 2-LTR primers used require a known primer efficiency for fold change calculation. A 5-point standard of plasmid containing the 2-LTR amplicon was serial diluted out and quantified as previously described (Figure 11C). Using the standard dilution Cq values an appropriate R2 value of 0.994 was achieved and the 2-LTR primer set was determined to have 80% amplification efficiency (Table 2). A Pfaffl efficiency was calculated at 1.80 for the purpose of quantifying relative fold change.

During previous qPCR analysis for early RT products low template number was a concern for failed experiments. 2-LTR circles are a byproduct formed in small quantities post-import (86). In addition, fewer viral complexes complete nuclear import over those that only complete reverse transcription. Due to the low number of 2-LTR circles formed a proper concentration of virus is needed for a detectable template number. To ensure that 2-LTR circles are detectable during qPCR HIV-GFP was serial diluted onto cells until 12 hours post-infection. Cell samples were harvested, extracted, and digested with DPN1 as previously described. A 1/8 dilution of HIV-GFP that was harvested at 0 hours post-infection served as a baseline for no 2-LTR products. Mock infected cells harvested at 12 hours post-infection were included as an additional negative control. Quantification of relative 2-LTR circles was carried out by comparing fold change to the 0-hour baseline. In doing so the accumulation of products at each dilution of virus could be assessed.

By plotting relative accumulation of products across the dilution series a concentration dependent increase in 2-LTR products was observed (Figure 31). At a 1/10 dilution of virus 2-LTR products only saw a negligible fold change increase of 1.26. In contrast, the 1/8 dilution resulted in a 4-fold increase over baseline at 4.09. Further, the ¼ dilution indicated a 2-fold

increase over the 1/8 dilution as expected for serial dilution. Lastly, 2-LTR products within this experiment reached a maximum at 1/2 dilution of virus at a 9.40-fold change relative to baseline (Table 12). Based on detectable products over background the 1/8 dilution was chosen for future experiments. In choosing a higher dilution of virus rather than the1/4 dilution the amount of stock virus needed was reduced per experiment.

Quantifying nuclear import. With virus concentration optimized for detection of 2-LTR product potential effects of CypA on nuclear import were tested by qPCR. Plated cells were infected by HIV-GFP in either constant CsA or ethanol containing media. Infection of CHME3 cells was carried out with cell harvesting at 0, 6, 12, and 24 hours post-infection to select for time-points within the expected window of nuclear import (79). Mock infected cells were included as a negative control to measure for contamination. Lastly, infected cells treated with constant NVP served as a no RT control. qPCR sample preparation was carried out by genomic DNA extraction and DPN1 digest. Early runs of the experiment failed to show a detectable increase in CsA treated samples (data not shown).

To ensure infection was progressing under CsA and ethanol treatment a troubleshooting experiment similar to the previously described Early RT troubleshooting assay was carried out. Cells were harvested at 0, 6, 12, and 24 hours post-infection while duplicate wells received NVP containing media to block further reverse transcription. A mock infected condition was included for qPCR and flow cytometry samples for background. Additionally, a set of well with virus received constant NVP treatment. Cell pellets were prepared for qPCR where the duplicate wells were harvested at 48 hours post-infection for Flow Cytometry. qPCR indicated an initial increase in products with ethanol treatment when fold change was calculated to the 0-hour time point. Interestingly, 2-LTR products under ethanol treatment peaked at 12 hours post-infection with

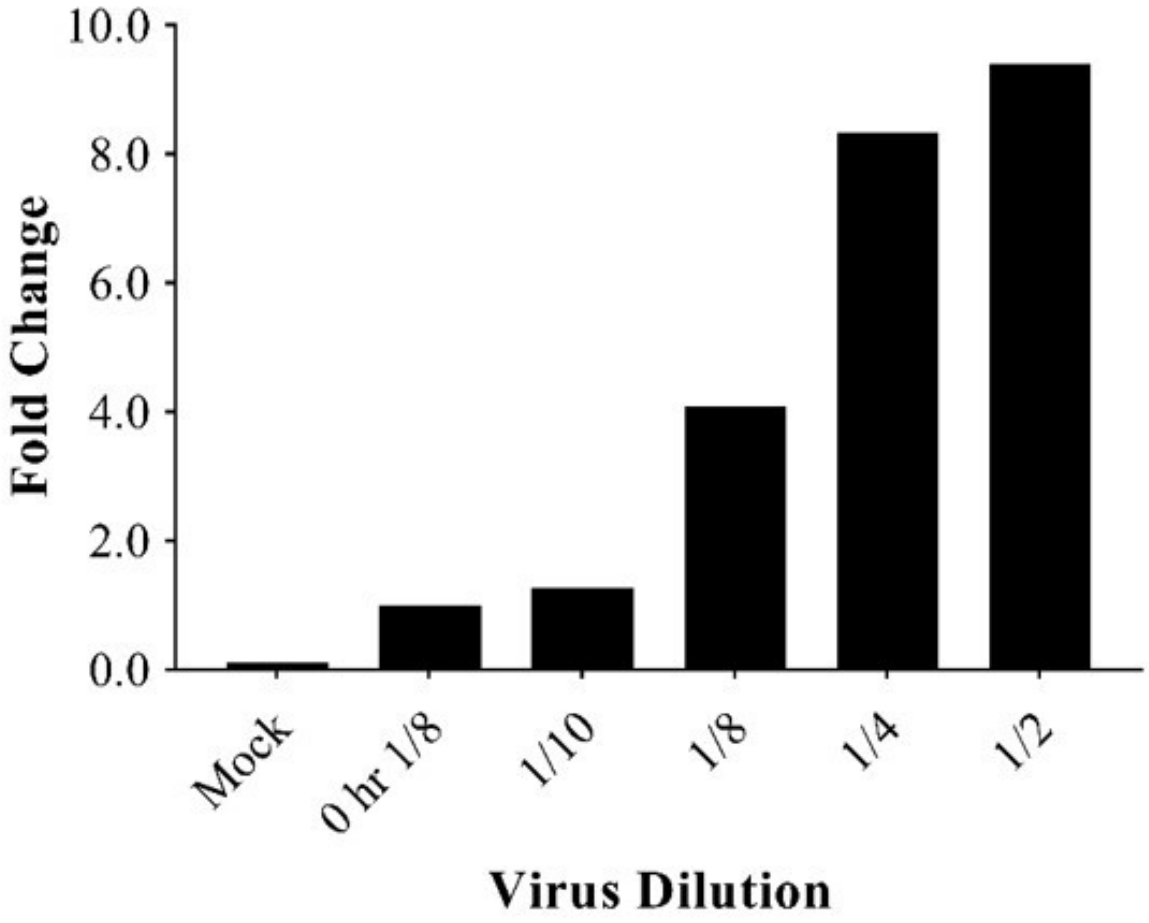

Figure 31. Serial Dilution of HIV for Optimized 2-LTR qPCR Detection. The 10/27/18 HIV-GFP stock was serial diluted to infect CHME3 cells. Cells were harvested at 24 hpi for qPCR quantification of 2-LTR products. A 0-hour control was included and harvested at 0 hpi. Relative accumulation of 2-LTR products was calculated through determining fold change of each dilution to the 0-hour control. All fold changes were normalized to a β-Actin housekeeping gene.

Table 12. Relative Fold Change of 2-LTR Products for Optimized Amplification

Virus Dilution	Fold Change Normalized
Mock	0.10
0 hr 1/8	1.00
1/10	1.26
1/8	4.09
1/4	8.34
1/2	9.40

relative product number decreasing at 24 hours post-infection (Figure 32A). In contrast, when CypA binding was disrupted an increasing trend in 2-LTR circles was not observed (Figure 32A). CsA treated cells with NVP addition at 0, 6, and 24 hours post-infection were then assessed by flow cytometry. Infectivity at 6- and 24-hours post infection increased over background indicating the progression of infection. While HIV infected the CsA treated cells the 24-hour time point only reached 14% GFP positive cells. The lower percentage of infection under CsA treatment has previously been observed in the CsA Addition data (Figure 8). Despite the progression of infection shown in the flow cytometry data the qPCR analysis failed to show an increasing trend (Figure 32A). Lower completion of nuclear import when CsA is present may result in low template number leading to a failure to detect subtle changes by qPCR.

With infection under ethanol and CsA treatment verified qPCR was carried out for 2-LTR circles. Following the completion of three independent experiments fold change values were combined for error analysis and statistical testing. The quantification of three individual experiments for 2-LTR circles was found to have a slight increase in nuclear import over time in the CsA treated samples. Ethanol treated samples demonstrated a higher fold change over the 24-analysis CsA treated cells were found to have a statistically significant decrease in 2-LTR hour time course likely indicative of increased levels of nuclear import. Upon products at 6, 12, and 24 hours post-infection relative to ethanol (Figure 33, Table 12). 2-LTR product accumulation was determined by calculating fold change relative to the 0-hour time point. (Table 13). A mixed ANOVA was carried out and found no significant differences. Since the sample size of these experiments is low effect size was calculated to estimate the magnitude of effect time has on product accumulation. Calculating Cohen's d for all time points relative to the mock condition revealed time to have a large to very large effect on product accumulation in CsA and ethanol

(Table 15, 16). Despite the lack of statistical significance, the large effect size estimated may suggest that were we to increase our sample size statistical significance would be detected.

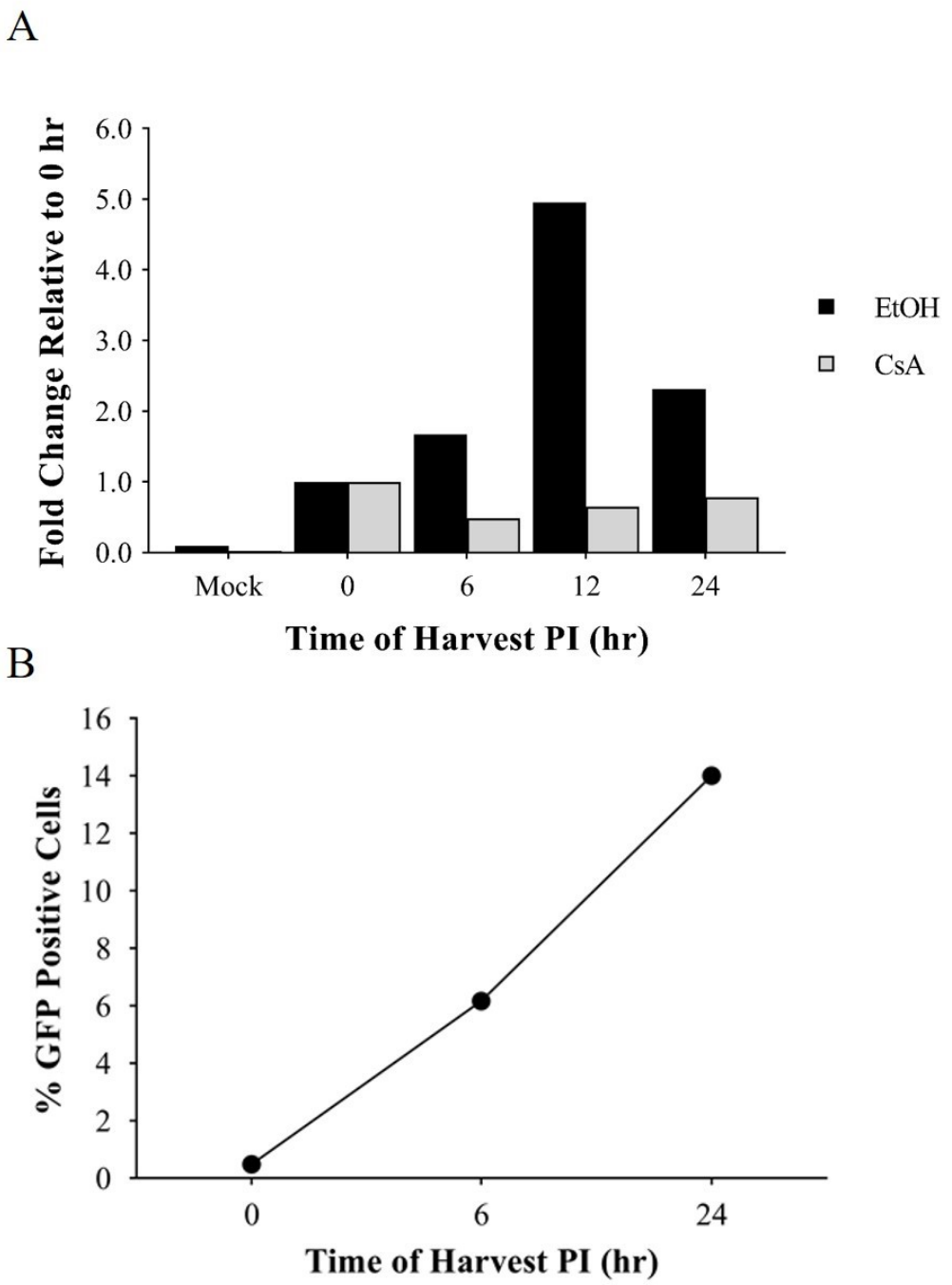

Figure 32. Verification of Infection by qPCR and Flow Cytometry. CHME3 cells were infected with a 1/8 dilution of HIV-GFP. A) Accumulation of 2-LTR products over time with CsA or ethanol containing media. Cells were infected in the presence of CsA or ethanol and harvested at each time point. The number of 2-LTR products relative to the 0 hr time point was determined by qPCR. B) Percentage of GFP positive CHME3 cells as a measure of end point infectivity. CHME3 cells were infected with constant CsA treatment. NVP was added for each time point with infection progression to 48 hpi.

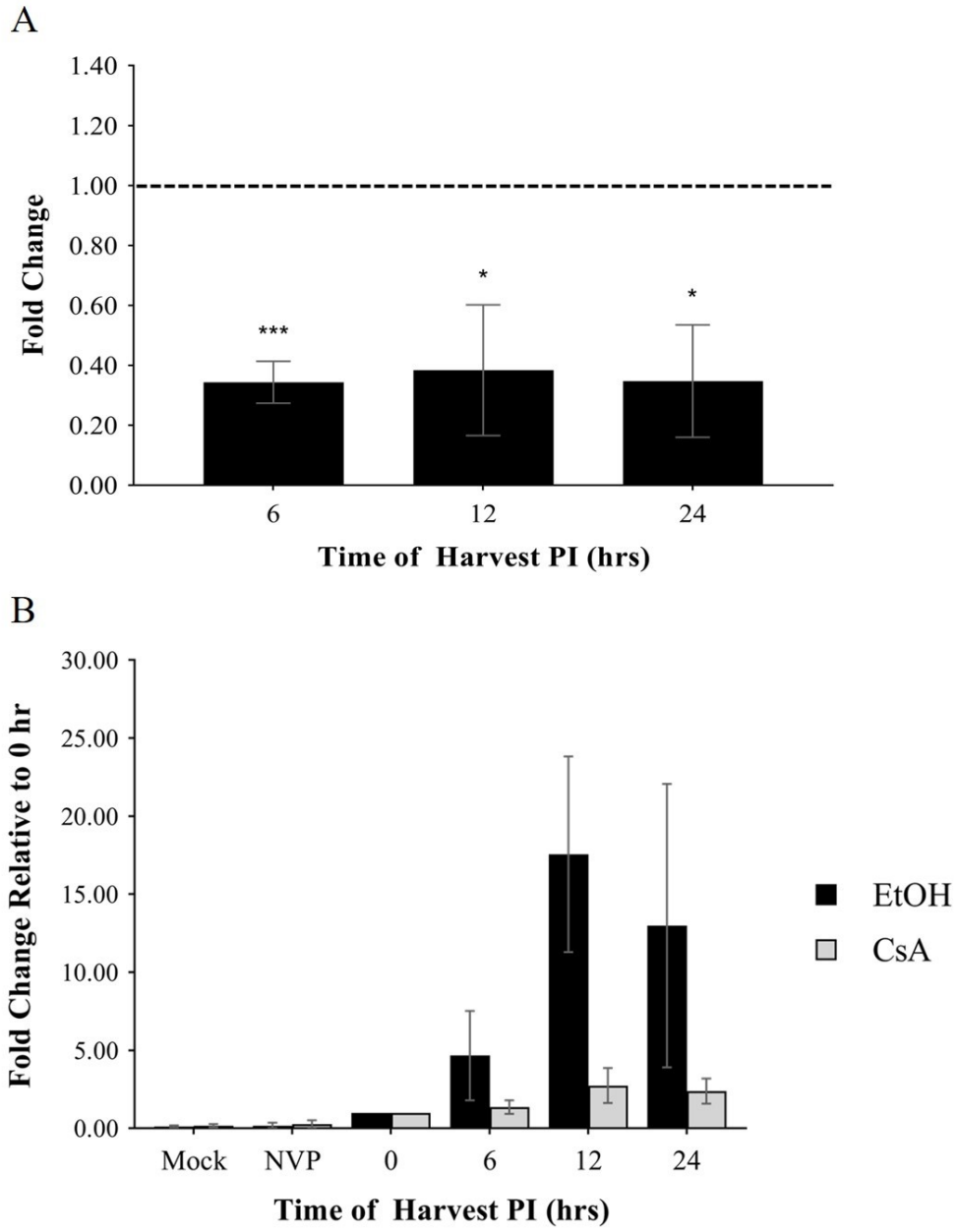

Figure 33. Quantification of Nuclear Import with CsA or Ethanol Treatment. CHME3 cells underwent infection with a 1/8 dilution of HIV-GFP in the presence of CsA or ethanol. Cell pellets were harvested at each time point followed by qPCR for 2-LTR products. Error bars represent ±SEM. Representative experiments from three independent experiments A) 2-LTR circle fold change ratio between of CsA relative to ethanol. Fold change was normalized to a β-Actin housekeeping gene. Statistical significance was determined by a Student T-test for each time point. *, $P < 0.05$, **, $P < 0.01$, ***, $P < 0.001$. B) Representation of 2-LTR accumulation over time under CsA or ethanol treatment. Relative fold change calculated by normalizing each time point to the 0-hour condition. A mixed ANOVA was carried out to detect statistical significance between group means. *, $P < 0.05$

Table 13. 2-LTR CsA/Ethanol Fold Change Ratio

Time of Harvest (hr)	Fold Change
6	0.34
12	0.38
24	0.35

Table 14. 2-LTR Fold Change Relative to 0-Hour Timepoint

Condition	CsA Fold Change	EtOH Fold Change
Mock	0.17	0.11
NVP	0.27	0.11
0 Hour	1.00	1.00
6 Hour	1.35	4.66
12 Hour	2.74	17.56
24 Hour	2.39	12.99

Table 15. Effect Size of Time on 2-LTR Accumulation in Ethanol

Variables		Cohen's d
Mock	NVP	-0.20
Mock	Hour 6	-1.29
Mock	Hour 12	-2.27
Mock	Hour 24	-1.15

Table 16. Effect Size of Time on 2-LTR Accumulation in CsA

Variables		Cohen's d
Mock	NVP	-0.20
Mock	Hour 6	-1.29
Mock	Hour 12	-2.27
Mock	Hour 24	-1.15

DISCUSSION

Synopsis

HIV infection of parenchymal microglial cells contributes to HIV associated neurocognitive disorders (11). Despite the clear relevance in HIV replication host-protein interactions are understudied within this cell type. Previously unpublished work has demonstrated that cyclophilin A (CypA) enhances endpoint infectivity in the CHME3 human microglial cell line. Here we have characterized the role of CypA in early HIV replication steps in the CHME3 cell line. Utilizing cell based, qPCR, and microscopy methods the effect of CypA on reverse transcription, uncoating, and nuclear import was assessed.

Reverse Transcription

By using the Nevirapine (NVP) Addition Assay the enhancement of reverse transcription by CypA was characterized. In this experiment decreases in infectivity correlate directly with the completion of reverse transcription. Completed reverse transcription was not detectable until two hours post-infection in either CsA or ethanol treatments. At 3, 4, 6, and 8 hours post-infection completed reverse transcription was significantly lower when CypA binding was blocked with CsA (Figure 18). Notably, completed reverse transcription under ethanol treatment resulted in 23% infectivity by 3 hours post-infection while CsA treatment was reported at 7.94%. At all time points beyond two hours post-infection CypA disruption corresponded with a >20% infectivity decrease compared to the vehicle control. The significant increase in reverse transcription when CypA can bind to the capsid indicates CypA enhances some aspect of reverse transcription. Previous work in the Jurkat T cell line has indicated a loss of CypA binding lowers reverse

transcription success (73). Importantly, use of the NVP Addition Assay alone is unable to differentiate an effect on early or late reverse transcription instead only measuring reverse transcription completion.

Early and late reverse transcription was uncoupled by the detection of early RT products by qPCR. Within the first two hours of infection disruption of CypA was found to have no effect on early reverse transcription. However, at 4- and 12- hours post-infection CypA disruption led to a significant decrease in products with a fold change of 0.70 and 0.51, respectively (Figure 17A). A decrease in later time points was also observed when tracking the RT accumulation up to 12 hours post-infection. Ethanol treated cells indicated an increasing trend of RT products that peaked at 12 hours-post infection. A gradual increase in RT products overtime is expected as replication progresses, and viral DNA accumulates. In contrast, disruption of CypA binding was associated with RT products peaking at 2 hours post-infection before remaining constant up to 12 hours. These data suggest that early reverse transcription is not detectably altered by CypA binding before 2 hours post-infection.

As shown in the NVP addition assay reverse transcription completion is detectable primarily past two hours post-infection. It is then expected that the first two hours of infection represent early reverse transcription. Over time late RT transcripts are generated marking the end of reverse transcription. Surprisingly, we found an agreement between our NVP addition assay and early RT qPCR data. Quantification of early RT products includes primers that target the R U5 sequence. At the onset of transcription, the R U5 region is unique to the early DNA product allowing specific detection. However, as reverse transcription proceeds a second R U5 sequence is introduced into the full-length DNA strand (Figure 3). Thus, as reverse transcription proceeds the detection of early RT products becomes less sensitive as late RT products are produced.

Within the early RT qPCR experiments no difference was found until beyond 2 hours post-infection. Importantly, completed reverse transcription was observed after 2 hours post-infection in the NVP Addition Assay, which aligns with the decrease in R U5 products. The later decrease then likely represents reduced completion of a later step in reverse transcription. Based on these findings CypA enhances late reverse transcription in the CHME3 microglial cell line and not early reverse transcription.

Uncoating

Considering that no direct interaction of CypA with the reverse transcription complex (RTC) has been identified the enhancement of reverse transcription may be indirect. During early replication the capsid protects the RTC from detection and degradation (32, 88) It is possible that alterations to uncoating kinetics would expose the RTC to proteasomal degradation and cytosolic sensors thereby explaining a decrease in products. To detect any changes in uncoating kinetics the In Situ Uncoating Assay was utilized. Signal intensities within treatments were first assessed to ensure that CsA and ethanol indicated a decreasing signal intensity from 0 to 4 hours post-infection. Uncoating in CsA containing media followed the expected trend with the 0-hour signal intensity at a maximum of 52.66 that decreased to 23.73 by 4 hours post-infection (Figure 29). Conversely, the ethanol signal intensity began at 41.99 at 0 hours post-infection before decreasing to 29.79 by 1 hour and increasing to 77.20 by 4 hours post-infection. The erratic change in intensity under ethanol treatment was unexpected as virions should see increasing uncoating overtime.

An alternative analysis of these data was carried out by grouping fused virions into uncoated or coated groups based on the lack or presence of any signal. Quantifying the

percentage of uncoating irrespective of CA intensity revealed an increase in uncoating under CsA treatment up to 4 hours post-infection (Figure 29B). Again, ethanol treated cells failed to show progressive uncoating with only 3% of the remaining virions uncoated at 4 hours post-infection. These discrepancies may indicate the corresponding data is not reliable and that replicate experiments are needed with increasing trends for CsA and ethanol.

Despite the unexpected uncoating trend in ethanol containing media the potential effect of CypA on uncoating was then investigated. Capsid intensity based on the mean max fluorescence of Cy5 was compared between CsA and ethanol at each timepoint. At 0- and 1-hour post-infection CsA CA signal was recorded as slightly increased over ethanol with 52.66 and 40.02 relative to 41.99 and 29.79. The observed increase may be negligible considering that the 0-hour time point was initially higher despite identical volumes of HIV per well. Differences between CsA and ethanol decreased at 2 hours post-infection with a difference of 1.64 between CA signal averages. A smaller difference between CsA and ethanol may suggest a similar level of capsid associated with fused virions at 2 hours post-infection. Unexpectedly, at 4 hours post-infection CA signal in ethanol containing media dramatically increased to 77.20 while CsA CA signal decreased to 23.73 (Figure 29A). By 4 hours post-infection we anticipated that CA signal would be at a minimum as observed with CsA treatment, but ethanol treatment corresponded with an opposite result.

It is important to note that during imaging of the 4-hour ethanol coverslip few cells remained adhered resulting in a lower particle count of 71 fused virions. Further, the 4-hour ethanol condition indicates a maximum signal at 77.2 above all other conditions. A maximum intensity at 4-hour post-infection is surprising as a decrease in CA overtime is expected as capsids uncoat. High CA intensity at 4 hours post-infection may be explained if the remaining

population of virions represent hyperstable capsid. As uncoating proceeds fluorophore labelled Vpr is lost due to protease and proteasomal mediated degradation (89). A low virion count in tandem with hyperstable capsids may be shifting the CA signal average to a higher value. Based on the distribution of CA signal a clustering of 0 and near 0 CA signal is present in all conditions except the 4-hour ethanol timepoint. Therefore, it is possible that with a higher sample size the signal intensity may lower as the uncoated population is detected.

Further optimization of the In Situ Uncoating Assay may come in the form of altering the viral marker used. In the work shown here GFP-Vpr represented post-fusion cores allowing assessment of colocalized CA stain for uncoating. Proper visualization of the RTC requires Vpr to remain associated during early replication prior to and post-uncoating. A concern with the continued use of GFP-Vpr is that Vpr may not remain associated with the RTC post-fusion. Researchers studying the import of YFP-Vpr found a loss of signal that was not dependent with capsid stability and may suggest rapid dissociation of Vpr from post-fusion cores (90). In the In Situ Uncoating Assay this would prove problematic as GFP-Vpr that dissociate from intact capsid could be erroneously recorded as an uncoated virus. To avoid poor colocalization of the viral marker GFP tagged Integrase (IN) could utilized in place of GFP-Vpr. IN remains associated with the RTC as well as the pre-integration complex (PIC) during early replication thereby solving the potential concerns of core dissociation. Future experiments would require dual-labelled viral stocks prepared with a IN-GFP containing plasmid and colocalization validation prior to carrying out the In Situ Uncoating Assay.

A key limitation of the In Situ Uncoating data shown in this work is that three independent experiments have yet to be completed. Due to time constraints stemming from troubleshooting and optimization only one experiment was successfully completed. Without

multiple replicates and statistical testing preliminary data cannot be used to draw strict conclusions. It is possible that discrepancies apparent within the individual run will be lost with further replicates. If the ethanol 4-hour timepoint demonstrates consistently high CA signal this unexpected finding will need to be addressed further.

In the current experiment shown the 0, 1, 2, and 4-hour time points were selected to include relevant windows for uncoating. In hindsight, future experiments may benefit from the inclusion of a 3-hour time point. At 3 hours post-infection in the NVP Addition Assay a significant decrease in the completion of reverse transcription is seen when CypA cannot bind to the capsid (Figure 18). The decrease in reverse transcription indicates CypA alters replication by at least 3 hours post-infection. Therefore, the inclusion of a 3-hour time point in the In Situ Uncoating Assay may provide vital information regarding altered uncoating.

During the process of optimizing the In Situ Uncoating Assay the approach to data analysis was addressed through development of a semi-automatic counting protocol in FIJI. The goal in designing this new workflow was to expedite data analysis while removing bias introduced through manual counting. Here we have established a simple protocol to automatically threshold images and carry out particle analysis. Time of analysis was significantly reduced using the semi-automatic method. Further, the automation of thresholding and particle counting is expected to increase detection sensitivity. Dual-labelled virus verification benefitted from the described protocol with relatively quick quantification of >1,000 particles (Figure 28). Completion of the semi-automatic protocol marks a key optimization of the In Situ Uncoating Assay. The time of analysis may be further reduced with the use of FJIJ integrated scripts. By scripting the FIJI dependent steps for analysis navigating software menus and applying settings could potentially be minimized to several button presses.

Without the completion of the In Situ Uncoating Assay our current hypothesis, that uncoating is the primary step altered by CypA, cannot be verified. At this time reverse transcription appears to be the earliest step enhanced by CypA interaction. However, loss of capsid structure could expose the RTC to protease and proteasomal degradation. Treatment with MG132, a protease and proteasomal inhibitor, has been shown to increase infectivity (91). Fluorophore labelled-Vpr signal is rapidly lost post-uncoating in live cell imaging experiments with proteasomal inhibition leading to the accumulation of GFP punctate (89, 91). In addition, GFP-labelled virus associated with the nucleus in higher numbers upon MG132 treatment (91).

While the completion of the In Situ Uncoating Assay experiments are priority investigating how CypA enhances reverse transcription may help verify our hypothesis. If capsids on average uncoat more rapidly in absence of CypA binding degradation of these products would explain decreased RT completion. To investigate if proteasomal degradation is responsible for the decrease in RT products MG132 can be used to identify notable differences under CsA and ethanol conditions. The time of pretreatment of cells with MG132 and working concentrations vary between cell lines and across publications. To ensure that a proper concentration is selected to avoid cell death a serial dilution of MG132 could be carried out on plated CHME3 cells with varying times of pretreatment. Cell death could then be assessed quickly and inexpensively with Trypan Blue. Trypan Blue, which is an organic dye, is unable to pass the cell membrane. Cell death is visible as Trypan Blue stains the cytoplasmic contents of cells with disrupted cell membranes allowing for cell death to be assessed. The percentage of cell death could then be quantified by counting total and dead cell number using a hemocytometer. Once an appropriate working concentration is selected a basic viral titration would be carried out in CsA and ethanol with either DMSO as a vehicle control or MG132. If MG132 rescues

infectivity to a larger extent under CsA treatment relative compared to ethanol, then RT and uncoating focused experiments would be justified with MG132.

Nuclear Import

Interaction between the pre-integration complex (PIC) and host proteins are required in facilitating nuclear import (43, 50, 92). Therefore, we investigated if CypA influenced nuclear import success. Relative amounts of 2-LTR circles were quantified by qPCR as a marker for nuclear import under CsA and ethanol treatment. Assessment of CypA binding on nuclear import revealed that blocking CypA binding led to significantly decreased nuclear import. At 6, 12, and 24 hours post-infection 2-LTR fold change decreased to 0.34, 0.38, and 0.35 relative to the vehicle control (Figure 33A). Under both CsA and ethanol treatment 2-LTR circles accumulated up to 12 hours-post infection before decreasing at 24 hours. (Figure 33B). Infection of CHME3 cells in ethanol resulted in a maximum fold increase to 17.56 above background. CsA treated infection demonstrated attenuated nuclear import with a maximum 2.74-fold increase over background. Similar experiments in the Jurkat T cell line have also shown a comparable decrease in nuclear import when CypA cannot bind (1).

While CypA may exert a direct effect on nuclear import the decrease in RT products may have downstream implications for nuclear import. An overall decrease in viral DNA would be expected to lower the number of pre-integration complexes undergoing nuclear import. Subsequent decreases in linear DNA would then result in decreased 2-LTR circle formation. In addition, the loss of the DNA flap lowers import success (26). Therefore, based on the experiments carried out here we cannot firmly conclude that nuclear import is the primary step altered by CypA.

Limitations and Future Experiments

Throughout this work the disruption of CypA binding was carried out through including cyclosporine A (CsA) within cell media. The competitive binding of CsA functionally prevents CypA binding to HIV CA making the described experiments possible (3, 59, 69). However, the inclusion of any drug includes off-target effects. CsA is an immunosuppressive drug and is known to bind indiscriminately to other cyclophilins (59, 61, 62). Therefore, we cannot account for off-target effects that could be influencing the data shown here. Alternative experiments exist to disrupt CypA binding, but within the scope of this work were not carried out due to time constraints.

To strengthen the findings shown here the knockdown of endogenous CypA could be used to verify our data. The design of a short-hairpin RNA (shRNA) containing vector would allow specific targeting of the CypA mRNA sequence. Once bound the transcript forms a hairpin that is recognized and degraded by the DICER/RISC complex (93). By utilizing shRNA knockdown, the presence of CypA protein can be depleted allowing for absence of CypA to be assessed. A strength of knocking down CypA is that off-target effects of the shRNA can be accounted for with an add back experiment. Careful design of the shRNA can allow for CypA to be reintroduced post-knockdown. Transfection of a vector containing a non-targetable CypA mRNA would allow exogenous expression functionally adding back CypA. Typically, this is carried out through altering wobble bases to maintain amino acid sequences but prevent shRNA recognition. Alternatively, CypA expression can be restored by a vector lacking the 3' UTR region if the shRNA targets the 3' UTR sequence on endogenous CypA mRNA. Off-target effects on the cell can be fully avoided using capsid mutants unable to bind CypA. Mutations to key residues at the CypA binding loop, consisting of HAGPIA, attenuate or prevent association

with CypA (64, 3). Well characterized capsid mutants P90A and G89V have been used to validate decreases in replication upon CsA treatment (94, 73). Infection of the CHME3 cell line with WT and P90A virus in CsA or ethanol would allow for an additional experiment to validate our findings.

Recent work has proposed a new model for CypA enhancement of HIV replication in which CypA binding physically blocks Trim5α from restricting infection at uncoating. Trim5α restriction is linked directly to the formation of hexagonal Trim5α nets around intact capsids leading to premature uncoating (40). Capsid dependent HIV restriction is also observed in owl world monkeys through Trim-Cyp by a similar mechanism, though relying on a retrotransposed CypA for capsid binding (95). In this study loss of CypA binding led to decreased infectivity in primary human blood cells that was rescued upon knockdown of Trim5α (96). Our current hypothesis proposes that CypA enhances infectivity of microglial cells through acting on the capsid in some way. With the newly established model for CypA and Trim5α interplay investigating the reported interaction in microglial cells will help to potentially strengthen this model. If knockdown of Trim5α in the CHME3 cell line were to restore infectivity in the presence of CsA we could verify the Trim5α-CypA dependent restriction. Alternatively, Trim5α and CypA have been identified to influence infectivity independently in the CEM-SS and TE671 cancer cell lines (97). While the use of cancer cell lines may not prove the best representation for HIV infectivity the CEM-SS cell line is derived from a T cell lineage. Comparison of the immortalized CHME3 cell line to CEM-SS cells may reveal that Trim5α and CypA function independently in early infection if Trim5α knockdown does not alter infection.

With the characterization of the CypA-HIV interaction in the CHME3 cell line the complete mechanism of CypA enhanced HIV is still not understood. In this work HIV with wild

type CA was assessed for altered replication. While studying wildtype CA does provide insight into host-protein interactions research regarding mutant CA can also reveal interesting findings. One such capsid mutant is the AC-1 CA in which the V86I, I91L, A92P, P93A, and M96L mutations are present within the CypA binding loop region. AC-1 was initially characterized with a higher affinity for CypA relative to WT CA that failed to efficiently infect dendritic cells, monocytes, and CD4+ T cells (88, 98). A significant decrease in nuclear import was identified without decreases in reverse transcription. Interestingly, the restriction of AC-1 was relieved upon CsA treatment or shRNA knockdown of CypA. Researchers identified the inner nuclear membrane protein SUN2 as a key protein in restriction of AC-1 as knockdown of SUN2 negated the CypA dependent restriction (98).

Contrary to these findings' others have reported that SUN2 influences infection independently of CypA in CD4+ T cells (99). Knockdown of SUN2 was shown to decrease infectivity regardless of CypA binding or disruption and instead each protein altered infection in an additive manner. AC-1 was not assessed in this work leaving the SUN2 dependence of AC-1 unexplained. Lastly, altering expression levels of SUN2 does raise some concerns as SUN2 represent a vital component of the Linker of Nucleoskeleton and Cytoskeleton (LINC) complex and influences nuclear envelope structure. In the CHME3 cell line overexpression of SUN2 drastically deformed nuclei and blocked infection (100).

Considering the AC-1 capsid mutant demonstrates a CypA dependent restriction the study of AC-1 may provide new insight into the CypA-CA interaction. To characterize AC-1 in the CHME3 cell line confirmation of restriction when CypA binds is needed. A simple viral titration in CsA or ethanol containing media would allow for infectivity to be quantified. Assuming CypA binding correlates with restriction reverse transcription, uncoating, and nuclear

import could then be assessed as shown in this work. If AC-1 is restricted in the CHME3 cell line this could suggest that a secondary factor in the cellular environment is responsible for AC-1 restriction. In addition, SUN2 knockdown could be carried out allowing for support or refutation of the previously proposed model.

Conclusion

Here we have characterized the role of CypA in the CHME3 microglial cell line. In agreement with past work CypA was found to enhance reverse transcription and nuclear import. Using alternative assays for quantifying reverse transcription we were able to demonstrate that CypA does not detectably alter initial reverse transcription, but rather a later step of reverse transcription. Unfortunately, the role of CypA in uncoating kinetics has not been fully established however replicate experiments are planned to identify any changes in uncoating. The establishment of the semi-automatic FIJI counting protocol will prove useful over the course of these future experiments. Lastly, nuclear import was shown to decrease upon disrupting CypA binding to CA. However, with the observed decrease in reverse transcription we cannot definitively conclude that nuclear import is the primary step effected. By characterizing the CypA-CA interaction in CHME3 cells this work establishes a starting point for future research in microglial cells to elucidate a concise mechanism.

REFERENCES

1. Heaton RK, Clifford DB, Franklin DR Jr, Woods SP, Ake C, Vaida F, Ellis RJ, Letendre SL, Marcotte TD, Atkinson JH, Rivera-Mindt M, Vigil OR, Taylor MJ, Collier AC, Marra CM, Gelman BB, McArthur JC, Morgello S, Simpson DM, McCutchan JA, Abramson I, Gamst A, Fennema-Notestine C, Jernigan TL, Wong J, Grant I, CHARTER Group. 2010. HIV-associated neurocognitive disorders persist in the era of potent antiretroviral therapy: CHARTER Study. Neurology 75:2087–2096.

2. Braaten D, Luban J. 2001. Cyclophilin A regulates HIV-1 infectivity, as demonstrated by gene targeting in human T cells. EMBO J 20:1300–1309.

3. Gamble TR, Vajdos FF, Yoo S, Worthylake DK, Houseweart M, Sundquist WI, Hill CP. 1996. Crystal structure of human cyclophilin A bound to the amino-terminal domain of HIV-1 capsid. Cell 87:1285–1294.

4. Bosco DA, Eisenmesser EZ, Pochapsky S, Sundquist WI, Kern D. 2002. Catalysis of cis/trans isomerization in native HIV-1 capsid by human cyclophilin A. Proc Natl Acad Sci U S A 99:5247–5252.

5. Wedemeyer WJ, Welker E, Scheraga HA. 2002. Proline Cis−Trans Isomerization and Protein Folding. Biochemistry 41:14637–14644.

6. Filipowicz AR, McGary CM, Holder GE, Lindgren AA, Johnson EM, Sugimoto C, Kuroda MJ, Kim W-K. 2016. Proliferation of Perivascular Macrophages Contributes to the Development of Encephalitic Lesions in HIV-Infected Humans and in SIV-Infected Macaques. Sci Rep 6:32900.

7. Lopez-Atalaya JP, Askew KE, Sierra A, Gomez-Nicola D. 2018. Development and maintenance of the brain's immune toolkit: Microglia and non-parenchymal brain macrophages. Dev Neurobiol 78:561–579.

8. Persidsky Y, Stins M, Way D, Witte MH, Weinand M, Kim KS, Bock P, Gendelman HE, Fiala M. 1997. A model for monocyte migration through the blood-brain barrier during HIV-1 encephalitis. J Immunol 158:3499–3510.

9. Fan Y, He JJ. 2016. HIV-1 Tat Induces Unfolded Protein Response and Endoplasmic Reticulum Stress in Astrocytes and Causes Neurotoxicity through Glial Fibrillary Acidic Protein (GFAP) Activation and Aggregation. J Biol Chem 291:22819–22829.

10. Eugenin EA, Clements JE, Zink MC, Berman JW. 2011. Human immunodeficiency virus infection of human astrocytes disrupts blood-brain barrier integrity by a gap junction-dependent mechanism. J Neurosci 31:9456–9465.

11. Chen NC, Partridge AT, Sell C, Torres C, Martín-García J. 2017. Fate of microglia during HIV-1 infection: From activation to senescence? Glia 65:431–446.

12. Lull ME, Block ML. 2010. Microglial activation and chronic neurodegeneration. Neurotherapeutics 7:354–365.

13. Antinori A, Arendt G, Becker JT, Brew BJ, Byrd DA, Cherner M, Clifford DB, Cinque P, Epstein LG, Goodkin K, Gisslen M, Grant I, Heaton RK, Joseph J, Marder K, Marra CM, McArthur JC, Nunn M, Price RW, Pulliam L, Robertson KR, Sacktor N, Valcour V, Wojna VE. 2007. Updated research nosology for HIV-associated neurocognitive disorders. Neurology 69:1789–1799.

14. Ances BM, Hammoud DA. 2014. Neuroimaging of HIV-associated neurocognitive disorders (HAND). Curr Opin HIV AIDS 9:545–551.

15. Vanhamel J, Bruggemans A, Debyser Z. 2019. Establishment of latent HIV-1 reservoirs: what do we really know? J Virus Erad 5:3–9.

16. Chan DC, Fass D, Berger JM, Kim PS. 1997. Core structure of gp41 from the HIV envelope glycoprotein. Cell 89:263–273.

17. Stine GJ. 2014. AIDS update 2014: an annual overview of acquired immune deficiency syndrome. McGraw-Hill. NY, NY.

18. McDonald D, Vodicka MA, Lucero G, Svitkina TM, Borisy GG, Emerman M, Hope TJ. 2002. Visualization of the intracellular behavior of HIV in living cells. J Cell Biol 159:441–452.

19. Jones KA, Kadonaga JT, Luciw PA, Tjian R. 1986. Activation of the AIDS retrovirus promoter by the cellular transcription factor, Sp1. Science 232:755–759.

20. Furtado MR, Callaway DS, Phair JP, Kunstman KJ, Stanton JL, Macken CA, Perelson AS, Wolinsky SM. 1999. Persistence of HIV-1 transcription in peripheral-blood mononuclear cells in patients receiving potent antiretroviral therapy. N Engl J Med 340:1614–1622.

21. Campbell EM, Hope TJ. 2015. HIV-1 capsid: the multifaceted key player in HIV-1 infection. Nat Rev Microbiol 13:471–483.

22. Ganser BK, Li S, Klishko VY, Finch JT, Sundquist WI. 1999. Assembly and analysis of conical models for the HIV-1 core. Science 283:80–83.

23. Sundquist WI, Kräusslich H-G. 2012. HIV-1 assembly, budding, and maturation. Cold Spring Harb Perspect Med 2:a006924.

24. Hughes SH. 2015. Reverse Transcription of Retroviruses and LTR Retrotransposons. Microbiol Spectr 3:MDNA3–0027–2014.

25. Coffin JM, Hughes SH, Varmus HE. 1999. Retroviruses. CSHL Press.

26. Zennou V, Petit C, Guetard D, Nerhbass U, Montagnier L, Charneau P. 2000. HIV-1 genome nuclear import is mediated by a central DNA flap. Cell 101:173–185.

27. Gitti RK, Lee BM, Walker J, Summers MF, Yoo S, Sundquist WI. 1996. Structure of the amino-terminal core domain of the HIV-1 capsid protein. Science 273:231–235.

28. Gamble TR, Yoo S, Vajdos FF, von Schwedler UK, Worthylake DK, Wang H, McCutcheon JP, Sundquist WI, Hill CP. 1997. Structure of the carboxyl-terminal dimerization domain of the HIV-1 capsid protein. Science 278:849–853.

29. Manocheewa S, Swain JV, Lanxon-Cookson E, Rolland M, Mullins JI. 2013. Fitness costs of mutations at the HIV-1 capsid hexamerization interface. PLoS One 8:e66065.

30. Ganser-Pornillos BK, Cheng A, Yeager M. 2007. Structure of full-length HIV-1 CA: a model for the mature capsid lattice. Cell 131:70–79.

31. Hulme AE, Kelley Z, Okocha EA, Hope TJ. 2015. Identification of capsid mutations that alter the rate of HIV-1 uncoating in infected cells. J Virol 89:643–651.

32. Forshey BM, von Schwedler U, Sundquist WI, Aiken C. 2002. Formation of a human immunodeficiency virus type 1 core of optimal stability is crucial for viral replication. J Virol 76:5667–5677.

33. Márquez CL, Lau D, Walsh J, Shah V, McGuinness C, Wong A, Aggarwal A, Parker MW, Jacques DA, Turville S, Böcking T. 2018. Kinetics of HIV-1 capsid uncoating revealed by single-molecule analysis. eLife 7:e34772

34. Xu H, Franks T, Gibson G, Huber K, Rahm N, Strambio De Castillia C, Luban J, Aiken C, Watkins S, Sluis-Cremer N, Ambrose Z. 2013. Evidence for biphasic uncoating during HIV-1 infection from a novel imaging assay. Retrovirology 10:70.

35. Fassati A, Goff SP. 2001. Characterization of intracellular reverse transcription complexes of human immunodeficiency virus type 1. J Virol 75:3626–3635.

36. Miller MD, Farnet CM, Bushman FD. 1997. Human immunodeficiency virus type 1 preintegration complexes: studies of organization and composition. J Virol 71:5382–5390.

37. Dismuke DJ, Aiken C. 2006. Evidence for a functional link between uncoating of the human immunodeficiency virus type 1 core and nuclear import of the viral preintegration complex. J Virol 80:3712–3720.

38. Campbell EM, Perez O, Melar M, Hope TJ. 2007. Labeling HIV-1 virions with two fluorescent proteins allows identification of virions that have productively entered the target cell. Virology 360:286–293.

39. Hulme AE, Perez O, Hope TJ. 2011. Complementary assays reveal a relationship between HIV-1 uncoating and reverse transcription. Proc Natl Acad Sci U S A 108:9975–9980.

40. Ganser-Pornillos BK, Chandrasekaran V, Pornillos O, Sodroski JG, Sundquist WI, Yeager M. 2011. Hexagonal assembly of a restricting TRIM5alpha protein. Proc Natl Acad Sci U S A 108:534–539.

41. Pawlica P, Berthoux L. 2014. Cytoplasmic dynein promotes HIV-1 uncoating. Viruses 6:4195–4211.

42. Lukic Z, Dharan A, Fricke T, Diaz-Griffero F, Campbell EM. 2014. HIV-1 uncoating is facilitated by dynein and kinesin 1. J Virol 88:13613–13625.

43. Bouyac-Bertoia M, Dvorin JD, Fouchier RA, Jenkins Y, Meyer BE, Wu LI, Emerman M, Malim MH. 2001. HIV-1 infection requires a functional integrase NLS. Mol Cell 7:1025–1035.

44. Lee K, Mulky A, Yuen W, Martin TD, Meyerson NR, Choi L, Yu H, Sawyer SL, Kewalramani VN. 2012. HIV-1 capsid-targeting domain of cleavage and polyadenylation specificity factor 6. J Virol 86:3851–3860.

45. Bejarano DA, Peng K, Laketa V, Börner K, Jost KL, Lucic B, Glass B, Lusic M, Müller B, Kräusslich H-G. 2019. HIV-1 nuclear import in macrophages is regulated by CPSF6-capsid interactions at the nuclear pore complex. eLife 8:e41800

46. De Iaco A, Santoni F, Vannier A, Guipponi M, Antonarakis S, Luban J. 2013. TNPO3 protects HIV-1 replication from CPSF6-mediated capsid stabilization in the host cell cytoplasm. Retrovirology 10:20.

47. Briggs JAG, Wilk T, Welker R, Kräusslich H-G, Fuller SD. 2003. Structural organization of authentic, mature HIV-1 virions and cores. EMBO J 22:1707–1715.

48. Panté N, Kann M. 2002. Nuclear pore complex is able to transport macromolecules with diameters of about 39 nm. Mol Biol Cell 13:425–434.

49. Burdick RC, Delviks-Frankenberry KA, Chen J, Janaka SK, Sastri J, Hu W-S, Pathak VK. 2017. Dynamics and regulation of nuclear import and nuclear movements of HIV-1 complexes. PLoS Pathog 13:e1006570.

50. Di Nunzio F, Danckaert A, Fricke T, Perez P, Fernandez J, Perret E, Roux P, Shorte S, Charneau P, Diaz-Griffero F, Arhel NJ. 2012. Human nucleoporins promote HIV-1 docking at the nuclear pore, nuclear import and integration. PLoS One 7:e46037.

51. Lin DH, Zimmermann S, Stuwe T, Stuwe E, Hoelz A. 2013. Structural and functional analysis of the C-terminal domain of Nup358/RanBP2. J Mol Biol 425:1318–1329.

52. Bichel K, Price AJ, Schaller T, Towers GJ, Freund SMV, James LC. 2013. HIV-1 capsid undergoes coupled binding and isomerization by the nuclear pore protein NUP358. Retrovirology 10:81.

53. Meehan AM, Saenz DT, Guevera R, Morrison JH, Peretz M, Fadel HJ, Hamada M, van Deursen J, Poeschla EM. 2014. A cyclophilin homology domain-independent role for Nup358 in HIV-1 infection. PLoS Pathog 10:e1003969.

54. Matreyek KA, Yücel SS, Li X, Engelman A. 2013. Nucleoporin NUP153 phenylalanine-glycine motifs engage a common binding pocket within the HIV-1 capsid protein to mediate lentiviral infectivity. PLoS Pathog 9:e1003693.

55. Cosnefroy O, Murray PJ, Bishop KN. 2016. HIV-1 capsid uncoating initiates after the first strand transfer of reverse transcription. Retrovirology 13:58.

56. Jacques DA, McEwan WA, Hilditch L, Price AJ, Towers GJ, James LC. 2016. HIV-1 uses dynamic capsid pores to import nucleotides and fuel encapsidated DNA synthesis. Nature 536:349–353.

57. Schaller T, Ocwieja KE, Rasaiyaah J, Price AJ, Brady TL, Roth SL, Hué S, Fletcher AJ, Lee K, KewalRamani VN, Noursadeghi M, Jenner RG, James LC, Bushman FD, Towers GJ. 2011. HIV-1 capsid-cyclophilin interactions determine nuclear import pathway, integration targeting and replication efficiency. PLoS Pathog 7:e1002439.

58. Koh Y, Wu X, Ferris AL, Matreyek KA, Smith SJ, Lee K, KewalRamani VN, Hughes SH, Engelman A. 2013. Differential effects of human immunodeficiency virus type 1 capsid and cellular factors nucleoporin 153 and LEDGF/p75 on the efficiency and specificity of viral DNA integration. J Virol 87:648–658.

59. Fischer G, Wittmann-Liebold B, Lang K, Kiefhaber T, Schmid FX. 1989. Cyclophilin and peptidyl-prolyl cis-trans isomerase are probably identical proteins. Nature 337:476–478.

60. Braaten D, Ansari H, Luban J. 1997. The hydrophobic pocket of cyclophilin is the binding site for the human immunodeficiency virus type 1 Gag polyprotein. J Virol 71:2107–2113.

61. Takahashi N, Hayano T, Suzuki M. 1989. Peptidyl-prolyl cis-trans isomerase is the cyclosporin A-binding protein cyclophilin. Nature 337:473–475.

62. Davis TL, Walker JR, Campagna-Slater V, Finerty PJ, Paramanathan R, Bernstein G, MacKenzie F, Tempel W, Ouyang H, Lee WH, Eisenmesser EZ, Dhe-Paganon S. 2010. Structural and biochemical characterization of the human cyclophilin family of peptidyl-prolyl isomerases. PLoS Biol 8:e1000439.

63. Franke EK, Yuan HE, Luban J. 1994. Specific incorporation of cyclophilin A into HIV-1 virions. Nature 372:359–362.

64. Luban J, Bossolt KL, Franke EK, Kalpana GV, Goff SP. 1993. Human immunodeficiency virus type 1 Gag protein binds to cyclophilins A and B. Cell 73:1067–1078.

65. Sokolskaja E, Sayah DM, Luban J. 2004. Target cell cyclophilin A modulates human immunodeficiency virus type 1 infectivity. J Virol 78:12800–12808.

66. Vajdos FF, Yoo S, Houseweart M, Sundquist WI, Hill CP. 1997. Crystal structure of cyclophilin A complexed with a binding site peptide from the HIV-1 capsid protein. Protein Sci 6:2297–2307.

67. Ambrose Z, Lee K, Ndjomou J, Xu H, Oztop I, Matous J, Takemura T, Unutmaz D, Engelman A, Hughes SH, KewalRamani VN. 2012. Human immunodeficiency virus type 1 capsid mutation N74D alters cyclophilin A dependence and impairs macrophage infection. J Virol 86:4708–4714.

68. Yoo S, Myszka DG, Yeh C-Y, McMurray M, Hill CP, Sundquist WI. 1997. Molecular recognition in the HIV-1 capsid/cyclophilin A complex 1 1Edited by J. A. Wells. J Mol Biol 269:780–795.

69. Handschumacher RE, Harding MW, Rice J, Drugge RJ, Speicher DW. 1984. Cyclophilin: a specific cytosolic binding protein for cyclosporin A. Science 226:544–547.

70. Huai Q, Kim H-Y, Liu Y, Zhao Y, Mondragon A, Liu JO, Ke H. 2002. Crystal structure of calcineurin-cyclophilin-cyclosporin shows common but distinct recognition of immunophilin-drug complexes. Proc Natl Acad Sci U S A 99:12037–12042

71. Liu J, Chen CM, Walsh CT. 1991. Human and Escherichia coli cyclophilins: sensitivity to inhibition by the immunosuppressant cyclosporin A correlates with a specific tryptophan residue. Biochemistry 30:2306–2310.

72. Bossard MJ, Koser PL, Brandt M, Bergsma DJ, Levy MA. 1991. A single Trp121 to Ala121 mutation in human cyclophilin alters cyclosporin A affinity and peptidyl-prolyl isomerase activity. Biochem Biophys Res Commun 176:1142–1148.

73. De Iaco A, Luban J. 2014. Cyclophilin A promotes HIV-1 reverse transcription but its effect on transduction correlates best with its effect on nuclear entry of viral cDNA. Retrovirology 11:11.

74. Liu C, Perilla JR, Ning J, Lu M, Hou G, Ramalho R, Himes BA, Zhao G, Bedwell GJ, Byeon I-J, Ahn J, Gronenborn AM, Prevelige PE, Rousso I, Aiken C, Polenova T, Schulten K, Zhang P. 2016. Cyclophilin A stabilizes the HIV-1 capsid through a novel non-canonical binding site. Nat Commun 7:10714.

75. Peng W, Shi J, Márquez CL, Lau D, Walsh J, Faysal KMR, Byeon CH, Byeon I-JL, Aiken C, Böcking T. 2019. Functional analysis of the secondary HIV-1 capsid binding site in the host protein cyclophilin A. Retrovirology 16:10.

76. Janabi N, Peudenier S, Héron B, Ng KH, Tardieu M. 1995. Establishment of human microglial cell lines after transfection of primary cultures of embryonic microglial cells with the SV40 large T antigen. Neurosci Lett 195:105–108.

77. Takeda E, Kono K, Hulme AE, Hope TJ, Nakayama EE, Shioda T. 2015. Fluorescent image analysis of HIV-1 and HIV-2 uncoating kinetics in the presence of old world monkey TRIM5α. PLoS One 10:e0121199.

78. Mandal D, Prasad VR. 2009. Analysis of 2-LTR circle junctions of viral DNA in infected cells. Methods Mol Biol 485:73–85.

79. Butler SL, Hansen MS, Bushman FD. 2001. A quantitative assay for HIV DNA integration in vivo. Nat Med 7:631–634.

80. Pfaffl MW. 2001. A new mathematical model for relative quantification in real-time RT-PCR. Nucleic Acids Res 29:e45.

81. Rodgers W. 2002. Making membranes green: construction and characterization of GFP-fusion proteins targeted to discrete plasma membrane domains. Biotechniques 32:1044–6, 1048, 1050–1.

82. Yamashita M, Perez O, Hope TJ, Emerman M. 2007. Evidence for direct involvement of the capsid protein in HIV infection of nondividing cells. PLoS Pathog 3:1502–1510.

83. Velasco FRD. 1980. Thresholding Using the ISODATA Clustering Algorithm. IEEE Trans Syst Man Cybern 10:771–774.

84. Ridler TW, Calvard S. 1978. Picture Thresholding Using an Iterative Selection Method. IEEE Trans Syst Man Cybern 8:630–632.

85. Muroi M, Shiragami N, Nagao K, Yamasaki M, Takatsuki A. 1994. Folimycin (concanamycin A) and Bafilomycin A1, Inhibitors Specific for V-ATPase, Exert Similar but Distinct Effects on Intracellular Translocation and Processing of Glycoproteins. Biosci Biotechnol Biochem 58:425–427.

86. Li L, Olvera JM, Yoder KE, Mitchell RS, Butler SL, Lieber M, Martin SL, Bushman FD. 2001. Role of the non-homologous DNA end joining pathway in the early steps of retroviral infection. EMBO J 20:3272–3281.

87. Jeanson L, Subra F, Vaganay S, Hervy M, Marangoni E, Bourhis J, Mouscadet J-F. 2002. Effect of Ku80 depletion on the preintegrative steps of HIV-1 replication in human cells. Virology 300:100–108.

88. Lahaye X, Satoh T, Gentili M, Cerboni S, Conrad C, Hurbain I, El Marjou A, Lacabaratz C, Lelièvre J-D, Manel N. 2013. The capsids of HIV-1 and HIV-2 determine immune detection of the viral cDNA by the innate sensor cGAS in dendritic cells. Immunity 39:1132–1142.

89. Sood C, Francis AC, Desai TM, Melikyan GB. 2017. An improved labeling strategy enables automated detection of single-virus fusion and assessment of HIV-1 protease activity in single virions. J Biol Chem 292:20196–20207.

90. Desai TM, Marin M, Sood C, Shi J, Nawaz F, Aiken C, Melikyan GB. 2015. Fluorescent protein-tagged Vpr dissociates from HIV-1 core after viral fusion and rapidly enters the cell nucleus. Retrovirology 12:88.

91. Francis AC, Melikyan GB. 2018. Single HIV-1 Imaging Reveals Progression of Infection through CA-Dependent Steps of Docking at the Nuclear Pore, Uncoating, and Nuclear Transport. Cell Host Microbe 23:536–548.e6.

92. Dharan A, Talley S, Tripathi A, Mamede JI, Majetschak M, Hope TJ, Campbell EM. 2016. KIF5B and Nup358 Cooperatively Mediate the Nuclear Import of HIV-1 during Infection. PLoS Pathog 12:e1005700.

93. Manjunath N, Wu H, Subramanya S, Shankar P. 2009. Lentiviral delivery of short hairpin RNAs. Adv Drug Deliv Rev 61:732–745.

94. Braaten D, Aberham C, Franke EK, Yin L, Phares W, Luban J. 1996. Cyclosporine A-resistant human immunodeficiency virus type 1 mutants demonstrate that Gag encodes the functional target of cyclophilin A. J Virol 70:5170–5176.

95. Sayah DM, Sokolskaja E, Berthoux L, Luban J. 2004. Cyclophilin A retrotransposition into TRIM5 explains owl monkey resistance to HIV-1. Nature 430:569–573.

96. Kim K, Dauphin A, Komurlu S, McCauley SM, Yurkovetskiy L, Carbone C, Diehl WE, Strambio-De-Castillia C, Campbell EM, Luban J. 2019. Cyclophilin A protects HIV-1 from restriction by human TRIM5α. Nat Microbiol. 4:2044–2051

97. Sokolskaja E, Berthoux L, Luban J. 2006. Cyclophilin A and TRIM5alpha independently regulate human immunodeficiency virus type 1 infectivity in human cells. J Virol 80:2855–2862.

98. Lahaye X, Satoh T, Gentili M, Cerboni S, Silvin A, Conrad C, Ahmed-Belkacem A, Rodriguez EC, Guichou J-F, Bosquet N, Piel M, Le Grand R, King MC, Pawlotsky J-M, Manel N. 2016. Nuclear Envelope Protein SUN2 Promotes Cyclophilin-A-Dependent Steps of HIV Replication. Cell Rep 15:879–892.

99. Donahue DA, Porrot F, Couespel N, Schwartz O. 2017. SUN2 Silencing Impairs CD4 T Cell Proliferation and Alters Sensitivity to HIV-1 Infection Independently of Cyclophilin A. J Virol 91.

100. Donahue DA, Amraoui S, di Nunzio F, Kieffer C, Porrot F, Opp S, Diaz-Griffero F, Casartelli N, Schwartz O. 2016. SUN2 Overexpression Deforms Nuclear Shape and Inhibits HIV. J Virol 90:4199–4214.